

INFORMATION TO USERS

This manuscript has been reproduced from the microfilm master. UMI films the text directly from the original or copy submitted. Thus, some thesis and dissertation copies are in typewriter face, while others may be from any type of computer printer.

The quality of this reproduction is dependent upon the quality of the copy submitted. Broken or indistinct print, colored or poor quality illustrations and photographs, print bleedthrough, substandard margins, and improper alignment can adversely affect reproduction.

In the unlikely event that the author did not send UMI a complete manuscript and there are missing pages, these will be noted. Also, if unauthorized copyright material had to be removed, a note will indicate the deletion.

Oversize materials (e.g., maps, drawings, charts) are reproduced by sectioning the original, beginning at the upper left-hand corner and continuing from left to right in equal sections with small overlaps. Each original is also photographed in one exposure and is included in reduced form at the back of the book.

Photographs included in the original manuscript have been reproduced xerographically in this copy. Higher quality 6" x 9" black and white photographic prints are available for any photographs or illustrations appearing in this copy for an additional charge. Contact UMI directly to order.

UMI

**A Bell & Howell Information Company
300 North Zeeb Road, Ann Arbor MI 48106-1346 USA
313/761-4700 800/521-0600**

University of Alberta

Punching Shear of High Strength Concrete Slabs with Perforations

by

Brian Wayne Kennedy



**A thesis submitted to the Faculty of Graduate Studies and Research in partial fulfillment
of the requirements for the degree of Master of Science**

in

Structural Engineering

Department of Civil Engineering

Edmonton, Alberta

Spring 1997



National Library
of Canada

Acquisitions and
Bibliographic Services

395 Wellington Street
Ottawa ON K1A 0N4
Canada

Bibliothèque nationale
du Canada

Acquisitions et
services bibliographiques

395, rue Wellington
Ottawa ON K1A 0N4
Canada

Your file Votre référence

Our file Notre référence

The author has granted a non-exclusive licence allowing the National Library of Canada to reproduce, loan, distribute or sell copies of his/her thesis by any means and in any form or format, making this thesis available to interested persons.

The author retains ownership of the copyright in his/her thesis. Neither the thesis nor substantial extracts from it may be printed or otherwise reproduced with the author's permission.

L'auteur a accordé une licence non exclusive permettant à la Bibliothèque nationale du Canada de reproduire, prêter, distribuer ou vendre des copies de sa thèse de quelque manière et sous quelque forme que ce soit pour mettre des exemplaires de cette thèse à la disposition des personnes intéressées.

L'auteur conserve la propriété du droit d'auteur qui protège sa thèse. Ni la thèse ni des extraits substantiels de celle-ci ne doivent être imprimés ou autrement reproduits sans son autorisation.

0-612-21178-9

University of Alberta

Library Release Form

Name of Author: Brian Wayne Kennedy

Title of Thesis: Punching Shear of High Strength Concrete Slabs with Perforations

Degree: Master of Science

Year this Degree Granted: 1997

Permission is hereby granted to the University of Alberta Library to reproduce single copies of this thesis and to lend or sell such copies for private, scholarly, or scientific research purposes only.

The author reserves all other publication and other rights in association with the copyright in the thesis, and except as hereinbefore provided, neither the thesis nor any substantial portion thereof may be printed or otherwise reproduced in any material form whatever without the author's prior written permission.

A handwritten signature in black ink, appearing to read 'B. Kennedy', written over a horizontal line.

20 Greenwood Way
Sherwood Park, Alberta
Canada T8A 0J5

January 27, 1997

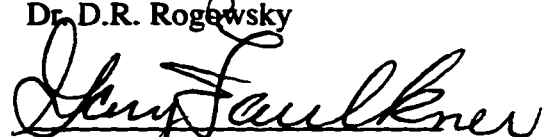
University of Alberta

Faculty of Graduate Studies and Research

The undersigned certify that they have read, and recommend to the Faculty of Graduate Studies and Research for acceptance, a thesis entitled Punching Shear of High Strength Concrete Slabs with Perforations by Brian Wayne Kennedy in partial fulfillment of the requirements for the degree of Master of Science in Structural Engineering.


Dr. S.D.B. Alexander


Dr. D.R. Rogowsky


Dr. M.G. Faulkner

To my parents Don and Faye Kennedy for their never-ending encouragement and support in all my chosen endeavors.

Abstract

This thesis presents the results of six tests conducted on reinforced high strength slabs. The tests were performed to evaluate the influence of perforations on the punching behavior and ultimate capacity of flat plate-column connections containing high performance concrete. In particular, the tests were designed to assess the impact of perforations on the load carrying mechanisms defined by the bond model, a lower bound solution for punching strength proposed by Alexander and Simmonds.

The test specimens consisted of two solid specimens, two specimens with perforations on the column faces, and two specimens with perforations on the column corners. The test results showed that perforations placed in the vicinity of the column have a significant effect both on the ductility and capacity of the connection. Effects on capacity were shown to be a result of disruptions to the load carrying mechanisms defined by the model, in particular on the development of shear and torsion in the vicinity of the perforation. Perforation placed at the column corners had a greater effect than perforations at the column faces.

The bond model is successfully applied to the six tests reported in the thesis as well as 32 others reported in the literature. In addition test results are compared to existing code predictions.

Acknowledgments

Financial support for this research was provided by Concrete Canada. Donations of materials were made by Lafarge, Inland Cement, W.R. Grace, and Master Builders. We are grateful for their contributions.

Sincere appreciation is expressed to Larry Burden and Richard Helfrich of the I.F. Morrison Structures Laboratory for their valuable assistance during fabrication and testing of test specimens.

TABLE OF CONTENTS

1. INTRODUCTION.....	1
1.1 DESCRIPTION OF PROBLEM.....	1
1.2 SCOPE OF STUDY	2
2. BACKGROUND	4
2.1 EXISTING DESIGN METHODS	4
2.1.1 CSA Standard CAN3-A23.3-M94(Canadian).....	4
2.1.2 BS 8110 : Part 1 : 1985 (British)	6
2.1.3 BBK79 Handbook(Swedish)	7
2.2 TREATMENT OF PERFORATIONS.....	9
2.3 HIGH STRENGTH CONCRETE.....	10
3. THE BOND MODEL.....	13
3.1 ELEMENTS OF THE BOND MODEL	13
3.1.1 The Radial Strip.....	13
3.1.2 Loading of The Radial Strip	14
3.2 CAPACITIES OF THE RADIAL STRIP	14
3.2.1 Flexural Capacity.....	15
3.2.2 Shear Capacity	17
3.3 DETERMINATION OF PUNCHING STRENGTH	18
3.3.1 Equilibrium of the Radial Strip.....	18
3.3.2 Optimized Loading of the Radial Strip	20
3.3.3 Effect of Slab Perforations on Punching Strength.....	23
3.4 MECHANISMS OF FAILURE.....	25
3.4.1 Limitations on Shear Development.....	26
3.4.2 Limitations on Flexural Support	27

3.4.3 Limitations on Torsional Shear and Moment.....	28
4. DESCRIPTION OF SPECIMENS AND TEST PROCEDURES.....	34
4.1 DESCRIPTION OF TEST SPECIMENS	34
4.1.1 Reinforcement.....	35
4.1.2 Concrete.....	35
4.1.3 Fabrication of Specimens.....	36
4.2 TEST SETUP AND INSTRUMENTATION	37
4.2.1 Test Apparatus	37
4.2.2 Strain Measurements.....	37
4.2.3 Linear Variable Differential Transformers(LVDT's)	38
4.2.4 Load Cells.....	38
4.3 TEST PROCEDURE	39
5. ANALYSIS OF TEST SPECIMENS.....	45
5.1 STRAIN MEASUREMENTS.....	45
5.1.1 Primary Shear Calculations.....	46
5.1.2 Moment at Column Face of Radial Strips.....	48
5.2 EQUILIBRIUM OF RADIAL STRIP	48
5.2.1 Vertical Equilibrium	48
5.2.2 Rotational Equilibrium	49
5.3 COMMENTS ON ANALYSIS	50
5.3.1 Shear Calculations	50
6. OBSERVATIONS AND EVALUATION.....	52
6.1 LOAD-DEFLECTION BEHAVIOR.....	52
6.2 SHEAR TRANSFER TO THE RADIAL STRIP.....	53
6.2.1 Solid Slab Specimens.....	54
6.2.2 Specimens with Perforations.....	56

6.3 DEVELOPMENT OF YIELD MOMENT AT COLUMN FACE	57
6.4 DEVELOPMENT OF TORSION	57
6.5 COMPARISON OF TEST RESULTS TO PREDICTED CAPACITIES	60
6.5.1 Bond Model Predictions	60
6.5.2 CSA Standard CAN3-A23.3-M84	62
6.6 COMMENTS ON THE BOND MODEL	62
7. CONCLUSIONS AND RECOMMENDATIONS FOR FUTURE WORK.....	77
7.1 CONCLUSIONS	77
7.2 RECOMMENDATIONS FOR FUTURE WORK	78
8. REFERENCES	80
9. APPENDIX A	82

LIST OF TABLES

TABLE 4.1 DESCRIPTION OF TEST SPECIMENS	44
TABLE 6.1 TEST TO PREDICTED RATIOS	73

LIST OF FIGURES

FIGURE 2.1 REDUCTION OF CRITICAL PERIMETER	12
FIGURE 3.1 ISOLATED RADIAL HALF STRIP	30
FIGURE 3.2 OPTIMIZED LOADING OF RADIAL HALF-STRIP	31
FIGURE 3.3 OPTIMIZED LOADING OF RADIAL HALF-STRIP WITH PERFORATION IN STRIP	31
FIGURE 3.4 OPTIMIZED LOADING OF RADIAL HALF-STRIP WITH PERFORATIONS ADJACENT TO STRIP	32
FIGURE 3.5 DEFORMED GEOMETRY OF RADIAL STRIP	33
FIGURE 4.1 TYPICAL TOP MAT REINFORCEMENT LAYOUT	40
FIGURE 4.2 TOP MAT REINFORCEMENT LAYOUT FOR SPECIMEN #5-4C	40
FIGURE 4.3 TYPICAL BOTTOM MAT REINFORCEMENT LAYOUT	41
FIGURE 4.4 TEST SPECIMEN PERFORATION PATTERNS	41
FIGURE 4.5 STRAIN GAUGE LAYOUT FOR TEST SPECIMENS	42
FIGURE 4.6 TYPICAL STRESS-STRAIN CURVES FOR 15M AND 20M REINFORCING BARS	42
FIGURE 4.7 STANDARD TEST SETUP	43
FIGURE 5.1 GAUGE LOCATIONS FOR ANALYSIS OF TEST SPECIMENS	51
FIGURE 5.2 INFLUENCE OF TORSIONS ON MEASURED FORCE GRADIENTS	51
FIGURE 6.1 LOAD DEFLECTION BEHAVIOR - ALL SPECIMENS	64
FIGURE 6.2 LOAD DEFLECTION BEHAVIOR - SOLID SPECIMENS	64
FIGURE 6.3 LOAD DEFLECTION BEHAVIOR - 4F SPECIMENS	65
FIGURE 6.4 LOAD DEFLECTION BEHAVIOR - 4C SPECIMENS	65
FIGURE 6.5 PERIMETER BAR SHEARS - SPECIMEN #1-SS	66
FIGURE 6.6 PERIMETER BAR SHEARS - SPECIMEN #4-SS	66
FIGURE 6.7 PERIMETER BAR SHEARS - SPECIMEN #2-4F	67
FIGURE 6.8 PERIMETER BAR SHEARS - SPECIMEN #6-4F	67
FIGURE 6.9 PERIMETER BAR SHEARS - SPECIMEN #3-4C	68
FIGURE 6.10 PERIMETER BAR SHEARS - SPECIMEN #5-4C	68

FIGURE 6.11 RATIO OF MEASURED LOAD TO TOTAL LOAD - SS SPECIMENS	69
FIGURE 6.12 RATIO OF MEASURED LOAD TO TOTAL LOAD - 4F SPECIMENS	69
FIGURE 6.13 RATIO OF MEASURED LOAD TO TOTAL LOAD - 4C SPECIMENS	70
FIGURE 6.14 DEVELOPMENT OF NEGATIVE MOMENT AT COLUMN FACE	70
FIGURE 6.15 TORSION REQUIREMENTS - SS SPECIMENS	71
FIGURE 6.16 TORSION REQUIREMENTS - 4F SPECIMENS	71
FIGURE 6.17 TORSION REQUIREMENTS - 4C SPECIMENS	72
FIGURE 6.18 TEST TO PREDICTED RATIOS- BOND MODEL	75
FIGURE 6.19 TEST TO PREDICTED RATIOS - CAN-A23.3-M94	75
FIGURE 6.20 TEST TO PREDICTED RATIOS - BOND MODEL	76
FIGURE 6.21 TEST TO PREDICTED RATIOS - CAN3-A23.3-M84	76

LIST OF SYMBOLS

b	width of plate strip for definition of reinforcement ratio
b_o	perimeter length of critical section
c	side dimension of column
c_{eff}	effective width of radial strip
d	effective depth of reinforcement measured from center of mat to slab soffit
f'_c	cylinder compressive strength of concrete
f_y	static yield stress of steel
h_n	width of perforation perpendicular to strip
h_r	width of perforation parallel to strip
j	ratio of flexural moment arm to d
k_r	restraint factor
l	loaded length of radial strip
m_n	distributed bending moment on side face of radial strip
m_t	distributed torsional moment on side face of radial strip
s	spacing of reinforcement
v	distributed shear in plate
v_c	permissible shear stress
v_p	distributed primary shear in plate
v_t	distributed torsional shear in plate
w	bond model loading term
A_{bar}	area of single reinforcing bar
A_s	total area of flexural reinforcement
A_{sT}	total negative flexural reinforcement associated with width b
A_{sB}	total positive flexural reinforcement associated with width b
A_{Bcol}	total area of positive flexural reinforcement within the radial strip
A_{Tcol}	total area of negative flexural reinforcement within the radial strip
B	diameter or nominal diameter of column
C	horizontal component of compressive arch

L	total length of radial strip
M_{neg}, M_{pos}	negative and positive flexural capacities of radial strip
M_s	flexural capacity of radial strip
P_s	load carried by single radial strip
P_{ult}	summation of all loads carried by all radial strips to column
T	tensile force in reinforcing bar
α	angle of concrete compressive arch relative to horizontal at column face
β_c	aspect ratio of column
ε	strain in reinforcement
λ	factor to account for low density concrete
ρ_{neg}	effective negative reinforcement ratio for radial strip
ρ_{pos}	effective positive reinforcement ratio for radial strip

1. INTRODUCTION

1.1 Description of Problem

Several advantages are obtained through the use of flat plate structural systems. These systems consist of reinforced concrete slabs supported on columns. As there are no beams, drop panels, or column capitals formwork is greatly simplified. Additionally, as this leaves a level soffit, the installation of services, as well as interior finishes becomes less complicated. These benefits make flat plate structures a favorable method of construction.

In utilizing a flat plate system, a designer must consider punching failures which can become increasingly critical with this type of structure. A punching shear failure occurs when the column is essentially pushed through the slab. This mode of failure becomes increasingly complex in situations where it is necessary to incorporate perforations, or holes, through the slabs in order to convey services to the floors above. Perforations near support columns are of particular concern due to their influence on the resistance to punching failure of the slab-column connection. Current building code design procedures for punching strength, which are semi-empirical in nature in the absence of perforations, add another degree of empiricism in their presence. A simple yet general mechanical model which describes the transfer of load between the slab and the column would be desirable.

In addition, there is some concern that as material properties change, such as the use of high strength concrete or alternate forms of reinforcement, the existing design procedures may not be adequate. Current design procedures are largely based on research conducted utilizing relatively low strength concrete, typically no higher than about 40

MPa. Extrapolation of these methods to cases involving high strength concrete, for which relatively little information is available, is justifiably cause for concern.

The use of high strength concrete in two-way slab systems is becoming more common for two reasons. The first is deflection control. In order to minimize deflections under load, particularly with longer spans, a designer may opt to use higher strength concrete. This will provide a stiffer load-deformation behavior as a result of the increase in the modulus of elasticity.

The second situation arises from the use of high strength concrete columns, already common in construction. In order to prevent a “sandwich” column (a layer of normal strength concrete at slab elevations sandwiched between high strength concrete columns above and below) high strength concrete is sometimes puddled around the column and forms part of the surrounding slab. Since this puddled high strength concrete is in the zone of punching failures it is natural to take advantage of any increases in punching strength resulting from its presence.

1.2 Scope of Study

Alexander and Simmonds(1991) propose a model to predict the punching strength of slab-column connections. This model is encouraging as it describes the load carrying mechanisms as well as appears to be adaptable to a wide variety of load cases. Additionally, through previous testing, it appears to have good correlation with observed behavior.

The bond model describes all load entering the column through defined portions of the slab termed radial strips. Shear transfer to the column occurs through arching action of

the radial strip. The radial strips, equal to the width of the column, extend from the face of the column to the point of zero shear and are loaded on their side faces by both primary shear and torsion. The primary shear is developed through bending moment gradient perpendicular to the radial strip and is assumed to be dominated by beam action. Torsional moments and shears are developed by the two way behavior of the plate.

A total of six specimens were tested and are reported in this thesis. The principal goal was to check the validity of the bond model with a focus on the influence of perforations and their effect on the above described load carrying mechanisms. Secondary to this, the specimens utilized high strength concrete to expand the database of experimental work conducted with respect to the bond model. There are few sources in the literature for punching behavior of high strength concrete and no sources were found with the combination of high strength concrete and slab perforations. Based on the results of these tests and those reported in the literature, the validity and suitability of the bond model are discussed. Comparisons of test results to existing code methods are also made.

2. BACKGROUND

Current methods of estimating the punching capacity of slab-column connections are largely based on the concept of a limiting shear stress on a defined critical perimeter. Variations exist between different codes as to the location of the critical perimeter and the permissible stress. While the two are interrelated, the seemingly arbitrary manner in which they are defined speaks to the empirical nature of the method. The following section briefly outlines the methods for predicting punching capacity contained in the Canadian, British, and Swedish Codes. For ease of comparison the notation utilized to define similar parameters has been standardized.

2.1 Existing Design Methods

2.1.1 CSA Standard CAN3-A23.3-M94(Canadian)

The characteristic punching strength for non-prestressed two-way slabs without shear reinforcement as defined in the Canadian code is:

$$V_c = (1 + \frac{2}{\beta_c}) \times 0.2\lambda\sqrt{f'_c}b_o d \leq 0.4\lambda\sqrt{f'_c}b_o d \quad \text{where}$$

β_c = ratio of long side to short side of concentrated load or reaction area

λ = factor to account for low density concrete

b_o = perimeter of critical section

d = average flexural depth of negative reinforcement

It can be determined from the limit imposed on the punching strength that the aspect ratio becomes influential only for aspect ratios greater than 2. This factor becomes

important for elongated columns which tend to promote unsymmetric behavior in the plate in regions near the column. Neglecting this as well as the reduction factor for low density concrete it can be seen that the punching capacity is dependent only upon the concrete strength, flexural depth of the reinforcement, and column size. The critical section defined in the Canadian code is located at a distance of one-half of the flexural depth from the perimeter of the column.

The simplicity and transparency of the Canadian design equation, which is conceptually identical to the ACI(American) code, make it attractive for design purposes. Inconsistencies and omissions, however, bring into question the reliability and accuracy, particularly when used for cases outside the parameter ranges for which it was calculated (i.e. high strength concrete).

For example, the critical value of shear utilized for punching strength is twice that used for one-way shear. This “apparent” increase in shear strength is attributed to the confinement effects provided by the two-way behavior of the plate. This critical stress however is not determined from tests designed to quantify the beneficial influence of confinement but rather by calibration of the design equation to existing test data.

Another inconsistency in the design method concerns the failure surface itself. While the defined location of the critical perimeter is more or less consistent with the location of inclined cracking observed in tests, typically 25° to 35° from the horizontal (Regan and Braestrup, 1985) beginning near the column face, there is no explanation offered as to why fully developed inclined cracking is observed at loads as low as 70% of the ultimate capacity. If indeed punching failures are governed by a limitation on shear

stresses developed on the critical perimeter it would be anticipated that the formation of inclined cracking (rupture surface) would be accompanied by the punching failure itself.

2.1.2 BS 8110 : Part 1 : 1985 (British)

The characteristic punching strength defined in the British code is

$$V_c = \varepsilon v_c b_o d \quad \text{where}$$

$$v_c = 0.79 \times \sqrt[3]{100\rho} \times \sqrt[3]{f'_c/25} \quad \text{with } 25 \leq f'_c \leq 40$$

$$\varepsilon = \sqrt[4]{400/d} \geq 1.0$$

ρ = average reinforcement ratio in x and y-directions

(constrained to be less than or equal to 0.03 and evaluated in regions extending 1.5d on either side of the column)

The primary difference noted between the Canadian and British codes is the defined critical perimeter and the permissible stress permitted on the critical perimeter. The permissible stress in the British Code, which includes the beneficial effect of increased reinforcement, provides consistent treatment of shear within the code. However, as would be anticipated, the lower allowable stress (compared to North American codes) requires a much larger critical perimeter in order to fit existing test data. The defined critical perimeter in the British code is located a distance of 1.5d away from the loaded area. This places the critical perimeter at the outer edges and even beyond observed rupture surfaces.

Also of note in the British code equation is the parameter ε . This parameter is dependent on the flexural depth and is essentially a scale effect. Such factors are common

in empirical methods, and are utilized to provide better accuracy in the calibration of design equations.

Comparing the Canadian and British codes the empirical nature of such design procedures becomes readily apparent. While the Canadian code adopts a critical perimeter more consistent with the location of inclined cracking observed in punching failures and defines a limiting “two-way shear stress” which fits existing data, the British code uses the one way shear value and best fits a critical perimeter to associate with the limiting shear. In addition both models fail to account for the formation of inclined cracks at loads as much as and even greater than 30% below the failure loads.

2.1.3 BBK79 Handbook(Swedish)

The Swedish code rules for punching capacity are based on a mechanical model proposed by Kinnunen and Nylander. The characteristic punching strength is calculated as:

$$V_c = f_{v1}\pi(B+d)d \text{ where}$$

$$B = \text{diameter or nominal diameter of column} = \sum b/\pi$$

$$b = \text{side dimension of column}$$

Although this equation appears similar to the previously listed, namely a limiting shear stress, f_{v1} , on a defined perimeter, the strength parameter, f_{v1} , is derived from the equilibrium of an assumed deformed behavior and criterion of failure.

The mechanics of the model are based on tests conducted on circular slabs supported by circular columns, hence the circumferential perimeter. The criterion for failure is the attainment of a limiting compressive circumferential strain at the slab soffit. The strength parameter is defined as:

$$f_{v1} = 0.5\xi\alpha \times f_{v1,d} \text{ where}$$

$$f_{v1,d} = \frac{2\rho f_y}{(1+\frac{B}{d})(1-\frac{B}{c})} \times \frac{z}{d} \quad \frac{z}{d} = \frac{3+200k\rho}{3+300k\rho} \text{ and}$$

$$k = \frac{1}{0.57 + 0.43 \frac{f_c'}{13} \sqrt{\frac{400}{f_y}}}$$

The factor α is dependent upon the system geometry and material properties and is determined using the following relations.

$$\text{If } B/d \leq 2 \text{ for } 100k\rho \leq 1.0 \text{ then } K_1 = \frac{3.8 + 0.4 \frac{d}{B} \frac{1}{100k\rho}}{100k\rho + \frac{d}{B}}$$

$$\text{for } 100k\rho > 1.0 \text{ then } K_1 = \frac{3.8 + 0.4d/B}{100k\rho + d/B}$$

If $B/d > 2$ then the above expressions for K_1 are multiplied by $(0.7 + 0.15B/d)$

$$\frac{r_s}{d} = \frac{380}{f_y} K_1 \quad \frac{c_o}{d} = \frac{B}{2d} + 1.8$$

$$\text{If } \frac{c_o}{d} < \frac{r_s}{d} < \frac{c}{2d} \quad \alpha = \frac{r_s}{d} \times 2 \frac{d}{c} \left[1 + \ln\left(\frac{c}{2d} \frac{d}{r_s}\right) \right]$$

$$\text{If } \frac{r_s}{d} < \frac{c_o}{d} \quad \alpha = \frac{r_s}{d} \times 2 \frac{d}{c} \left[1 + \ln\left(\frac{c}{2d} \frac{d}{c_o}\right) \right]$$

$$\text{If } \frac{r_s}{d} \geq \frac{c}{2d} \quad \alpha = 1.0$$

The parameter ξ is a scale effect dependent on the flexural depth. It is determined as follows.

$$\text{For } d < 0.2 \quad \xi = 1.4 \quad d \text{ in metres}$$

$$\text{For } 0.2 < d < 0.5 \quad \xi = 1.6 - d$$

$$\text{For } d > 0.5 \quad \xi = 1.3 - 0.4d$$

c = distance between sections of contraflexure on either side of column

While mechanical models are typically preferable to empirical models it is apparent that this method is quite convoluted and iterative in nature. Additionally, the complexity of equations such as these does not provide the designer with a very good feel for the influence of the individual variables.

Also of note is that Kinnunen and Nylander's model was developed based on polarsymmetric loading and behavior. This is cause for concern when the method is used in cases where it is clear that there is not polarsymmetric behavior.

2.2 Treatment of Perforations

Given the existing design methods for punching shear contained in current codes, namely a limiting shear stress on a defined critical perimeter, it is not surprising the manner in which perforations are treated. The presence of perforations are typically accounted for by reducing the critical perimeter by an amount associated with the perforation size, geometry, and proximity to the column. While slight variations exist between codes, the most common method adopted is to reduce the critical perimeter by the radial projection of the perforation on the defined perimeter.

Figure 2.1 illustrates the reduction resulting from both straight and radial projections. While the straight projection would appear to be more consistent with the

actual loss of perimeter such a projection is very sensitive to the location of the perimeter and leads to unconservative results when used with larger perimeters such as in the British code (Regan and Braestrup, 1985). Radial projections are virtually unaffected by the proximity of the perimeter to the column and are more widely utilized by building codes. Regan and Braestrup suggest however that the use of radial projections tends to be overconservative.

The removal of critical perimeter also has a secondary effect. Ultimately the designer is concerned with not just the shear transfer to the column but the total shear moment interaction. Unsymmetric removal of critical section results in unbalanced moment which must also be transferred to the column. Such cases require the calculation of section properties based on the reduced perimeter and can become significantly more complex.

2.3 High Strength Concrete

The increasing use of high strength concrete brings with it the necessity to accurately predict the behavior and assess the strength of structural components made from it. Extrapolation of existing empirical design methods developed from tests done on normal strength concrete to newer high strength materials brings with it an inherent danger. While the use of high strength concrete is expanding and becoming more popular, relatively little data exists regarding its performance under various conditions.

In research conducted by Marzouk and Hussein (1991) on the performance of high strength slabs subjected to concentrated loads it was noted that using the square root of the concrete strength, such as contained in the Canadian code, tends to overestimate the

influence of that parameter for higher strength concrete. Other concerns regarding high strength concrete include load-deformation behavior and ductility.

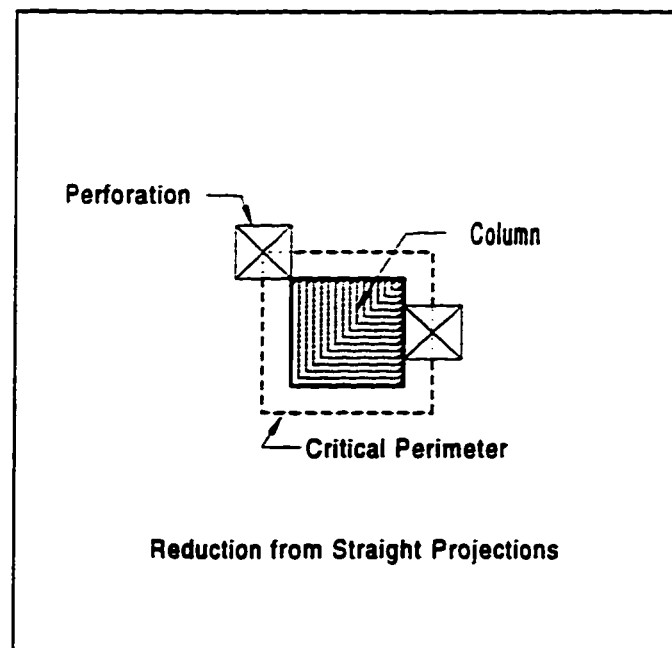
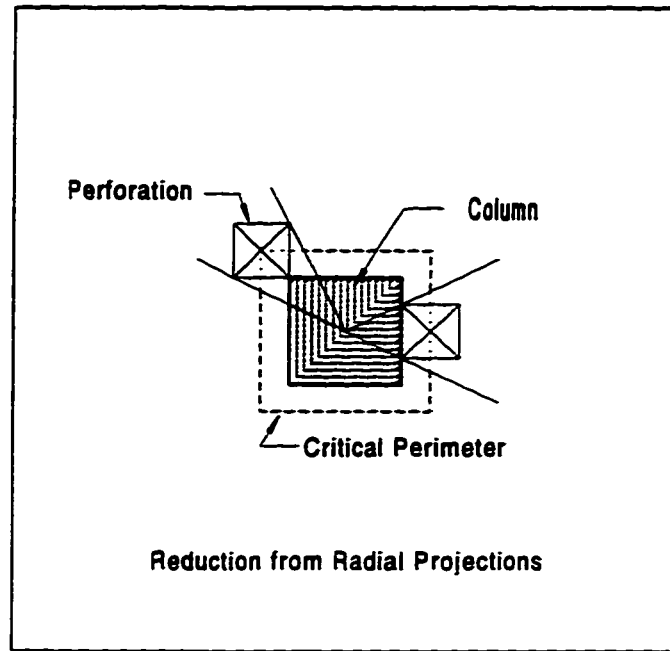


Figure 2.1 Reduction of Critical Perimeter

3. THE BOND MODEL

3.1 Elements of The Bond Model

The bond model, subject to certain constraints, provides a lower bound solution for the punching strength of a slab-column connection. The advantage of this model over methods such as those contained in the Canadian and British codes is that it is a mechanical model, thus eliminating much of the empiricism inherent in these methods. The advantage over existing mechanical models, such as the Kinnunen and Nylander model which forms the basis of the Swedish code, is that it is simple and general in its development and use.

The following section details the concepts and components of the bond model as developed by Alexander and Simmonds(1991). In addition the consequences of slab perforations, with particular reference to the bond model, are discussed.

3.1.1 The Radial Strip

The radial strip, illustrated in Figure 3.1, is the ultimate source of all vertical load entering the column. For rectangular columns it has a width equal to the column width perpendicular to the strip. For a circular column it has a width equal to the column diameter. The radial strip extends from the column face to the point of zero shear, hereinafter termed the remote end. The total length of the radial strip is denoted as L . For a continuous plate the remote end is at the position of maximum positive moment, while for typical test specimens it is at the free edge.

The radial strips are parallel to the slab reinforcement and thus the bond model is constrained to orthogonally reinforced slabs. Two directions are defined parallel and perpendicular to the radial strip and are denoted as the r-axis and n-axis respectively. These directions are equivalent to the radial and circumferential directions of the slab column connection.

3.1.2 Loading of The Radial Strip

The radial strip is loaded by self weight and directly applied loads as well as through the adjacent quadrants of plate. Primary shear is developed along the strip faces through moment gradient perpendicular to the strip. Additionally, both torsional shears and moments are developed by the two-way behavior of the plate.

It is suggested by Alexander and Simmonds that the primary shear developed on the radial strip faces is mainly the result of beam action while the shear transfer from the radial strip to the column is dominated by arching action. Beam action shear is a result of force gradient in the flexural steel and is influenced by factors such as bond and anchorage. Shear is generated by arching action as a result of a constant tensile force in the flexural steel acting over a varying flexural depth.

3.2 Capacities of The Radial Strip

To determine the ultimate punching capacity of the slab column connection using the bond model, it is necessary to evaluate the individual capacities of the load carrying mechanisms defined by the model. The following section details these mechanisms and provides methods for estimating their individual capacities. Based on these capacities the development of design procedures based on the bond model are described.

3.2.1 Flexural Capacity

The flexural capacity of the radial strip is determined by the effective reinforcement ratio of the strip, the concrete strength, and the flexural depth of the reinforcement. In the bond model analysis, for a continuous plate, it is assumed that both the negative and positive flexural capacities of the radial strip are attained prior to punching. This assumption requires that the reinforcing bars have adequate development lengths and/or anchorage.

In determining the effective reinforcement ratio of the radial strip Alexander and Simmonds suggest the following.

$$\rho_{neg} = \frac{A_{sT}}{bd}$$

$$\rho_{pos} = \frac{A_{sB}}{bd}$$

A_{sT} is equal to the area of top steel passing through the column plus one half the area of the first bar on either side of the column. The distance b is the associated distance between these two outer bars. The effective positive reinforcement ratio is defined in the same manner. The rationale behind including bars outside of the radial strip is that the ratio, for a uniformly spaced mat, should not depend on whether the mat is bar centered or space centered.

In situations with symmetric perforations it seems reasonable that any steel passing through the column may be utilized for the associated flexural capacity M_{neg} . This reasoning becomes very evident if considering a situation in which there are perforations on either side of the radial strip. Such a situation will force the steel contained within the

strip to act within the strip width. It is therefore suggested that these equations be expanded to include the following conditions for the purposes of this test program.

$$\rho_{neg} = \frac{A_{sT}}{bd} \geq \frac{A_{Tcol}}{cd} \quad [3.1]$$

$$\rho_{pos} = \frac{A_{sB}}{bd} \geq \frac{A_{Bcol}}{cd} \quad [3.2]$$

In these equations A_{Tcol} and A_{Bcol} are the areas of top and bottom steel respectively within the effective radial strip width c .

Having defined the effective reinforcement ratios the total flexural capacity of the radial strip, M_s , can be estimated as:

$$M_s = M_{neg} + M_{pos} = \rho_{neg} f_y j d^2 c + k_r \rho_{pos} f_y j d^2 c \quad [3.3]$$

where k_r is a restraint factor dependent on the degree of rotational restraint provided at the remote end of the radial strip. For a continuous slab the restraint factor would be equal to one, while for a rotationally free edge such as those in the test specimens, the restraint factor would be zero

3.2.1.1 Comments on Effective Reinforcement

The effective reinforcement ratio utilized for bond model predictions plays a significant role in the overall strength of the slab column connection. The rules previously outlined have been developed for this test program and may not represent a general rule to evaluate all cases. Situations that the above rules might not accurately reflect include the existence of banded reinforcement through the column and or dramatic changes in reinforcement distribution across the slab. In such cases an effective reinforcement ratio

evaluated over a wider slab width, perhaps $1.5d$ on either side of the column may prove to be more appropriate.

3.2.2 Shear Capacity

Primary shear forces are developed on the side faces of the radial strip as a result of moment gradient perpendicular to the strip. In the bond model it is assumed that these shear forces are generated primarily through beam action and are limited by the force gradients attainable in the reinforcement. Bond of the reinforcement to the surrounding concrete is seen as a governing factor of the force gradients which can be attained, hence the name “bond model”. Since force gradients in the reinforcement may be determined utilizing strain gauges and the stress strain relationship of the reinforcement, an estimation of the shear forces developed in a test specimen can be made. This provides a direct method of evaluating the model and the load carrying mechanisms described within.

Based on the concept that a limiting force gradient is synonymous with a limiting shear stress, and that beam action dominates, Alexander and Simmonds go on to suggest that code methods for the concrete contribution to one way shear should provide reasonable estimates for the primary shear capacity w . The one way shear capacity as defined in the American code is as follows.

$$\text{ACI 318} \quad w_{ACI} = 0.166 \times d \times \sqrt{f'_c} \quad [3.4]$$

Since the development of beam action shear is dependent on force gradient through the face of the radial strip it is apparent that progressive yielding of this steel diminishes the ability to transfer shear by beam action. Widespread yielding however is consistent with the development of a folding mechanism which can be associated with the

flexural capacity of the plate. Only punching failures that occur prior to widespread yielding are of concern.

3.3 Determination of Punching Strength

Utilizing the capacities developed in the previous section and statics of the radial strip a method of estimating the punching capacity of the slab column connection has been developed. With reference to the freebody diagram shown in Figure 3.1, the method is outlined below.

3.3.1 Equilibrium of the Radial Strip

Vertical loading of the half radial strip shown in Figure 3.1 includes the line load q , which is the sum of the self weight of the radial strip and any loads applied directly to the strip, as well as ν , the plate shear. The plate shear is a combination of the primary shear and torsional shear developed on the side face of the radial strip. The total reaction at the column end for a single radial strip, P_s , can then be calculated as:

$$P_s = 2 \times \int_0^L (\nu + q) dr$$

Separating the plate shear into its individual components, the primary shear (ν_p) and the torsional shear (ν_t), and integrating the torsional shear results in:

$$P_s = 2 \times \int_0^L (\nu_p + q) dr + 2 \times \int_0^L \nu_t dr$$

$$P_s = 2 \times \int_0^L (\nu_p + q) dr + 2 \times m_t \Big|_0^L$$

Although the exact distribution of the torsional moments is unknown it was argued by Alexander and Simmonds(1991) that the torsional moment should reduce to zero at either end of the radial strip. Justification for this was that the remote end is at a position of zero shear while the column end is very near the axis of symmetry where the torsional moment is constrained to be zero. While this reasoning holds true at the remote end it is simply incorrect at the column end. Being near the axis of symmetry is not synonymous with being at the axis. Considering the column end is located in a region dominated by two-way behavior the presence of significant torsional gradients, and hence a nonzero torsional moment at the column end is very much possible, and in fact quite likely. As such, evaluation of the definite integral of m_t results in the following equation of vertical equilibrium:

$$P_s = 2 \times \int (v_p + q) dr - 2m_t(0) \quad [3.6]$$

As defined by the equation a negative value of $m_t(0)$ would mean that some portion of the total column reaction is carried directly by torsion. This force would appear as a point load at the column corners and would be consistent with previous research which has commonly shown higher vertical compressive strain levels at the column corners than in the middle of the column face. In addition it would be anticipated that the integration of primary shear over the length of the radial strip would underestimate the total column reaction if indeed a nonzero negative value of $m_t(0)$ existed.

Considering the rotational equilibrium of the radial strip yields:

$$M_s + 2M_t = 2 \times \int_0^L (v_p + q) r dr + \int_0^L v_t r dr$$

Integration of the torsional shear by parts results in:

$$M_s + 2M_t = 2 \int_0^L (v_p + q) r dr + 2 \times m_t r \Big|_0^L - 2 \times \int_0^L m_t dr$$

$$M_s + 4M_t = 2 \int_0^L (v_p + q) r dr \quad [3.7]$$

The significance of Equations 3.6 and 3.7 is that they provide a means of evaluating the model and its mechanisms. In both equations an estimate of the integral on the right hand side of the equations may be made. Considering the integral of q to be negligible estimates of the primary shear may be made utilizing the methods developed in Chapter 5. By having direct means of evaluating the model the appropriateness and suitability of the model can be addressed.

3.3.2 Optimized Loading of the Radial Strip

The development of a method for predicting the ultimate strength of a slab column connection involves the optimization of loading on the radial strip. This is done by maximizing the shear at the column end of the strip utilizing a rectangular distribution of shear with intensity w . The total length that the maximized shear acts over, l , may then be solved for using equations of equilibrium. Given the freebody diagram shown in Figure 3.2 and assuming the self weight of the radial strip to be negligible the equations are:

$$M_s = 2 \times \int_0^l (wr) dr = 2 \times \frac{wl^2}{2} = wl^2 \quad [3.8]$$

$$P_s = 2 \times \int_0^l (w) dr = 2wl \quad [3.9]$$

Solving Equation 3.8 for l and substituting in Equation 3.9 gives the capacity of a single radial strip.

$$P_s = 2 \times \sqrt{M_s \times w} \quad [3.10]$$

Utilizing the capacities of M_s and w discussed previously the punching strength may then be estimated by summing the contributions of each radial strip.

$$P_{ult} = \sum P_s \quad [3.11]$$

This method of estimating the punching strength of a slab column connection constitutes a lower bound solution provided that:

- i.) equilibrium is satisfied
- ii.) internal stresses nowhere exceed the stress capacity
- iii.) system has sufficient ductility

Requirement i.) is satisfied in the development of the solution. Requirement ii.) is satisfied provided that the flexural requirements in the associated quadrants of plate do not exceed the flexural capacity, reasonable estimates of M_s and w have been made, and the compressive stresses in the radial arches are not excessive. Exceedance of the flexural capacity of the plate would be accompanied by the development of a folding mechanism and therefor design would be governed by the capacity of the plate.

Requirement iii) is somewhat difficult to evaluate since it is not clearly defined or quantified. Alexander and Simmonds(1991) suggest that punching failures fall into two categories, namely ductile shear failures and proper punching failures. Ductile shear failures are defined as failures caused by extensive yielding of the reinforcement. The term proper punching failures refers to overreinforced flexural failures and brittle shear failures.

By definition overreinforced flexural failures occur as a result of crushing in the concrete compression block prior to yielding of the flexural reinforcement. Clearly this type of failure would violate the ductility requirements of a lower bound solution because the column steel does not yield. However in the case of an underreinforced slab that fails prior to reaching the flexural capacity of the plate, a “brittle” punching failure, it becomes uncertain whether or not the overall system meets the ductility requirements.

Since it is unclear how the ductility may be assessed in design perhaps the best method of evaluating the model as a lower bound solution is by direct comparison of model predictions to extensive test results. These comparisons have been done by Alexander and Simmonds(1991) and based on their results it indeed appears that the model approaches a lower bound solution. While comparison of model predictions to test results are presented in this thesis, the comparisons contained within are quite limited and are not made to validate the model as a lower bound solution.

Unconservative predictions of punching capacity indicate that the chosen shear distribution overestimates the ability of the connections to optimize the shear forces at the column end of the strip through the development of torsion and load redistribution. This could be accounted for by using a more conservative shear distribution such as one which varies linearly from a maximum at the column face to zero at some distance away. Such a distribution would reduce the predicted capacity to approximately 87 percent of that predicted utilizing the rectangular distribution.

It should be noted that in the development of the design procedures there is no requirement for the development of torsion on the side faces of the radial strip. Torsion

does however provide an explanation for how the shear forces entering the radial strip may be optimized near the column.

3.3.3 Effect of Slab Perforations on Punching Strength

3.3.3.1 Perforations Within the Radial Strip

Perforations within the radial strip will have several effects on the ultimate strength of a slab column connection due to their influence on the load carrying mechanisms. Firstly, if the perforations are at or near the column face, and within the radial strip, the effective width of the column will be reduced. This reduction will decrease the negative moment capacity of the strip and may result in an increase in the compressive stresses developed within the radial arches. The reduction in moment capacity may be accommodated in the bond model by modifying the effective reinforcing ratio as follows:

$$\rho_{neg} = \frac{A_{sr}}{b_{eff}} \geq \frac{A_{rcol}}{c_{eff}} \quad \text{where} \quad [3.12]$$

$$b_{eff} = b - h_n \quad \text{and} \quad c_{eff} = c - h_n \quad [3.13]$$

The negative moment capacity is then:

$$M_{neg} = \rho_{neg} f_y j d^2 c_{eff}$$

where c_{eff} is the effective width of the column which is equal to the column width minus the perforation width perpendicular to the strip, h_n . In situations where a significant portion of the column width is rendered ineffective by the perforation there is a danger of locally overreinforcing the radial strip. Care should be taken to ensure that this does not occur.

In addition, as can be seen in Figure 3.3, the perforation will dramatically reduce the development of shear forces on the side faces of the radial strip over the width of the perforation parallel to the strip due to an inability to carry moment gradient across the perforation. If the perforation is sufficiently far away from the column, that is to say if:

$$l_1 \geq \sqrt{M_s/w}$$

then all of the shear transfer can occur within the distance l as solved for utilizing Equation 3.8. If however this condition is not satisfied then shear transfer must extend beyond the perforation. Considering rotational equilibrium of the radial strip shown in Figure 3.3 results in a quadratic equation which may be solved for the unknown length l_2 .

Simplification of this solution results in:

$$l_2 = \sqrt{(l_1 + h_r)^2 - l_1^2 + \frac{M_s}{w}} - (l_1 + h_r) \quad [3.14]$$

and the punching contribution of the strip is:

$$P_s = 2 \times w \times (l_1 + l_2) \quad [3.15]$$

If the perforation is adjacent to the column face then l_1 is equal to zero and these equations can be further simplified to:

$$l_2 = \sqrt{h_r^2 + \frac{M_s}{w}} - h_r \quad [3.16]$$

$$P_s = 2 \times w \times l_2 \quad [3.17]$$

3.3.3.2 Perforations Adjacent to Radial Strips

Perforations adjacent to the radial strips will have slightly different effects on the punching strength than those placed within the strip. Considering the radial strip shown in

Figure 3.4, with perforations on both sides of the strip, it is apparent that the tensile force available to generate negative moment at the column face is limited to reinforcing bars within the radial strip. It would therefore seem reasonable that when calculating the effective reinforcement ratio only the second term on the right hand side of Equation 3.12 should be considered.

In addition shear transfer on the side faces will be disrupted similarly to when the perforation is within the strip. Since there is no moment gradient generated over the length of the perforation parallel to the strip there will be no shears developed and Equations 3.14 and 3.15 become applicable to this case as well.

3.4 Mechanisms of Failure

The mechanisms of failure with respect to the bond model may be examined by considering the load carrying mechanisms and the requirements demanded of them with increasing load. Considering equilibrium of the radial strip in Figure 3.2 it can be seen that an increment in load requires both an increase in shear along the side faces of the radial strip as well as increase in the flexural support provided to the strip. Additionally an increase in load will cause additional deformation of the system.

3.4.1 Limitations on Shear Development

The ability to develop shear on the radial strip faces is dependent on several factors. The development of beam action shear requires force gradient in the reinforcement perpendicular to the strip at the strip face. Force gradient in the reinforcement may be limited by both bond and anchorage. In addition the progression of yielding ultimately leads to the inability to generate shear through beam action.

Anchorage of the reinforcement will typically not be of concern. Good design practices will ensure adequate development lengths to effectively engage the reinforcement. Limitations on bond however may have a more significant influence. Loss of bond may result from splitting failures in the concrete around the reinforcement. Splitting of the concrete typically occurs in the plane of the reinforcement and/or in wedge shape splits around individual bars.

Loss of bond or progressive yielding which leads to a reduced ability to generate beam action shear may result in two situations. As force gradient in the reinforcement is lost there may be a significant loss in the ability to develop shear on the strip face in the zone of yielding. More likely however would be a transition in which shear that may have been previously carried by beam action is partially or fully generated through arching action.

In either event the zone of shear transfer, as calculated by the bond model, is usually confined to a very small length of the radial strip near the column, typically less than 500mm. Considering this it seems reasonable that the ability to generate additional shear along the remaining length of the radial strip is not of concern. The development of additional shear however imposes a requirement for additional flexural support.

3.4.2 Limitations on Flexural Support

Flexural support, as defined by the model, is provided by the development of negative moment at the column end of the strip and positive moment at the remote end. Although not directly included in the bond model additional support is provided by the development of torsional moments along the side faces of the radial strips. This

mechanism of flexural support is consistent with previous testing which typically reveals yielding of the column steel at loads significantly less than the failure loads. This mechanism of flexural support also introduces an element of conservatism in the bond model since the model does not provide for any flexural support to the strip from the development of torsional moments.

The flexural capacity may be limited by yielding of the flexural reinforcement and/or rupture of the concrete compression block. Rupture of the concrete prior to yielding occurs in overreinforced sections and typically results in sudden, brittle failures. These types of failures are undesirable by their very nature and can be prevented through proper flexural design procedures.

Ideally the flexural capacity the radial strip is attained through yielding of the flexural reinforcement. Excluding strain hardening of the reinforcement, any further flexural support afforded to the radial strip must be developed through torsional shears and moments on the strip faces. The ability of the system to provide flexural support through torsion will be limited by both yielding of the reinforcement outside the strip as well as the ductility of the connection.

3.4.3 Limitations on Torsional Shear and Moment

If it is now assumed that the negative and positive flexural capacities of the strip have been reached but the punching resistance has not, it may be concluded that additional flexural support is being provided to the strip through the development of torsion on the strip faces. This conclusion is drawn by considering Equations 3.8 and 3.10. Equation 3.10 requires that additional capacity must be accompanied by either an increase in the shear

intensity w or the flexural capacity of the strip, M_s . An increase in the shear intensity w however would result in a decreasing loaded length l by virtue of Equation 3.8. Since this is not consistent with test observations which show progressive yielding of the radial strip steel away from the column it may be concluded that the flexural resistance of the radial strip is being augmented through the development of torsions.

Considering now the geometry and statics of the radial arch the following equations are derived:

$$\tan \theta \sim 2d/l$$

$$P_r = C \tan \theta \quad \text{where:}$$

θ = effective angle of compressive arch at column face

C = horizontal component of compressive arch

These equations imply that if the loaded length l is increasing the effective angle of the arch must be decreasing and the horizontal component of the compressive arch must be increasing.

Considering the compressive arch shown in Figure 3.5 it is apparent that additional load and deformation will require that:

1. The effective angle of the arch, α , must decrease.
2. The effective point at which the arch is tied to the top reinforcement (Point B) will propagate further away from the column due to progressive yielding.
3. The vertical distance of Point B relative to Point A (entry point of compressive arch into column) will decrease due to rigid body rotation of the radial strip.

The implication of these requirements is that all reduce the effectiveness and efficiency of the arch, both geometrically as well as mechanically while at the same time demanding more of it.

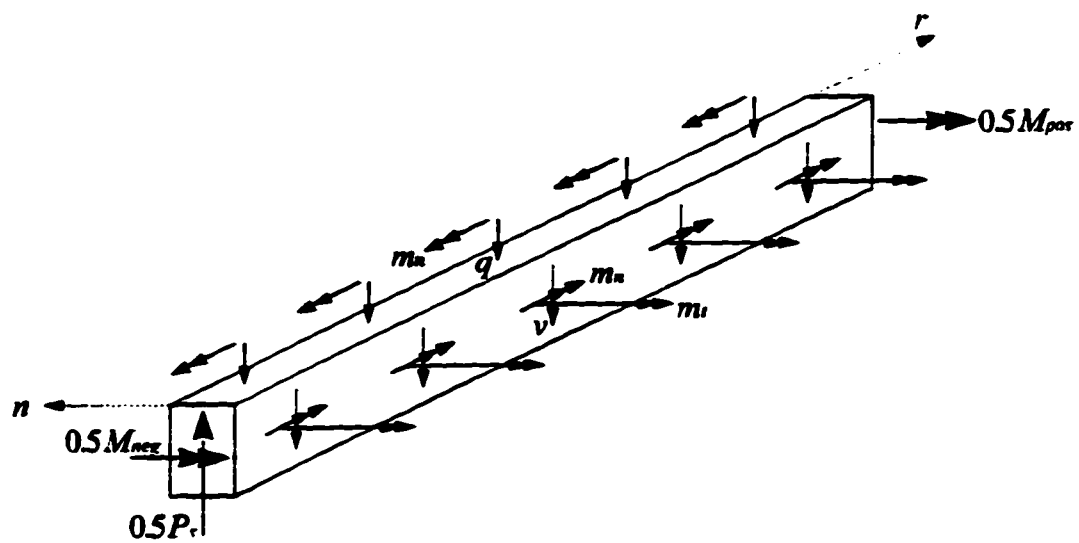
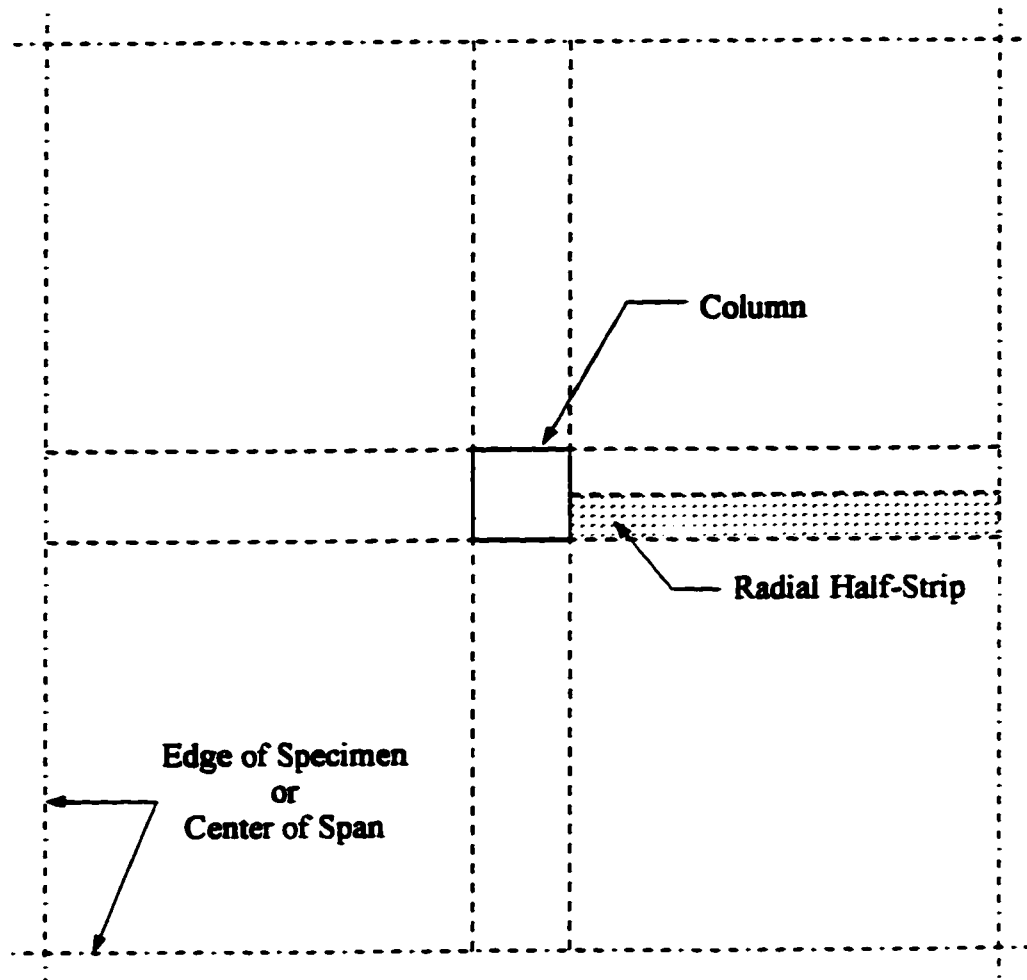


Figure 3.1 Isolated Radial Half-Strip

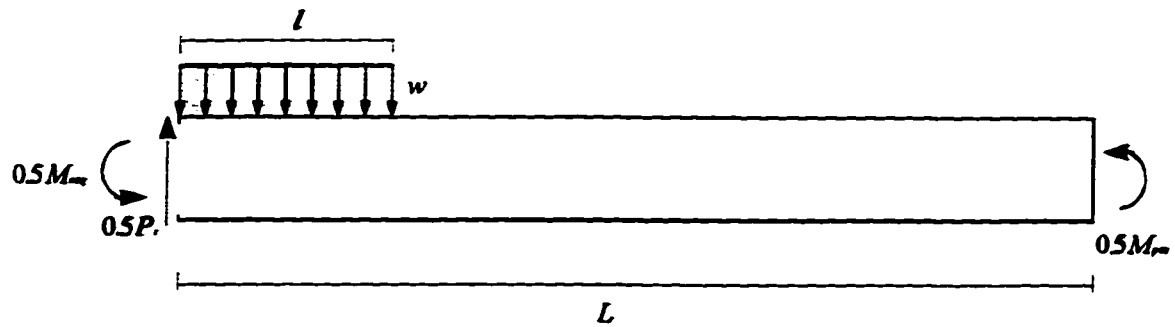


Figure 3.2 Optimized Loading of Radial Half-Strip

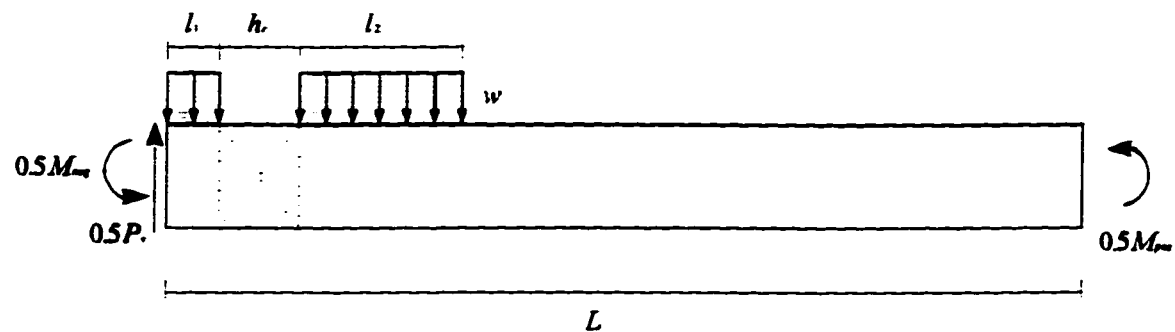
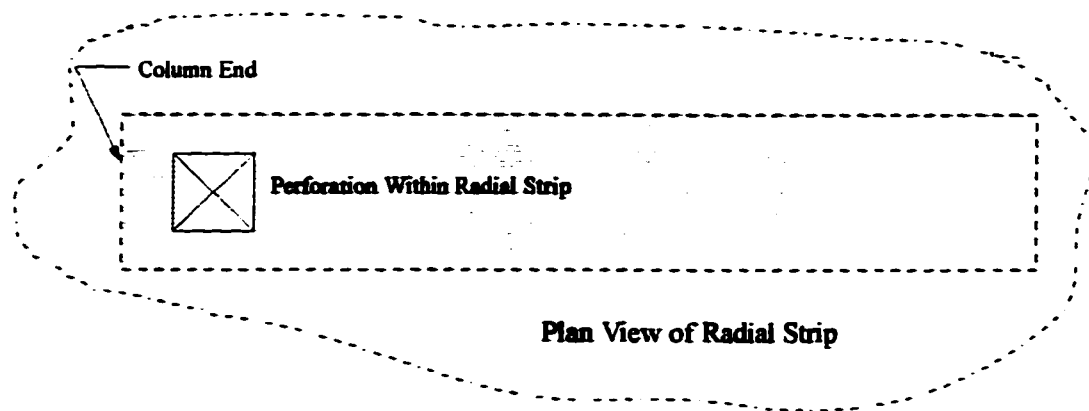


Figure 3.3 Optimized Loading of Radial Half-Strip with Perforation in Strip

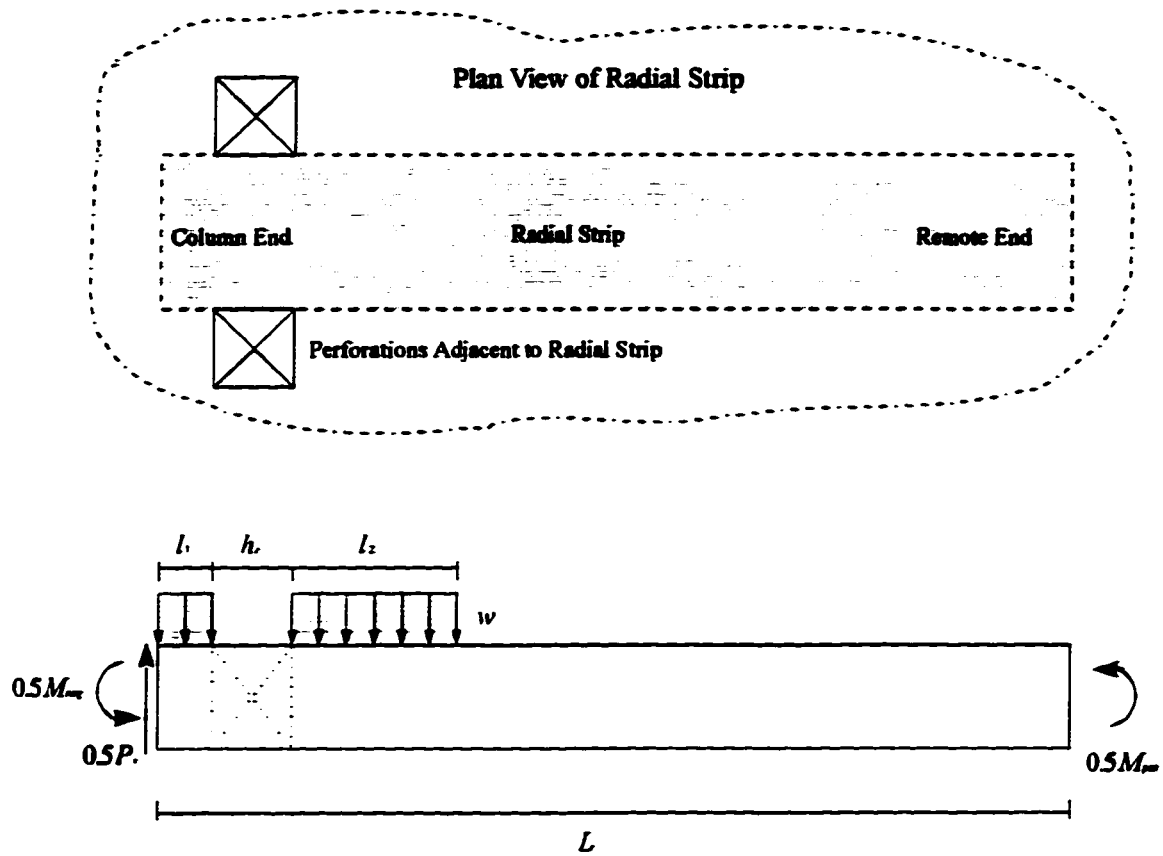


Figure 3.4 Optimized Loading of Radial Half-Strip with Perforations Adjacent to Strip

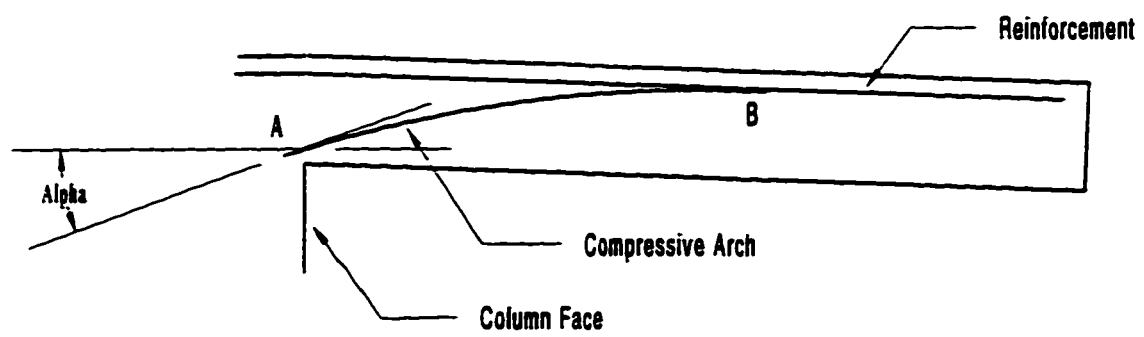


Figure 3.5 Deformed Geometry of Radial Strip

4. DESCRIPTION OF SPECIMENS AND TEST PROCEDURES

4.1 Description of Test Specimens

The testing program consisted of six specimens designed to represent the typical geometry of an interior column-flat plate connection. The plates were all 2100mm square with 250x250x300mm deep monolithic column stubs at the center of the plates. The slabs all had a configuration of perforations placed around the column with the exception of specimens #1-SS and #4-SS which were solid. The testing was conducted in two stages, each consisting of three specimens, as it was felt that analysis of the first stage specimens would yield information which would be suggestive for the remaining specimens.

The first three specimens consisted of Specimen #1-SS, a solid slab, and Specimens #2-4F and #3-4C each of which had four 125x125mm holes placed at the column faces and column corners respectively. The top mat for each of these specimens was identical consisting of #15M bars spaced at 190mm except for the outside bar on each side which was spaced at 95mm. The nominal flexural depth of the top mat reinforcement was 115mm. All of the top mat bars had 180 degree hooks at either end to prevent anchorage failure of these bars.

The remaining three specimens consisted of Specimens #4-SS, #5-4C, and #6-4F. Specimen #4-SS was cast to provide a solid slab with a concrete strength similar to the remaining specimens as the concrete mix was altered after the casting of specimen #1-SS. Specimens #5-4C and #6-4F had four hole patterns placed on the column corners and faces respectively. These two specimens differed in that they had an increased reinforcement within the radial strip. All six of the test specimens had column

reinforcement consisting of 4 #10M bars. Details of the reinforcement layouts and perforation patterns are illustrated in Figures 4.1 through 4.4.

4.1.1 Reinforcement

All specimens except #6-4F were reinforced with a top mat of #15M and a bottom mat of #10M deformed reinforcing bars. Specimen #6-4F also contained 4 #20M bars in the top mat. Tensile strength tests were conducted on random samples of the #15M bars and #20M bars which have nominal areas of 200 and 300mm² respectively. The bars had a minimum specified yield strength of 400 MPa. All steel used in the testing was from the same shipment and no significant differences were noted in the testing of the random samples. Based on the nominal areas of the reinforcement the #15M bars had a yield strength of 400 MPa and a modulus of elasticity of 183000 MPa. The #20M bars had a yield strength of 407 MPa and a modulus of elasticity of 189000 MPa. Typical stress strain curves for both the 15M and 20M bars are shown in Figure 4.6.

4.1.2 Concrete

A high strength concrete mixed in the lab was utilized for each of the six specimens. The mixing was done in a 7 cubic foot pan-type batch mixer and each specimen casting required four batches. The mix had a water to cement ratio of 0.33 and naphthalene sulphanate superplasticizer was added at a rate of 8.8 liters per cubic meter. The estimated 28 day strength of the concrete was 70 MPa.

The concrete for the first specimen exhibited poor workability and significant bleeding during placement and therefor the mix was altered slightly for the remaining specimens. Silica fume was added to the mix at a rate of 7% (by weight) of cementitious

material. In addition the superplasticizer dose was increased to 9.6 liters per cubic meter. These changes were successful in both improving workability and reducing bleedwater, but led to a significant increase in compressive strength.

A total of twelve compression cylinders, three from each batch, were cast for each specimen. The cylinders were nominally 100mm in diameter and 200mm in length. The cylinders were air cured alongside their associated specimen and were all tested the same day as the test specimen. The compressive strength of the concrete for each test specimen was calculated by averaging the average compressive strength of each of the four batches. Results of these tests are included in Table 4.1.

4.1.3 Fabrication of Specimens

All test specimens were cast upside down resulting in several benefits. First, having the heavier structural mat on short chairs near the forms allowed for much better control of the clear cover and spacing. In addition it allowed the strain gauge lead wires to exit through the forms, interfering with the concrete as little as possible and leaving the screeded surface uninterrupted. Lastly it allowed for the use of an independent column stub form to which the perforation blockouts were attached.

As mentioned each specimen required four batches to complete. Batches were placed in each of the four quadrants as they were mixed. After placement the concrete was mechanically vibrated and hand finished. After casting the specimens were covered with polythene and allowed to cure for approximately one week. Casting of each specimen took approximately 1.5 hours to complete.

4.2 Test Setup and Instrumentation

4.2.1 Test Apparatus

The test apparatus was identical for all specimens. The central load was applied to the column stub with a 200 kip ram controlled by a manual hydraulic pump. A spherical seat assembly was placed between the jack and column stub to allow for slight seating rotations of the stub. The central load was reacted against eight 19mm tie rods connected to the laboratory strong floor through a hollow structural steel frame. Details of the test setup are illustrated in Figure 4.7.

4.2.2 Strain Measurements

The strain gauge layout was also similar for each of the six test specimens. A total of 48 gauges were placed on 16 different bars which included both column bars(bars passing through the column) and perimeter bars(bars outside of the column). Specimen #4-SS had an additional 12 gauges placed on the four outermost bars. Specimen #5-4C had an additional two gauges placed on the two additional bars passing through the column. Gauges on the column bars were placed at the column faces in order to estimate the negative moment in the radial strip at this location. Gauges were placed on perimeter bars in order to estimate the shear transfer on the side faces of the radial strips through the use of measured force gradients.

Neglecting differences between the outer and inner layers of steel the 48(60) gauges represented a total of twelve(fifteen) distinct locations within the slab. This allowed an average of up to four gauges to be used to determine the bar force at any one

of these locations resulting in more reliable data. In general gauge performance was good with at least 85 percent of the gauges remaining functional for the duration of the tests.

All gauges were attached to the bars with the use of an epoxy adhesive. Following connection of the lead wires the gauges were covered with a thin layer of rubber cement, a protective wrap of electrical tape and a layer of silicone sealant. Protection of the gauges was kept to as small an area as possible to minimize the effects on bond. All gauges used had a nominal resistance of 120 ohms and gauge length of 5mm. Details of gauge layouts for all test specimens are contained in Figure 4.5.

4.2.3 Linear Variable Differential Transformers(LVDT's)

A total of five 15 Volt LVDT's were used for each specimen to measure deflection. A single LVDT was placed at the centerline of each side of the specimen and the fifth measured deflection of the column stub. The net specimen deflection could then be calculated by subtracting the average deflection of the four edges from the center deflection.

4.2.4 Load Cells

To monitor the total vertical load acting through the column a single load cell was placed beneath the column stub. As a vertical equilibrium check a full bridge arrangement of gauges was applied to each tie rod thereby allowing each individual rod to also act as a load cell. All load cells were calibrated prior to testing.

4.3 Test Procedure

Prior to testing all specimens were initially centered and leveled using an adjustable three point support scheme. After positioning was complete the tie rods were put in place

and the load transferred from the three points to the column stub by extending the jack. This allowed the specimen weight to be determined prior to testing. At this point a preload of approximately 10 to 15% of the predicted failure load was applied and the tie rods were balanced by adjusting the fastening nuts at the top end of the rods. The preload was then removed and testing commenced.

During testing, load was typically applied in 15 to 20 kN increments. The specimen was allowed to relax for approximately 30 seconds and measurements were recorded. Testing of each specimen took approximately 2 hours to complete.

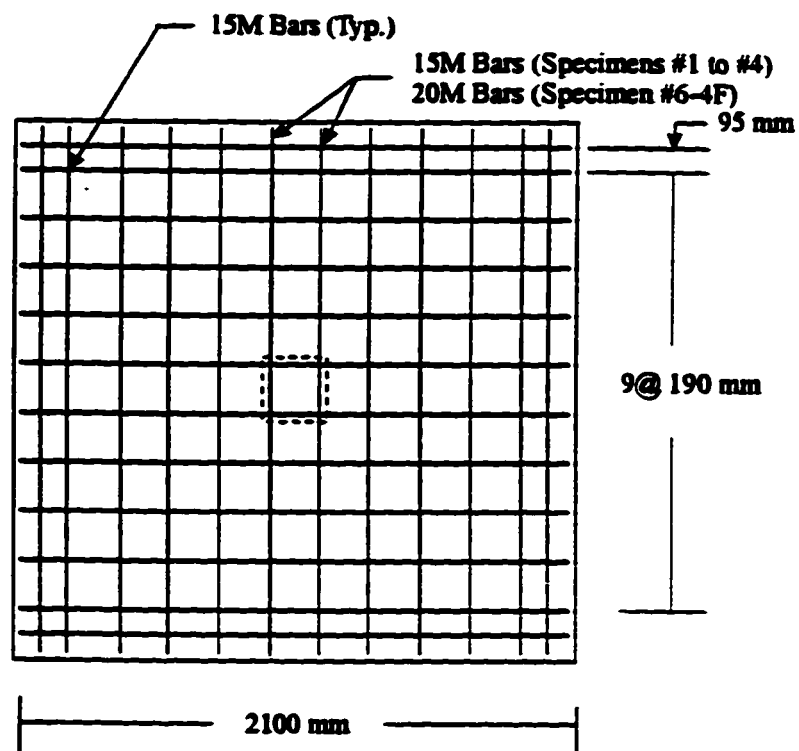


Figure 4.1 Typical Top Mat Reinforcement Layout

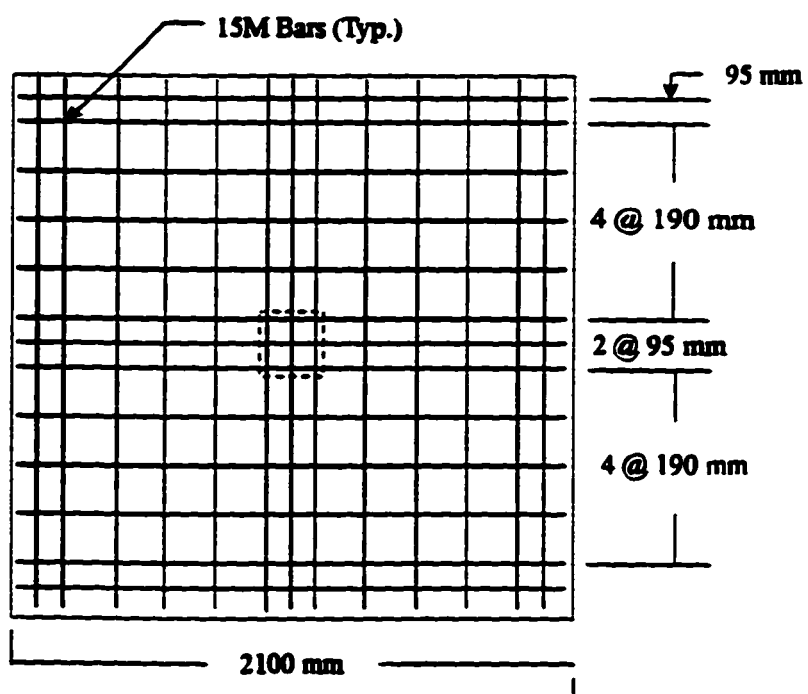


Figure 4.2 Top Mat Reinforcement Layout for Specimen #5-4C

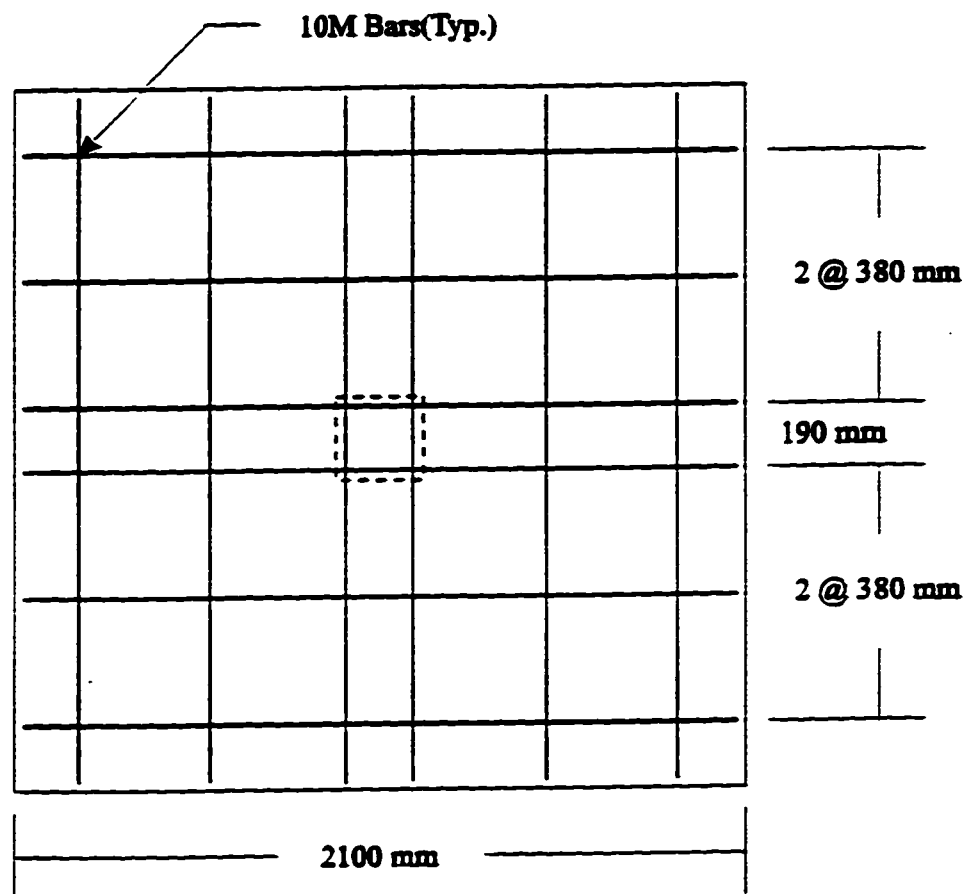


Figure 4.3 Typical Bottom Mat Reinforcement Layout

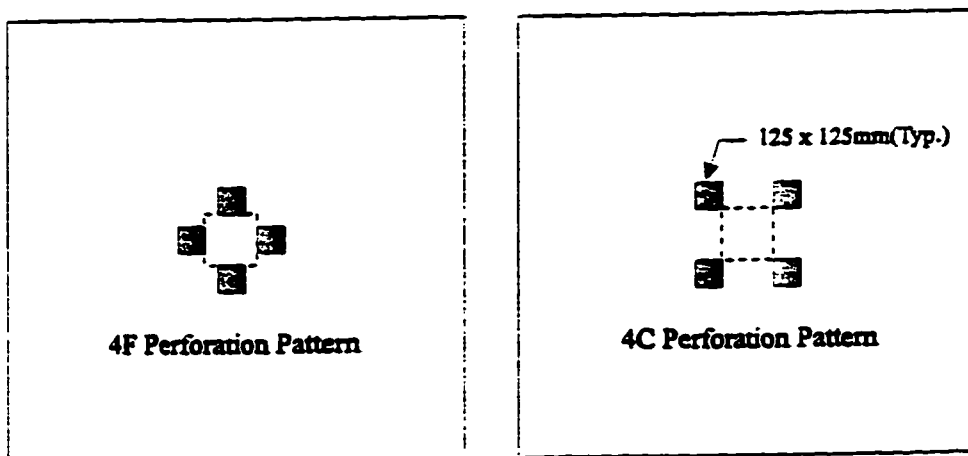


Figure 4.4 Test Specimen Perforation Patterns

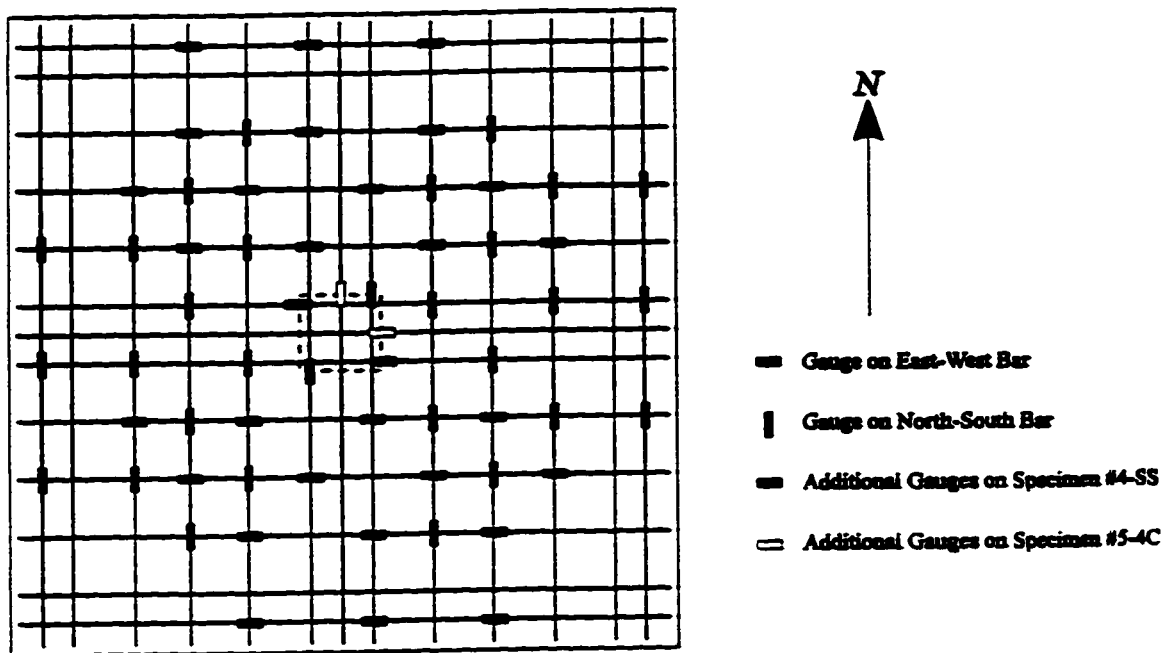


Figure 4.5 Strain Gauge Layout for Test Specimens

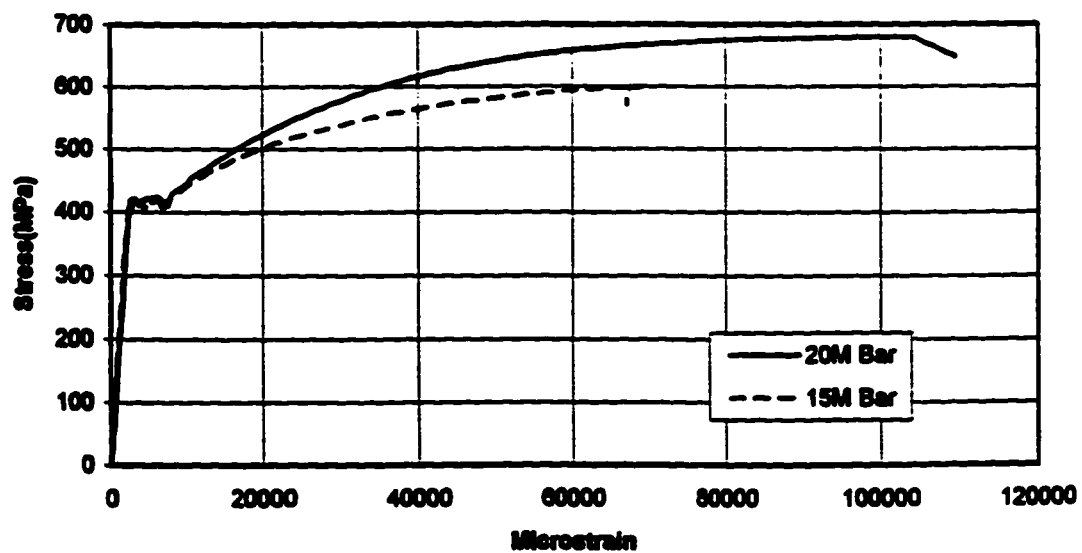


Figure 4.6 Typical Stress-Strain Curves for 15M and 20M Reinforcing Bars

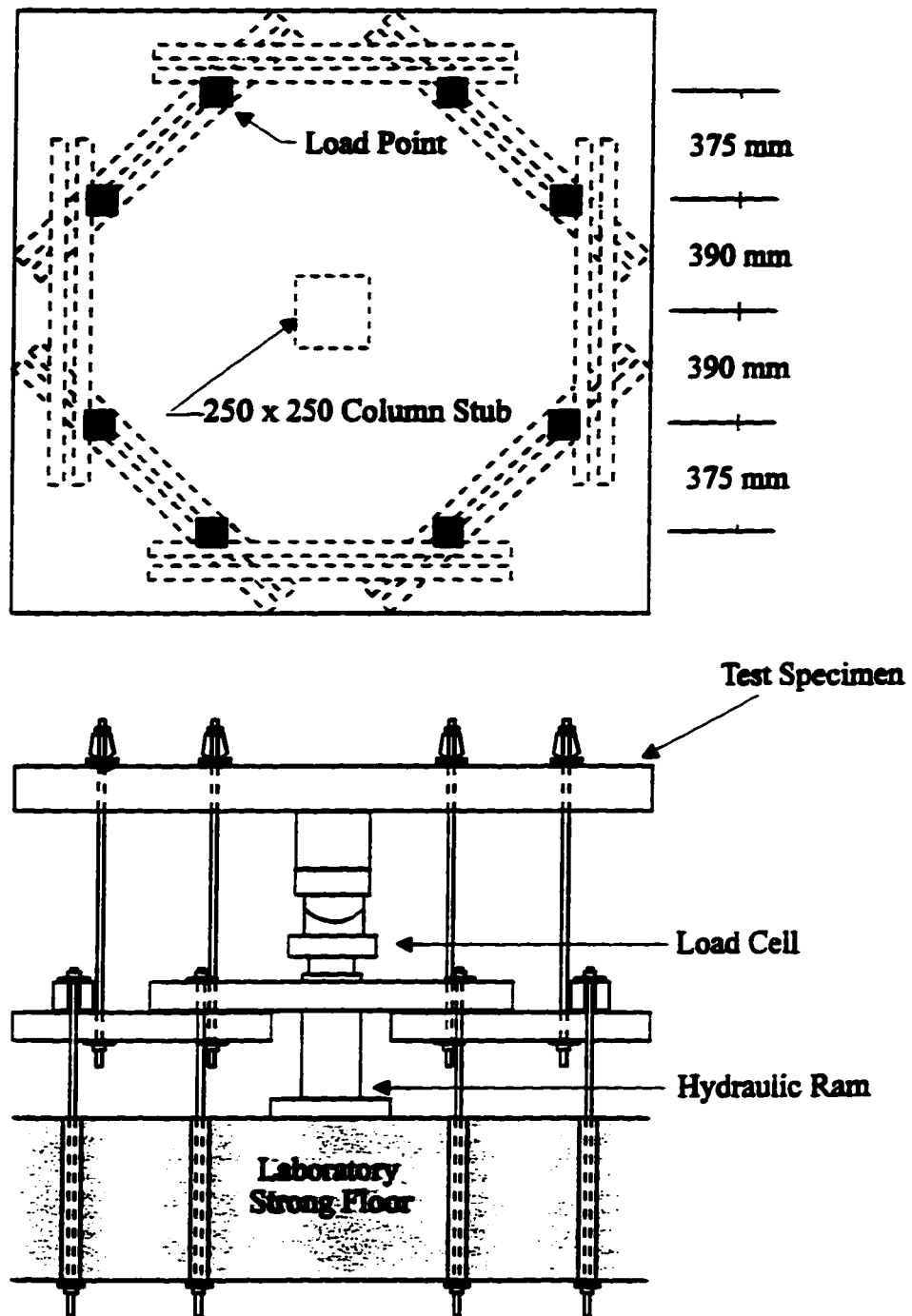


Figure 4.7 Standard Test Setup

Specimen #	f_c (MPa)	15M Bars		20M Bars		t (mm)	d (mm)
		f_y (MPa)	E_s (MPa)	f_y (MPa)	E_s (MPa)		
1-SS	78	400	183000	N/A	N/A	156	116
2-4F	96	400	183000	N/A	N/A	157	117
3-4C	93	400	183000	N/A	N/A	156	116
4-SS	101	400	183000	N/A	N/A	156	116
5-4C	99	400	183000	N/A	N/A	156	116
6-4F	94	400	183000	407	187000	157	117

Table 4.1 Description of Test Specimens

5. ANALYSIS OF TEST SPECIMENS

5.1 Strain Measurements

Each of the six test specimens had a series of strain gauges placed on reinforcing bars within the slab. With the exception of Specimens #4-SS and #5-4C the specimens had a total of forty-eight gauges placed at twelve distinct locations within the slab. These twelve locations, as illustrated in Figure 5.1, include the column bars at the column face, four locations on each of perimeter bars P1 and P2, and three locations on perimeter bar P3. Specimen #4-SS had an additional twelve gauges at three distinct locations on perimeter bar P5. Specimen #5-4C had an additional two gauges located on the centerline column bars at the column face.

Except where gauges were nonfunctional and on the centerline column bars of Specimen #5-4C an average of four strain measurements were utilized to produce a single bar force measurement at each distinct location. This was accomplished by first converting each strain measurement to a bar force using the results of coupon tests conducted on samples of the reinforcing steel. An average was then calculated from the bar forces measured at corresponding locations. Due to nonfunctional gauges an average of only three gauges were utilized to produce bar force measurements at six locations within Specimen #1-SS and at two locations within Specimen #2-4F. By using an average of multiple gauges any single bar force measurement at a distinct location is considered reproducible.

5.1.1 Primary Shear Calculations

5.1.1.1 Beam Action Shear

To evaluate how load is being carried in the test specimens it is necessary to make estimates of the shear forces developed on the side faces of the radial strip. Based on the average bar force at each location, force gradients in the reinforcement may be calculated for each gauged bar. Recalling that beam action shear is a result of force gradient in the reinforcing bars, and assuming that beam action shear dominates, an estimate of the shear contribution of each gauged perimeter bar, V_{bar} can be made using the following approximation.

$$V = \frac{dM}{dx} = \frac{d(T)}{dx} jd + \frac{d(jd)}{dx} T \approx \frac{d(T)}{dx} jd$$
$$V_{bar} = \frac{T_1 - T_2}{s} jd_1 \quad [5.1]$$

$$\text{where} \quad jd_1 = d - \frac{A_{bar} f_y}{2\alpha_1 f_c' b} \quad [5.2]$$

$$\text{and} \quad \alpha_1 = 0.85 - 0.0015 f_c'$$

The tensile forces T_1 and T_2 are the bar forces at sections 1 and 2 respectively as illustrated in Figure 5.1. The term s is the distance between the two sections. The width b is the associated width over which the individual bar acts.

5.1.1.2 Arching Action Shear

In addition to beam action shear, it is possible that shear is transferred to the radial strip through limited arching action near the radial strip face. This mechanism of shear

transfer is typically a result of progressive yielding which diminishes the capacity to develop beam action shear at the face of the radial strip. Owing to this, estimates of V_{bar} are made assuming arching action occurs over a specified interval.

The first estimate is made under the assumption that all shear in the second interval, between sections 2 and 3, is carried by beam action and a combination of beam and arching action occurs between sections 1 and 2. From these assumptions the following equations are derived.

$$V_{bar1} = \frac{M_1 - M_2}{s} = \frac{T_1 j d_1 - T_2 j d_2}{s} \quad [5.3]$$

$$V_{bar2} = \frac{T_2 - T_3}{s} j d_2 \quad [5.4]$$

If it is now assumed that V_{bar1} is equal to V_{bar2} then Equation 5.4 may be solved for $j d_2$ and substituted in Equation 5.3. This substitution results in:

$$V_{bar} = \frac{T_2 - T_3}{s} j d_1 \times \frac{T_1}{2T_2 - T_3} \quad [5.5]$$

A second estimate of arching action shear can similarly be made assuming that all shear is carried by beam action between sections 3 and 4 and arching occurs between sections 1 and 3. Utilizing the derivation of Equation 5.5 the equations may be written as below.

$$V_{bar1} = \frac{M_1 - M_2}{s} = \frac{T_1 j d_1 - T_2 j d_2}{s} \quad [5.6]$$

$$V_{bar2} = \frac{T_3 - T_4}{s} j d_2 \times \frac{T_2}{2T_3 - T_4} \quad [5.7]$$

Assuming that V_{bar1} is equal to V_{bar2} solving for jd_2 and substituting in Equation 5.7 results in:

$$V_{bar} = \frac{T_1}{s} jd_1 \times \frac{T_3 - T_4}{3T_3 - 2T_4} \quad [5.8]$$

This calculation requires strain measurements at a fourth distinct location along the bar.

As a result this calculation may only be conducted for perimeter bars P1 and P2.

5.1.2 Moment at Column Face of Radial Strips

Strain measurements of the reinforcing bars passing through the column are used to estimate of the total tensile force available for flexural resistance. Assuming a fully cracked section the resisting moment of the radial strips at the column face is computed as:

$$M_{neg} = A_{Tcol} \frac{\epsilon}{\epsilon_y} f_y \times \left(d - \frac{A_{Tcol} \frac{\epsilon}{\epsilon_y} f_y}{1.7 f_c' c_{eff}} \right) \quad [5.9]$$

where the ratio of strain to yield strain is constrained to be less than or equal to one.

5.2 Equilibrium of Radial Strip

5.2.1 Vertical Equilibrium

With estimates of the shear forces delivered to a side face of a radial strip for each of the gauged perimeter bars, vertical equilibrium of the radial strip is utilized to determine the total shear contributions of the ungauged perimeter bars and torsional shears. The ungauged perimeter bars typically included bars P4 and P5 except for Specimen #4-SS in which only perimeter bar P4 was ungauged.

Considering that each test specimen has four radial strips and that each radial strip has two faces the summation of shears along a single side face should equal one-eighth the total load being carried by the slab for any given load step. This relationship provides a method for estimating the shear contributions of the ungauged bars and torsional shear by subtracting the sum of the calculated shears for each of the gauged bars from one eighth of the total load for any given load step

5.2.2 Rotational Equilibrium

With estimates of the shear contribution of all perimeter bars as well as the negative moment at the column face it is possible to backcalculate the contribution of torsion by considering the rotational equilibrium of the strip. Rearrangement of Equation 3.7 yields:

$$M_t = \frac{1}{4}[(2 \times \int v_p r dr) - M_s] \quad [5.10]$$

The integration of primary shear over the total length of the radial strip is estimated by summing the individual contributions of each perimeter bar. This may be written as:

$$\int v_p r dr \approx \sum_{i=1}^s V_{bar(i)} r_{(i)}$$

where $r_{(i)}$ is the radial distance from the column face to the corresponding perimeter bar.

By using this approximation and considering the total flexural support afforded to the radial strip, M_s , is equal to M_{neg} as calculated in Equation 5.9 estimates of the torsional requirements of the strip may be computed as:

$$M_t = \frac{1}{4}[(\sum_{i=1}^5 V_{bar(i)} r_{(i)}) - M_{neg}] \quad [5.11]$$

5.3 Comments on Analysis

5.3.1 Shear Calculations

Except on the column bars strain gauges were placed at the intersections of orthogonal bars. This was done intentionally in efforts to measure strains in the reinforcement at locations where cracking is likely to occur. By doing so slight nuances in force gradient measurements which may occur as a result of in and out bond are eliminated. Additionally the analysis is conducted under the assumption that the plate is fully cracked and therefor is not valid prior to reaching this state.

The analysis has several limitations inherent in its development. The development of torsions in the plate imposes a requirement for additional forces in the top mat reinforcement. Since there is no method to separate the torsion requirements from the shear requirements a gradient in the torsions orthogonal to the radial strip will introduce additional error into the shear computations.

It would be anticipated that force gradients in the reinforcement resulting from torsion would likely be in opposition to the force gradients generating shear at the radial strip face. This seems likely since the gauges at Section 1 are very close to the centerline of the radial strip which, by symmetry, is a line of zero torsion. If this is indeed the case then the analysis would tend to underestimate the shear forces developed along the strip face. This type of error is illustrated in Figure 5.2

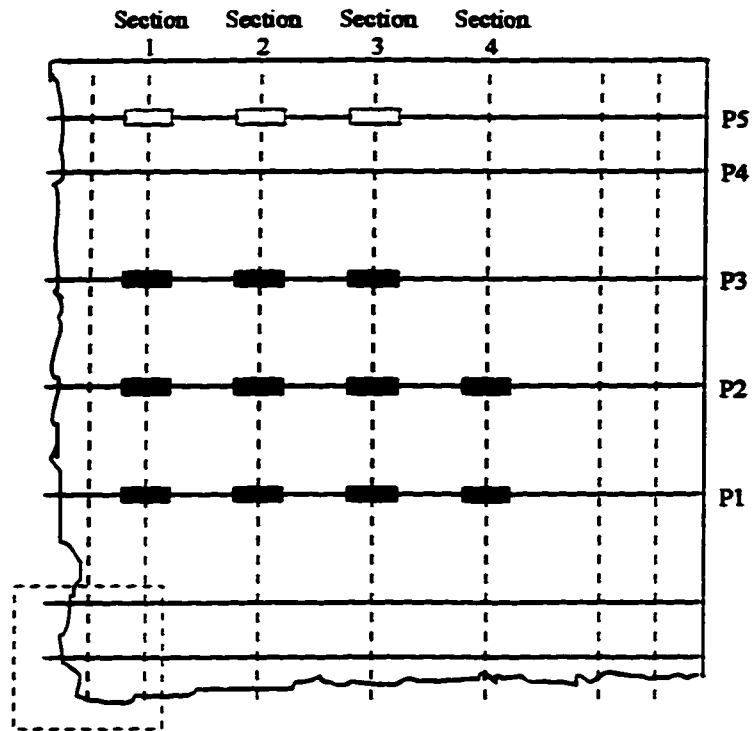


Figure 5.1 Gauge Locations for Analysis of Specimens

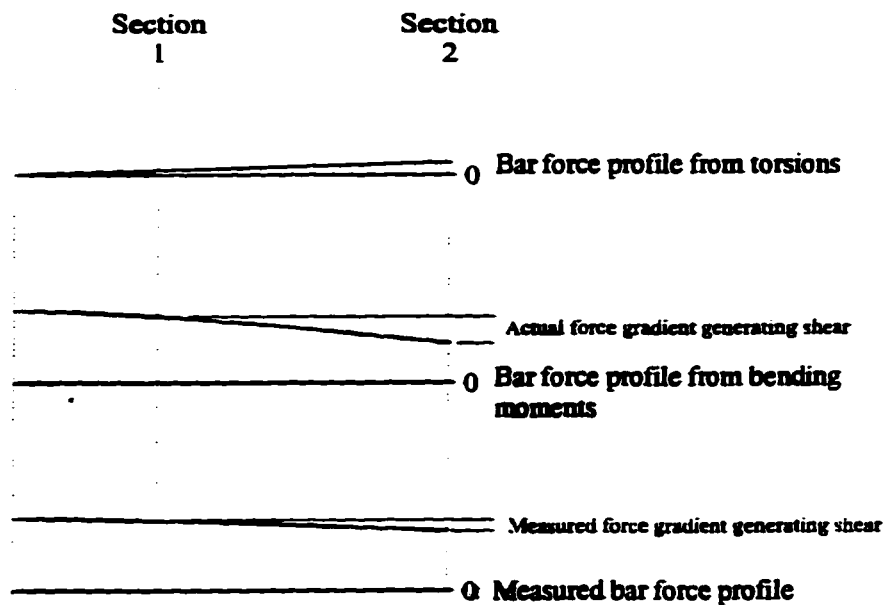


Figure 5.2 Influence of Torsions on Measured Force Gradients

6. OBSERVATIONS AND EVALUATION

6.1 Load-Deflection Behavior

Load-deflection diagrams for all test specimens are shown in Figures 6.1 through 6.4. Generally speaking the load -deflection response can be divided into three stages of behavior. Initially, as shown in the figures, the test specimens exhibited a similar linear behavior up to a load of approximately 100 to 125 kN. This first stage corresponds to the uncracked elastic behavior of the plates.

Cracking of the slab occurred at a deflection of about 1.5 mm and was accompanied by a significant loss in stiffness. From initial cracking up to a deflection of approximately 13 to 15 millimeters the slabs exhibited a gradual loss of stiffness. The slight loss of stiffness through this stage is consistent with progressive cracking throughout the slab and localized yielding of the reinforcement in the column region. All of the test specimens with perforations failed in this stage after full cracking of the slab but prior to extensive yielding of the reinforcement.

The two solid specimens entered a third stage of behavior at a deflection of approximately fifteen millimeters. This stage is marked by a continuing loss of stiffness associated with progressive yielding of the reinforcement and the development of a folding mechanism within the plate. During this stage the specimens undergo increasing deformations with relatively small increases in load. Based on a yield line analysis the flexural capacities of the plates correspond to a load of approximately 420 kN. This load is consistent with entry into the third stage of behavior. At failure the solid specimens had exceeded the calculated flexural capacity by nearly 20 percent. Exceedance of the flexural

capacity in this order is common in the literature and is often attributed to membrane action and second order effects(Long, 1975).

From Figure 6.1 it can be seen that the presence of perforations on the column faces did not have a detrimental effect on the stiffness of the plates. In fact both Specimen #2-4F and #6-4F exhibited a slightly stiffer load deflection behavior than the solid specimens. Specimen #3-4C, with perforations at the column corners, exhibited a slight loss of stiffness, in comparison to the solid specimens, at a deflection of approximately eight millimeters. The increased reinforcement through the column of Specimen #5-4C had a noticeable influence on the stiffness as illustrated in Figure 6.4. The increased reinforcement, however did not have a similar influence on the specimens with perforations at the column faces, as shown in Figure 6.3.

6.2 Shear Transfer to the Radial Strip

Figures 6.5 through 6.10 show the results of the analysis of shear transfer to the radial strip. The figures detail the calculated shears of all gauged perimeter bars as well as the shear required from both the ungauged perimeter bars and torsion to satisfy equilibrium. Except for Specimen #4-SS, where only perimeter bar P4 was ungauged, the figures illustrate one half of the combined shear requirements of bars P4 and P5 as well as the torsional shear contribution ($m_t(0)$).

The shear contribution of each individual bar V_{bar} was calculated assuming that shear development was generated either through beam action or by a combination of beam and arching action. In all cases, at each load step, the maximum shear calculated was

attributed to each of the gauged bars. For each of these bars the transition point, where the combined action became dominant over beam action alone, is marked by a black circle.

As a second method of evaluation of shear transfer to the radial strip, a comparison of the shears from all gauged perimeter bars to the total load being carried is made. By summing the shears from each gauged bar and dividing by one-eighth of the total load, the percentage of load which may be accounted for by the gauged bars is determined. These comparisons are shown graphically in Figures 6.11 through 6.13.

When considering these figures it should be noted that the calculation of shear forces is made under the assumption of a fully cracked section. As a result, the analysis is not valid unless the specimens are fully cracked. Based on strain measurements of perimeter bar P3 this does not occur until a deflection of approximately 2.5 to 3 millimeters.

6.2.1 Solid Slab Specimens

What is noted immediately when examining the perimeter bar shears in Figures 6.5 and 6.6, and indeed for all of the test specimens, is that arching action contributes early to shear development on the radial strip. This result is not surprising for two reasons. Firstly, accepting that shear transfer to the column from the radial strip is the result of radial arching within the strip, it does not seem unreasonable, considering requirements of strain compatibility, that arching is occurring outside the strip, particularly in areas near the column. Secondly, the progression of yielding ultimately leads to the inability to generate beam action shear and therefor must be accompanied by a loss in ability to generate shear or the engagement of other load carrying mechanisms.

Examination of the calculated shears for Specimens #1-SS and #4-SS suggest a relatively uniform distribution of shear along the total length of the radial strip at failure. Specimen #4-SS however required a significantly higher shear from the ungauged perimeter bar P4 than the shears calculated for the gauged bars. Clearly this does not seem reasonable and suggests that: (1) the analysis is underestimating the shears developed by the gauged bars, (2) torsion is playing an increasing role in shear development, or (3) load is being transferred through other mechanisms.

The first explanation is quite possible for several reasons. Firstly, the governing shears for perimeter bars P1 and P2 during the latter stages of the test were calculated with Equation 5.8, which requires arching between sections 1 and 3. Recalling that this calculation was not possible for perimeter bar P3 and considering the shear calculated for perimeter bar P3 is significantly less than those calculated for bars P2 and P5, on either side of P3, it seems quite likely that the analysis is underestimating the shear contribution of this bar.

It seems unlikely that during the latter stages of the test that torsion is providing the means for increasing shear development. At this stage yielding of the reinforcement has occurred in the column vicinity and is radiating outward. As a result of the progressive yielding the ability to generate additional torsional shears is diminished.

Alternatively there may be some limited strutting of load directly from the load points to the column. In either case, however, the results for this specimen during the latter stages of the test are seen as questionable and therefor further analysis of Specimen #4-SS, in terms of torsional requirements, include adjustments to account for this. The

adjustments are made assuming a uniform distribution of shear over the entire length of the radial strip (i.e.: the total load carried is distributed equally and uniformly to each of the eight strip faces).

6.2.2 Specimens with Perforations

Figure 6.12 reveals similar behavior of the two test specimens with perforations on the column faces. The figure shows that for both specimens the first three perimeter bars accounted for approximately 70 to 85 percent of the total load being carried up until failure of the specimens. For specimens #3-4C and #5-4C the first three perimeter bars accounted for approximately 80 to 85 percent of the total load. This required only relatively modest shears in the outer two perimeter bars to satisfy equilibrium as illustrated in Figures 6.7 and 6.10.

Some differences are noted however in the perimeter bar shears developed in specimens #2-4F and #6-4F. While Specimen #6-4F appears to have a more even distribution among the first three perimeter bars, the first perimeter bar of Specimen #2-4F developed a significantly higher shear than perimeter bars P2 and P3. Even more interesting is that similar differences are noted between Specimens #3-4C and #5-4C. These similarities would tend to suggest that the increased reinforcement within the radial strips of Specimens #5-4C and #6-4F is enabling more efficient development of shear away from the column.

6.3 Development of Yield Moment at Column Face

Figure 6.14 shows the development of negative moment with progressive loading. Except for specimens #6-4F and #1-SS the development of negative moment is quite

consistent, with each specimen reaching the flexural capacity of the radial strip prior to failure. Specimen #6-4F reached approximately 90 percent of the flexural capacity with three of the four column bars reaching yield prior to failure.

Specimen #1-SS appears to exhibit a delayed development of negative moment at the column face. This anomaly is considered suspect for two reasons. The first reason is that it is the only specimen to exhibit such behavior. Secondly it is the only specimen in which the strain measurements indicate yielding of perimeter bar P1 prior to yielding in the column bars. Possible causes may include partial delamination of one or more of the gauges used in the average.

Neglecting Specimen #1-SS, yielding of the column steel for specimens having two #15M bars within the radial strip occurred at a load of approximately 300 to 320 kN. Yielding of the column steel for Specimens #5-4C and #6-4F, which contained increased reinforcement in the radial strip, occurred at a load of about 420 kN.

6.4 Development of Torsion

Figures 6.15 to 6.17 show the torsional requirements of the test specimens with increasing load. The figures reveal consistent behavior in the development of torsional moments. As the specimen becomes fully cracked the torsional requirements are quite modest, typically in the order of one to two kN-m. As loading continues the torsional moments steadily increase up until failure of the specimen.

At comparable load levels, the solid specimens developed higher torsional moments than specimens which had perforations placed near the column. Comparison of specimens with perforations at the column faces with specimens with perforations at the

column corners reveals that perforations at the column corners have a more significant influence on the ability to develop torsional moments along the side faces of the radial strips. This is not surprising considering the following factors. Firstly, for specimens with perforations at the column corners, the boundary conditions do not permit any torsion to be developed on the side faces of the radial strip over the length of the strip parallel and adjacent to the perforations. Additionally these perforations will enforce one way behavior in the length of radial strip adjacent to the perforations and perhaps slightly beyond. Since torsion is developed by two way behavior of the plate these perforations may dramatically reduce the ability to generate torsion.

As illustrated in Figure 6.16 the torsional requirements of Specimen #2-4F were consistently higher than that of Specimen #6-4F. This is primarily explained by the increased flexural capacity of the radial strips in Specimen #6-4F. What is more interesting however is that these two specimens failed at nearly identical loads. This fact may be suggestive of the mechanisms that led to the failure of these two specimens.

It would be anticipated that the torsional capacity of these two specimens would be similar and yet at ultimate load the torsional moments generated by Specimen #6-4F were roughly only 55 percent of those developed by Specimen #2-4F. This tends to suggest that Specimen #6-4F did not fail due to an inability to provide rotational support to the radial strips but by some other mechanism.

An analysis of the negative flexural capacity of the radial strips of these two specimens reveals important differences. Because of the increased reinforcement and the reduced effective width of the radial strip in Specimen #6-4F the depth of the concrete

compression block at first yield is increased by approximately 55 percent compared to Specimen #2-4F. As a result, at similar strains in the reinforcement, the concrete strains in Specimen #6-4F will be substantially higher. In addition, after yielding of the column steel, the horizontal component of the compression arch is substantially greater. Therefore, at similar load levels the compressive force carried by the arch will also be considerably larger. Based on the measured strains in the column steel it seems unlikely that crushing of the concrete in compressive arch solely from flexure led to the failure of Specimen #6-4F. It could be possible however that the combined effects of both flexure and torsion reached a limiting stress in the concrete.

Another possible failure mechanism is a limitation on the ratio of column width to flexural depth discussed by Alexander and Simmonds(1991). This limitation occurs as result of vertical tensile stresses that must be generated when shear forces developed on the side faces of the radial strip enter below the compressive arch within the strip. Alexander and Simmonds (1991) suggest a critical value of c/d calculated for a splitting failure of this type of 0.66. This limitation was initially thought to be of no great concern since typical slabs will have ratios in excess of 1.5. However a perforation placed on the column face has the influence of reducing this ratio. It should also be noted that the critical value is calculated based on assumed relationships between the compressive and tensile strength of the concrete. Due to high variability of this relationship estimates of the critical value may be low.

For Specimens #2-4F and #6-4F the effective column width is reduced to 125 mm resulting in a c/d ratio of 1.09. If the effective column width is also reduced by the bar

diameters, where minimal tensile strength is afforded, this ratio is further reduced to about 0.78. This value is fast approaching the critical value and may suggest that failure of these specimens was initiated by a splitting failure caused by high tensile stresses near the perforations.

6.5 Comparison of Test Results to Predicted Capacities

Comparisons of predicted capacities to the test results of three independent testing programs are contained in Table 6.1. The results contained in the table include tests done by Moe(1961), Marzouk and Hussein(1991), as well as those conducted by the authors. Comparisons are made to the predicted capacities as calculated by both the bond model as well as CSA Standard CAN3-A23.3-M84.

The test results of Moe which are included in the table consist of a series of tests conducted to examine the effects of perforations on punching capacity. Marzouk and Hussein's tests were a series of tests designed to study the punching behavior of high strength concrete slabs.

6.5.1 Bond Model Predictions

The bond model predictions for the punching capacity of slab-column connections correlate well with the observed behavior. The average test to predicted ratio of the 36 tests examined is 1.25 with a standard deviation of 0.13. In all but two cases the test to predicted ratios were greater than one, consistent with a lower bound solution.

The two cases which failed prior to reaching the predicted capacities were Specimens H13 and H14 tested by Moe. Specimen H13 failed at a test to predicted ratio of 0.87 however the following explanation is offered as to why the specimen failed to

reach the predicted capacity. Firstly the specimen was simply supported along all four sides with the corners free to lift. As such the majority of load is forced to enter the slab on the central portion of each of the four edges. Secondly the specimen had a 4C perforation pattern with 10" by 10" perforations. Given the loading conditions and the geometry of the specimen the mechanism of load transfer described by the model, namely shear transfer to the side faces of the radial strip is seriously compromised. Specimen H14 failed at a test to predicted ratio of 0.96. This specimen had a reinforcement ratio of 0.77 and a test capacity to flexural capacity ratio of 1.032 consistent with the onset of the development of a folding mechanism within the plate.

The test results contain a number of specimens that exhibited ductile punching failures as folding mechanisms were developing in the plates. In general the radial strip method conservatively predicted the failure loads even for specimens failing in this manner. This however is not entirely surprising given that the model gives consideration to the flexural capacity of the radial strip. It should also be noted that these failures do not need to be predicted by a punching shear model since they are flexural failures by definition.

6.5.2 CSA Standard CAN3-A23.3-M84

The code method of estimating the punching capacity gave an average test to predicted ratio of 1.15 with a standard deviation of 0.24. As shown in Figures 6.19 and 6.21 there are several instances where the test to predicted ratio falls below unity. Figure 6.21 shows the test to predicted ratios plotted against the effective reinforcement ratio of the radial strip and tends to suggest that the CSA Standard becomes less

conservative and indeed may overestimate the punching strength as reinforcement decreases.

6.6 Comments on the Bond Model

Based on this work, as well as the work of Alexander and Simmonds(1991), the bond model appears to approach a lower bound solution for the punching strength of slab-column connections. The modifications to account for the influence of perforations near the column contained in Chapter 3 also seem to correlate well with the observed behavior. It should be cautioned however that the research conducted to date is quite limited in terms of geometry of test specimens, loading conditions, and extremes of variables. Expansion of research to study the effects of these parameters is seen as necessary to format a general design procedure. In particular three key areas are noted.

The first is the behavior of edge and corner columns. While it is readily apparent that for such columns the free edges of the radial strips are unavailable for shear transfer, the discontinuity of the slab may have a dramatic influence on the ability to develop shear and/or torsions on the interior faces. In addition such loading will introduce significant torsions about the axis of the radial strip. As a large amount of experimental work regarding the behavior of edge and corner columns already exists, the application and correlation of the bond model to such cases, at least in a preliminary manner, could be evaluated with relative ease.

Another area of concern is the influence of increasing reinforcement. While increased reinforcement within the radial strip may increase the punching strength there is likely a crossover in which ductility is compromised and beneficial effects are no longer

realized. A better understanding of this transition and how to identify it is important to ensure safe design.

Somewhat related is the influence of positive reinforcement on the punching strength. In its current format the model would predict an increase of about 40 percent in the punching capacity of the slab-column connections tested as part of this thesis had they been fully continuous with equivalent positive reinforcement. This is a significant influence, particularly when current code methods would predict no increase in strength. While some comparisons of model predictions to tests on slabs designed to simulate continuity have yielded good results(Alexander and Simmonds, 1991), tests designed to specifically study this influence could prove invaluable to validating or disproving the model.

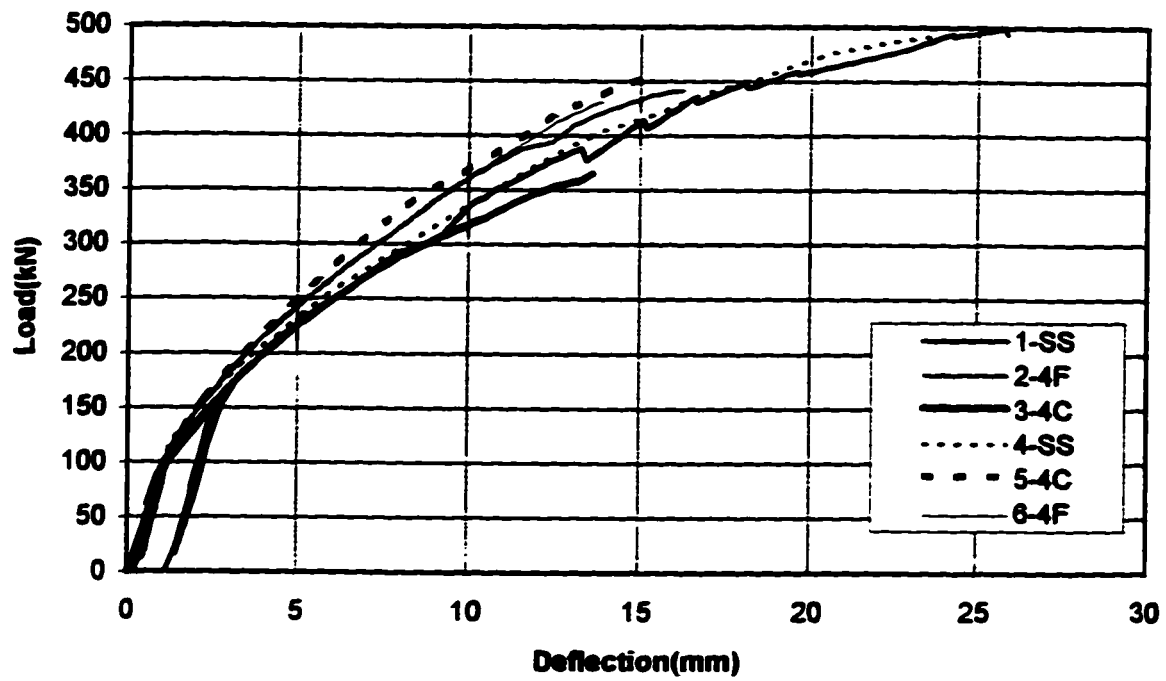


Figure 6.1 Load Deflection Behavior - All Specimens

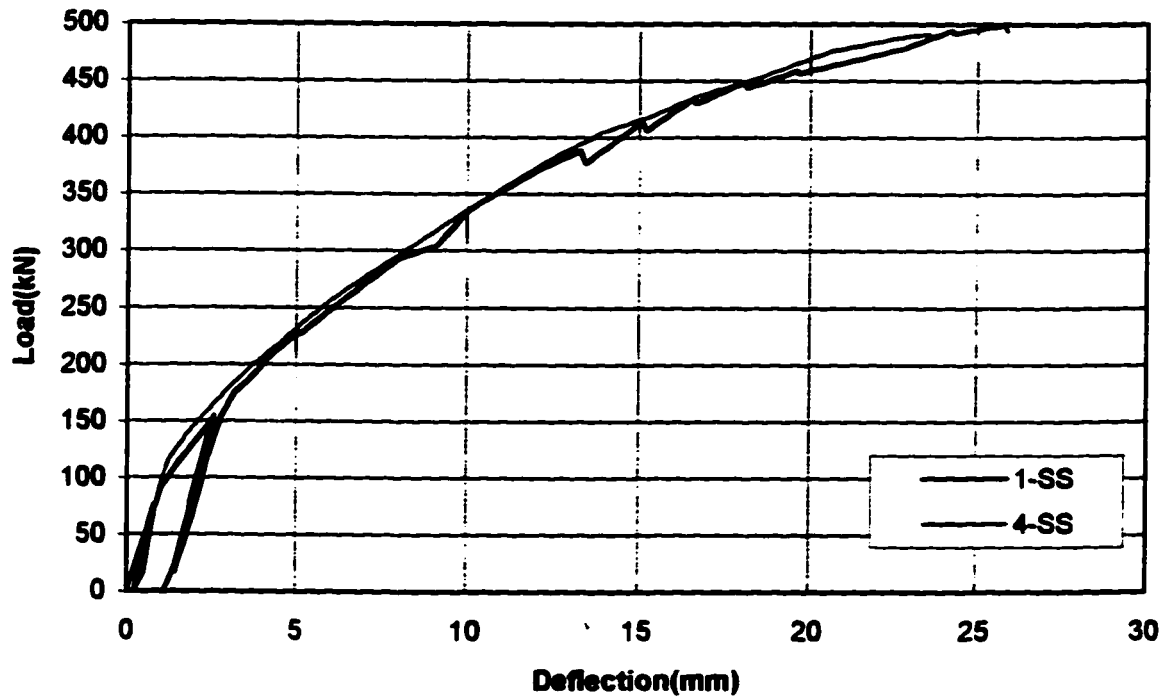


Figure 6.2 Load Deflection Behavior - Solid Specimens

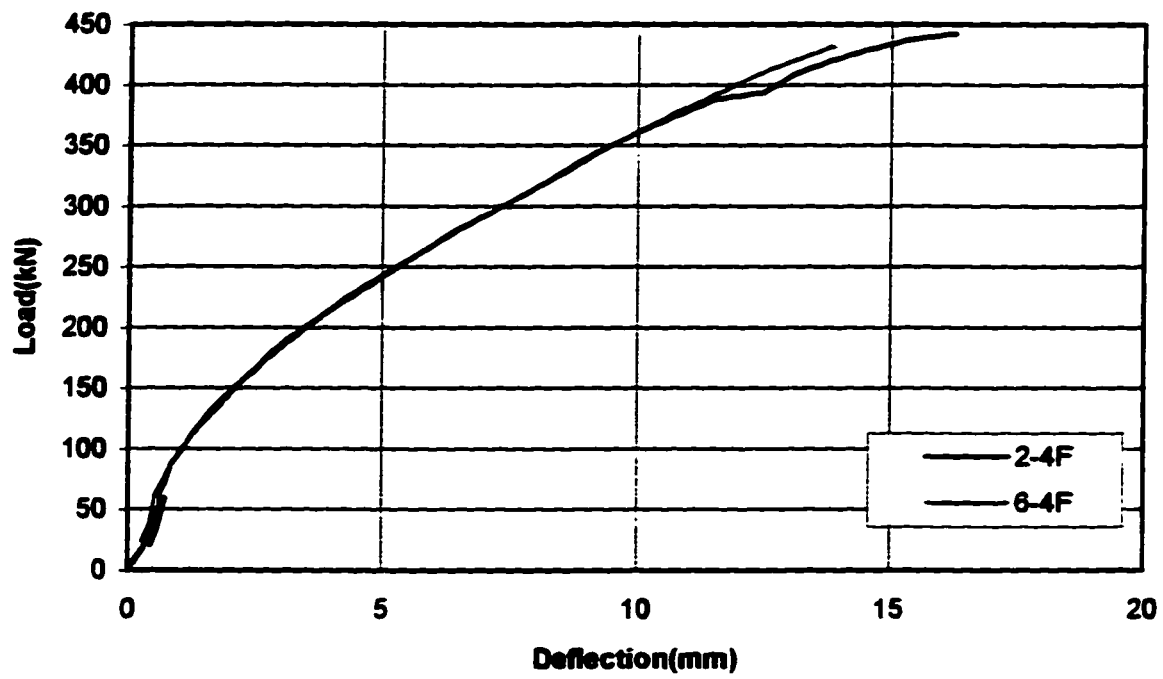


Figure 6.3 Load Deflection Behavior - 4F Specimens

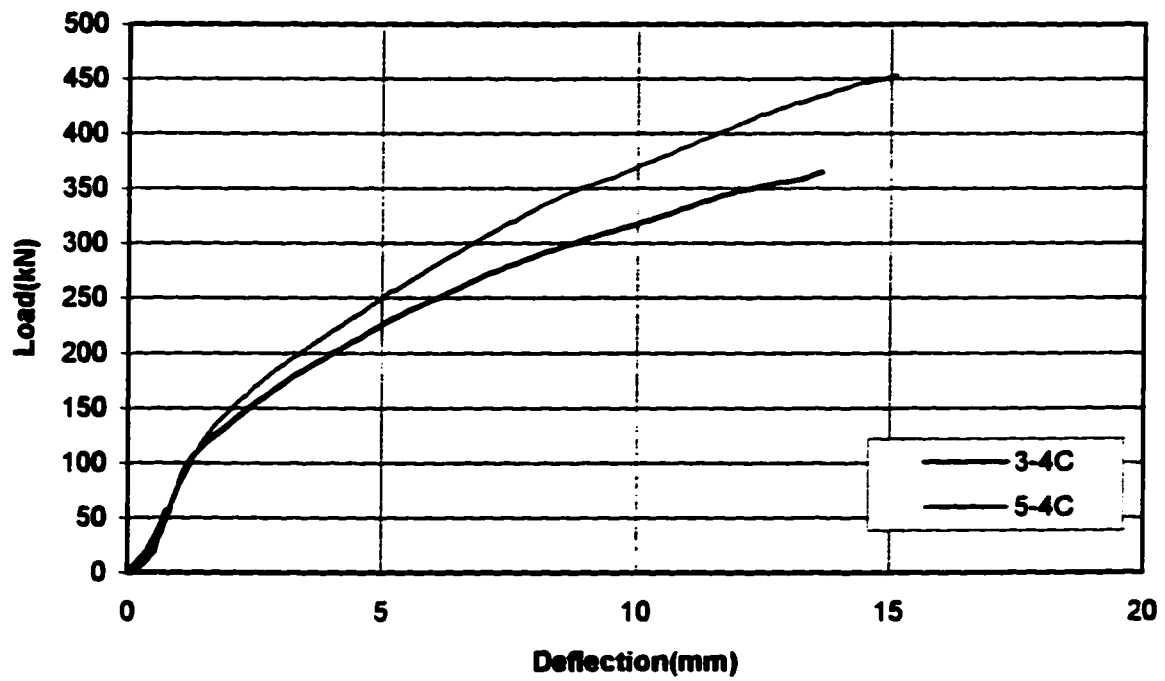


Figure 6.4 Load Deflection Behavior - 4C Specimens

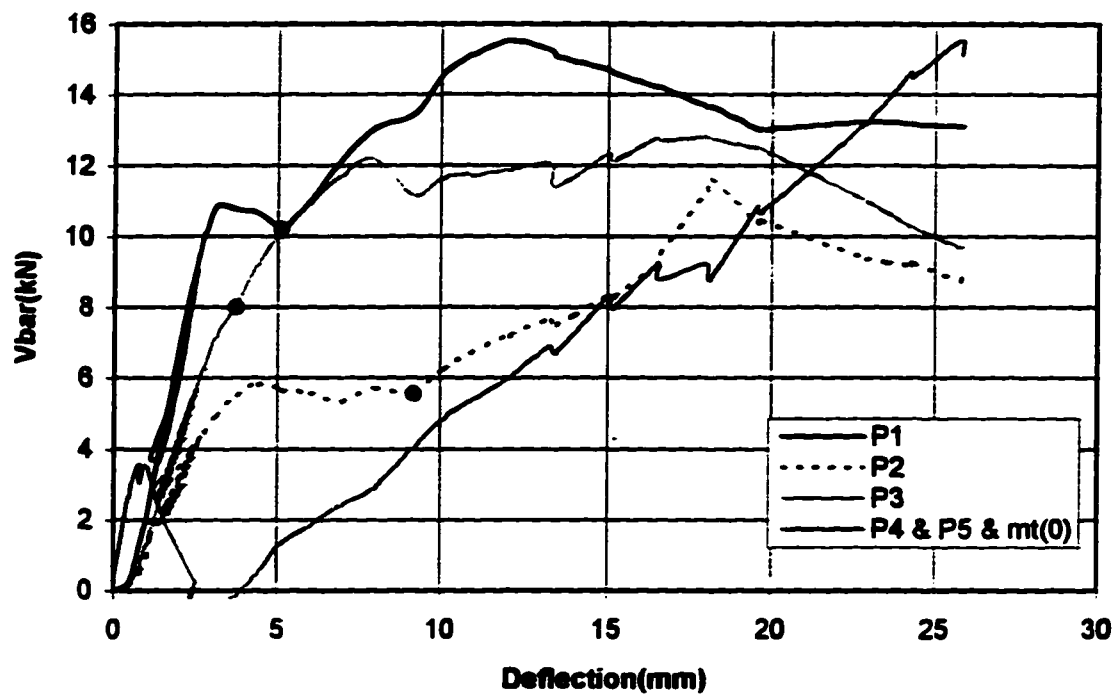


Figure 6.5 Perimeter Bar Shears - Specimen #1-SS

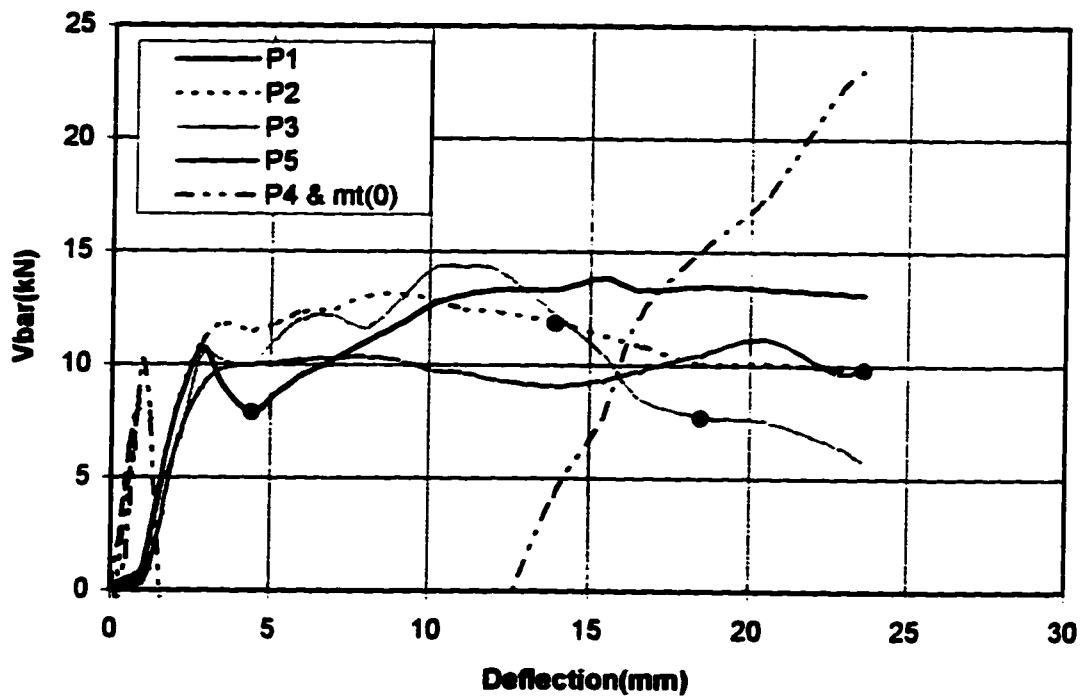


Figure 6.6 Perimeter Bar Shears - Specimen #4-SS

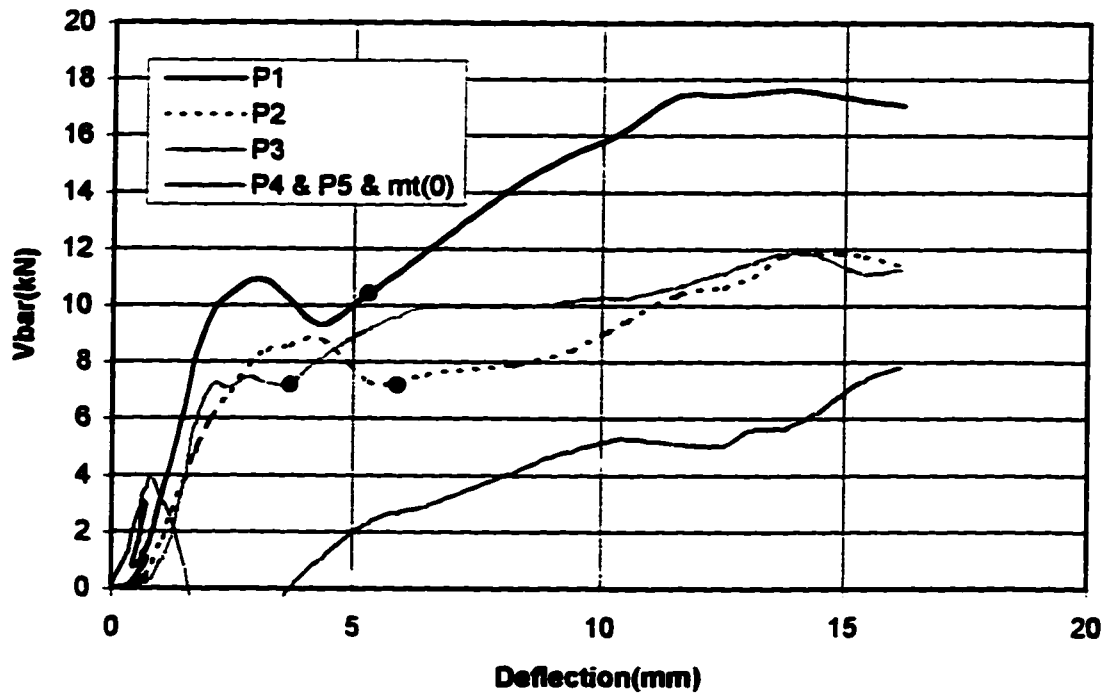


Figure 6.7 Perimeter Bar Shears - Specimen #2-4F

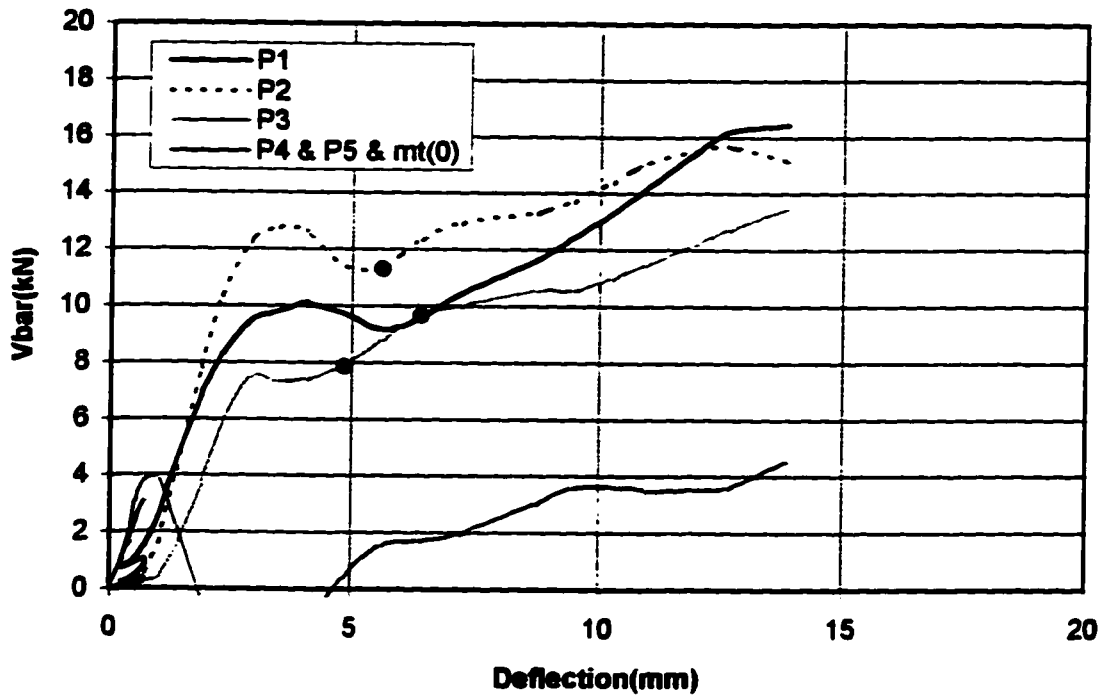


Figure 6.8 Perimeter Bar Shears - Specimen #6-4F

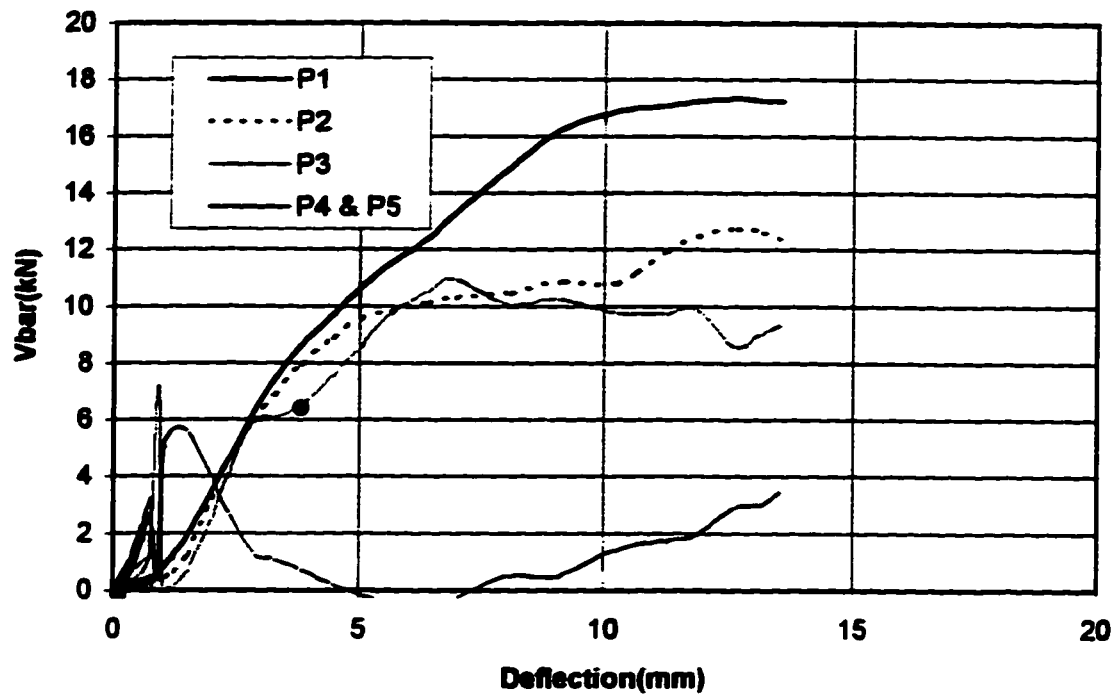


Figure 6.9 Perimeter Bar Shears - Specimen #3-4C

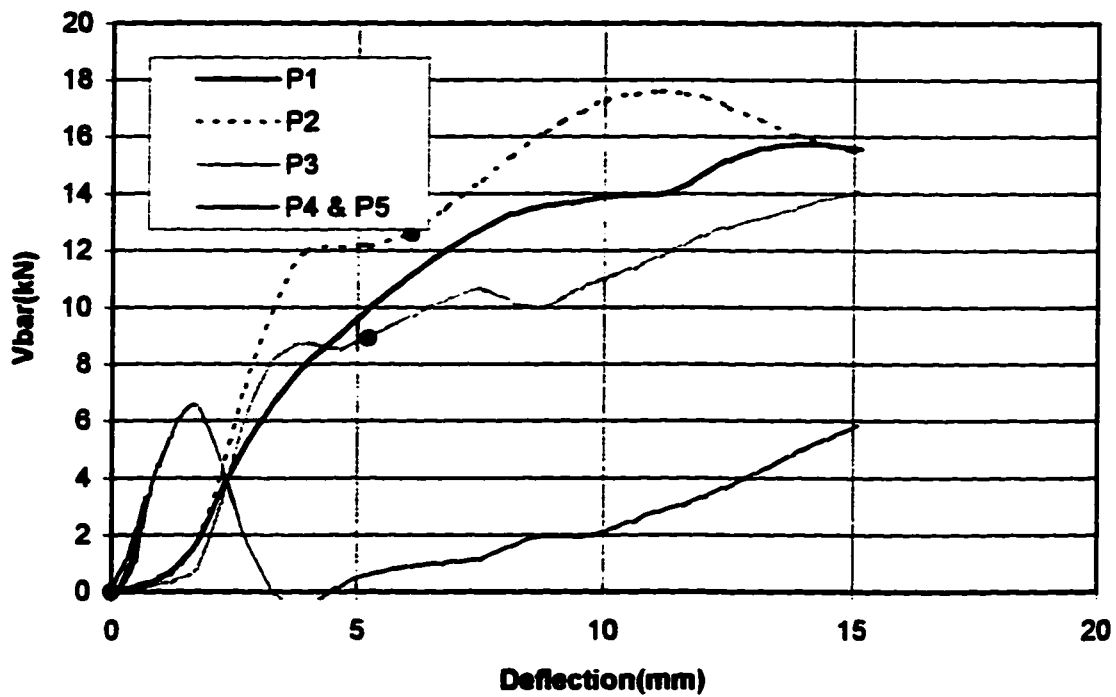


Figure 6.10 Perimeter Bar Shears - Specimen #5-4C

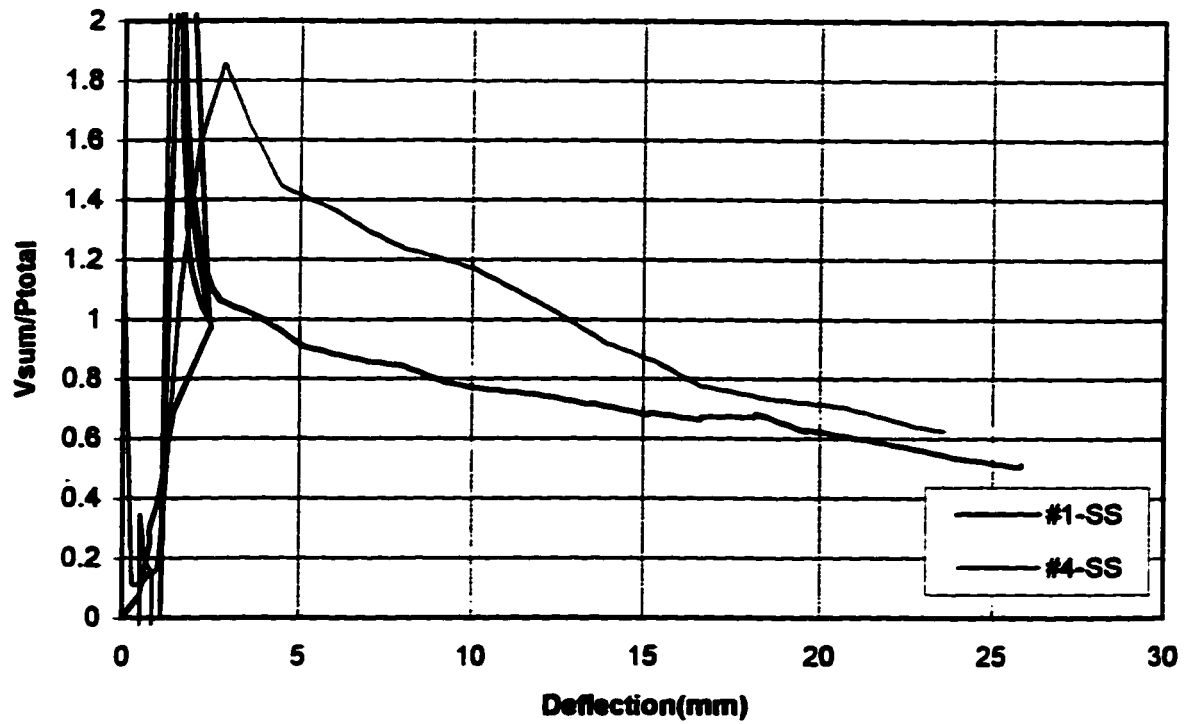


Figure 6.11 Ratio of Measured Load to Total Load - SS Specimens

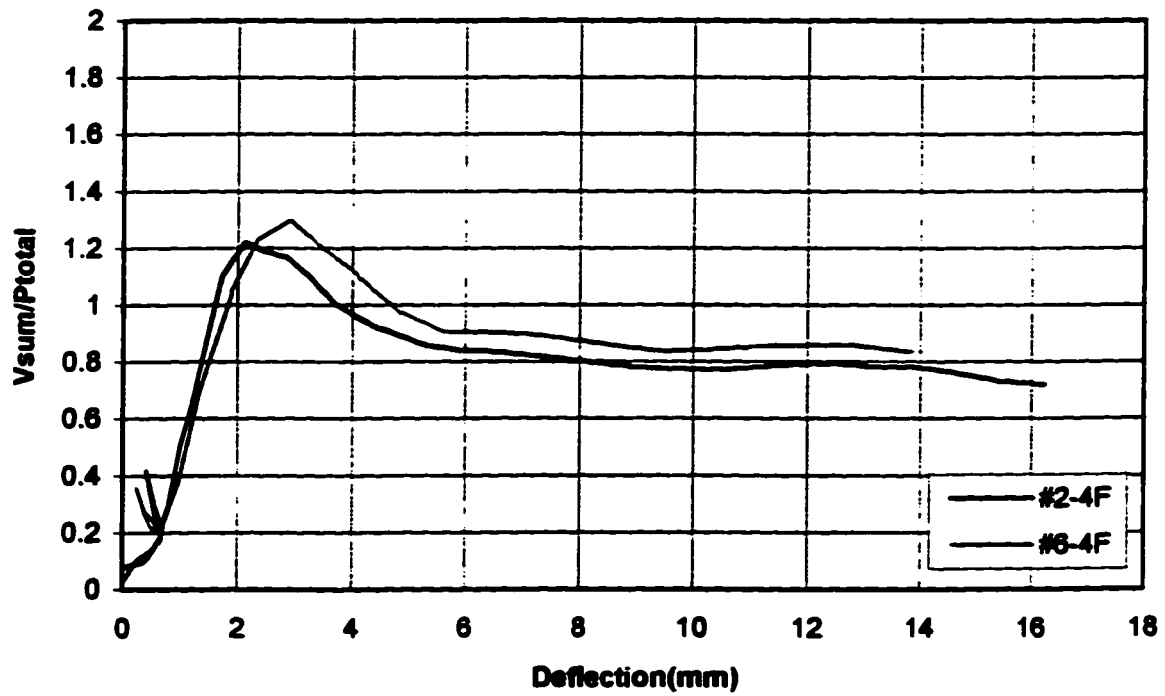


Figure 6.12 Ratio of Measured Load to Total Load - 4F Specimens

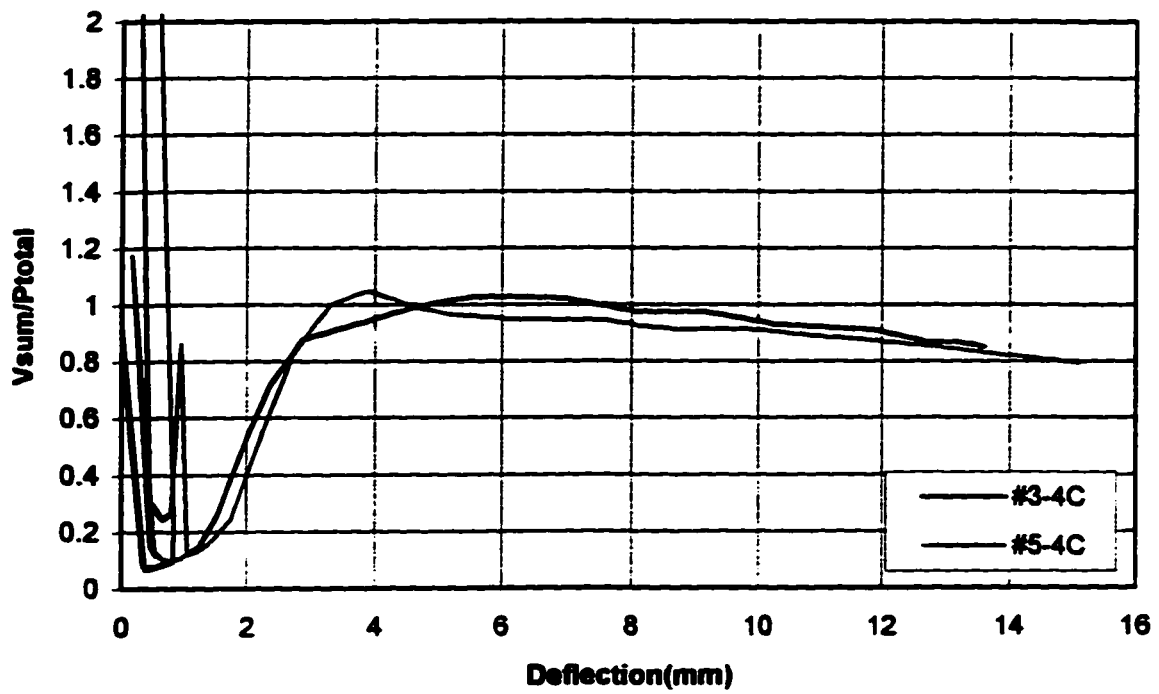


Figure 6.13 Ratio of Measured Load to Total Load - 4C Specimens

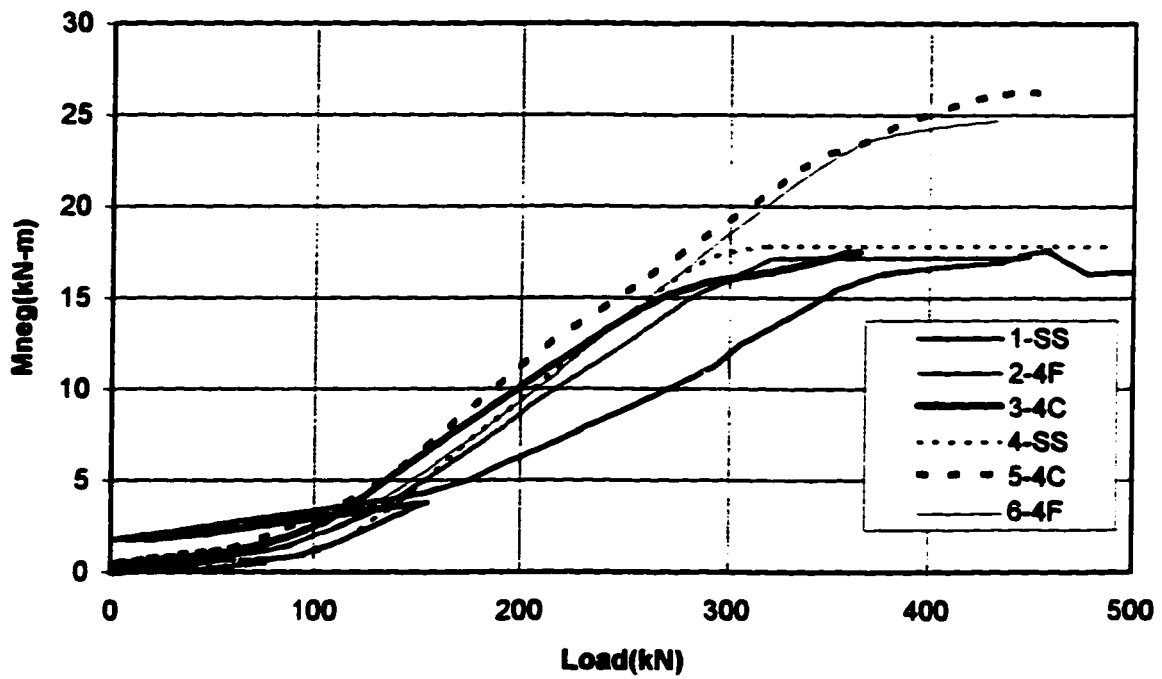


Figure 6.14 Development of Negative Moment at Column Face

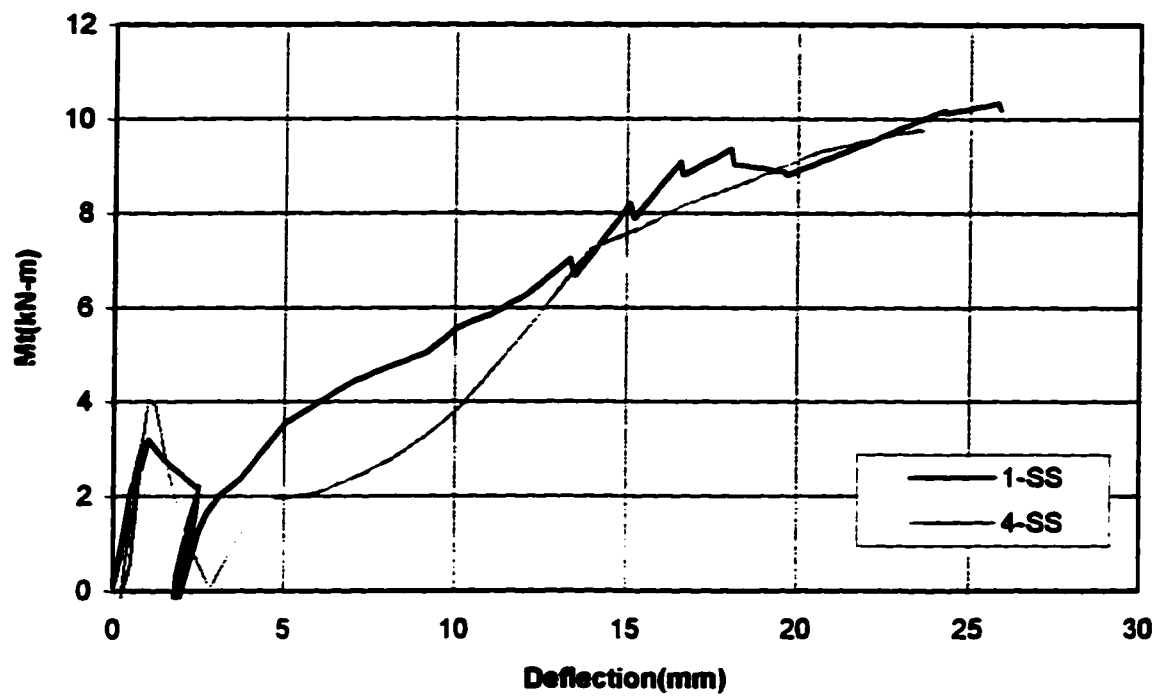


Figure 6.15 Torsion Requirements - SS Specimens

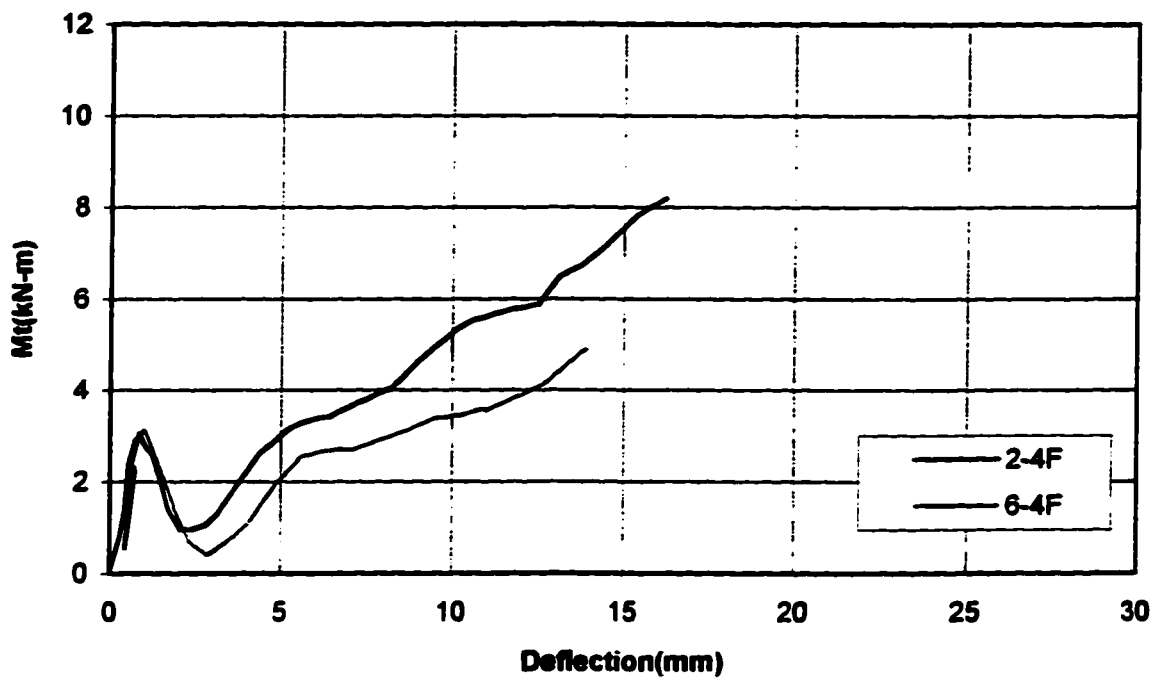


Figure 6.16 Torsion Requirements - 4F Specimens

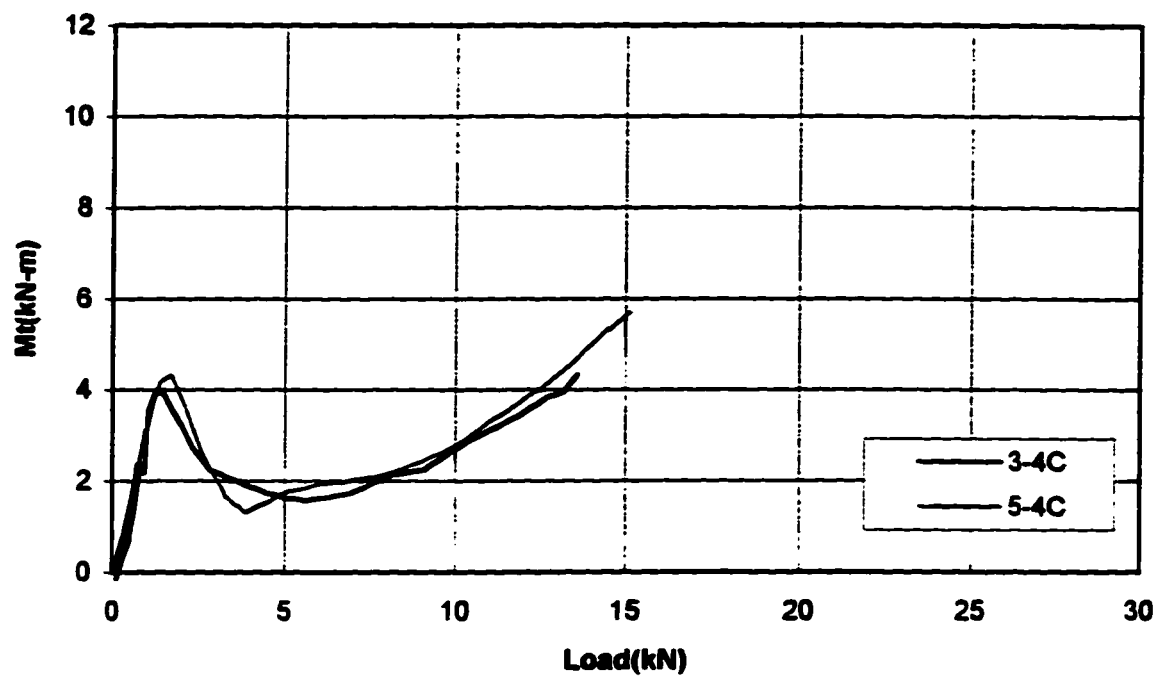


Figure 6.17 Torsion Requirements - 4C Specimens

Tests by Kennedy

Spec.	f _c	f _y (Acad)	f _y (Ap)	d	e	coeff	hr	h _m	Acad	w	ll	l ₂	M _{req}	P _{Acad}	P _{A23.3}	P _{ult}	T/P-Bond	T/P-A23.3
#1-SS	78	400	400	115	250	250	0	0	400	168.6	0	323	17.6	436	593	494	1.13	0.83
#2-4F	96	400	400	115	250	125	125	125	400	187.0	0	203	17.1	303	329	443	1.46	1.34
#3-4C	93	400	400	115	250	250	125	125	400	184.1	0	210	17.8	309	324	366	1.18	1.13
#4-SS	101	400	400	115	250	250	0	0	400	191.9	0	305	17.8	468	675	492	1.05	0.73
#5-4C	99	400	400	115	250	250	125	125	600	189.9	0	267	26.2	406	334	454	1.12	1.36
#6-4F	94	407	400	115	250	125	125	125	600	185.1	0	264	25.1	391	326	431	1.10	1.32

Tests by Marzouk and Hussein

Spec.	f _c	f _y (Acad)	f _y (Ap)	d	e	coeff	hr	h _m	Acad	w	ll	l ₂	M _{req}	P _{Acad}	P _{A23.3}	P _{ult}	T/P-Bond	T/P-A23.3
NS1	42	490	490	95	150	150	0	0	210	102.2	0	293	8.8	240	241	320	1.33	1.33
NS2	30	490	490	120	150	150	0	0	200	109.1	0	310	10.5	271	284	396	1.46	1.39
HS1	67	490	490	95	150	150	0	0	70	129.1	0	157	3.2	162	305	178	1.10	0.98
HS2	70.2	490	490	95	150	150	0	0	120	132.1	0	202	5.4	214	312	249	1.17	0.80
HS3	69.1	490	490	95	150	150	0	0	210	131.1	0	265	9.2	277	310	356	1.28	1.15
HS4	65.8	490	490	90	150	150	0	0	320	121.2	0	323	12.6	313	280	418	1.33	1.49
HS5	68.1	490	490	125	150	150	0	0	100	171.2	0	187	6.0	256	454	365	1.42	0.80
HS6	70	490	490	120	150	150	0	0	200	166.7	0	259	11.2	346	434	489	1.41	1.13
HS7	73.8	490	490	95	150	150	0	0	200	135.5	0	255	8.8	276	320	356	1.29	1.11
HS8	69	490	490	120	150	150	0	0	200	165.5	0	260	11.2	345	431	436	1.27	1.01
HS9	74	490	490	124	150	150	0	0	400	177.1	0	355	22.3	502	468	543	1.08	1.16
HS10	80	490	490	120	150	150	0	0	420	178.2	0	356	22.6	508	464	645	1.27	1.39
HS11	70	490	490	70	150	150	0	0	100	97.2	0	184	3.3	143	206	196	1.37	0.95
HS12	75	490	490	70	150	150	0	0	160	100.6	0	227	5.2	182	213	258	1.41	1.21
HS13	68	490	490	70	150	150	0	0	210	95.8	0	262	6.6	201	203	267	1.33	1.31
HS14	72	490	490	95	220	220	0	0	400	133.8	0	358	17.2	384	406	498	1.30	1.23
HS15	71	490	490	95	300	300	0	0	420	132.9	0	372	18.4	395	506	560	1.42	1.11

Table 6.1 Test to Predicted Ratios

Tests by Moe

Spec.	Pc	Dy(Accel)	Dy(Ap)	d	c	ceff	br	bm	Accl	w	ll	l2	Ming	Pband	PA23.3	Pult	T/P-Bond	T/P-A23.3
111	26	328	328	114	254	254	0	0	400	96.5	0	373	13.4	288	342	371	1.29	1.08
112	25	328	328	114	254	254	0	0	400	94.6	0	376	13.4	260	294	329	1.26	1.12
113	25	328	328	114	254	127	127	127	400	94.6	0	248	11.8					
113	24	328	328	114	254	254	0	0	400	92.7	0	379	13.3	233	247	325	1.40	1.32
114	24	328	328	114	254	127	127	127	400	92.7	0	249	11.6					
114	26	328	328	114	254	254	0	0	400	96.5	0	373	13.4	239	257	290	1.21	1.13
115	26	328	328	114	254	127	127	127	400	96.5	0	246	11.9					
115	25	328	328	114	254	254	0	0	400	94.6	0	376	13.4	212	210	250	1.18	1.19
116	25	328	328	114	254	127	127	127	400	94.6	0	248	11.8					
116	28	328	328	114	254	127	127	127	400	100.1	0	243	12.1	195	178	246	1.26	1.39
117	25	328	328	114	254	254	0	0	400	94.6	0	376	13.4	260	294	312	1.20	1.06
117	25	328	328	114	254	127	127	127	400	94.6	0	248	11.8					
118	28	328	328	114	254	254	0	0	400	100.1	0	368	13.5	245	267	312	1.28	1.17
118	28	328	328	114	254	127	127	127	400	100.1	0	243	12.1					
119	24	328	328	114	254	254	0	0	400	92.7	0	379	13.3	257	300	313	1.22	1.04
119	24	328	328	114	254	127	127	127	400	92.7	51	198	11.6					
1110	25	328	328	114	254	254	0	0	400	94.6	0	376	13.4	260	313	334	1.28	1.07
1110	25	328	328	114	254	127	127	127	400	94.6	102	146	11.8					
1111	26	328	328	114	254	254	0	0	400	96.5	0	373	13.4	267	326	339	1.27	1.04
1111	26	328	328	114	254	127	127	127	400	96.5	204	63	13.4					
1112	28	328	328	114	254	254	127	127	400	100.1	0	262	13.5	210	178	269	1.28	1.31
1113	25	328	328	114	254	254	254	254	800	94.6	0	306	23.5	231	112	201	0.87	1.80
1114	26	328	328	114	254	254	0	0	400	96.5	0	373	13.4	263	300	253	0.96	0.84
1114	26	328	328	114	254	127	127	127	400	96.5	0	246	11.9					
1115	23	328	328	114	254	254	0	0	400	90.8	0	382	13.2	253	282	331	1.31	1.17
1115	23	328	328	114	254	127	127	127	400	90.8	0	251	11.5					

AVE.	1.25	1.15
STDEV.	0.13	0.24

Table 6.1 Test to Predicted Ratios(cont.)

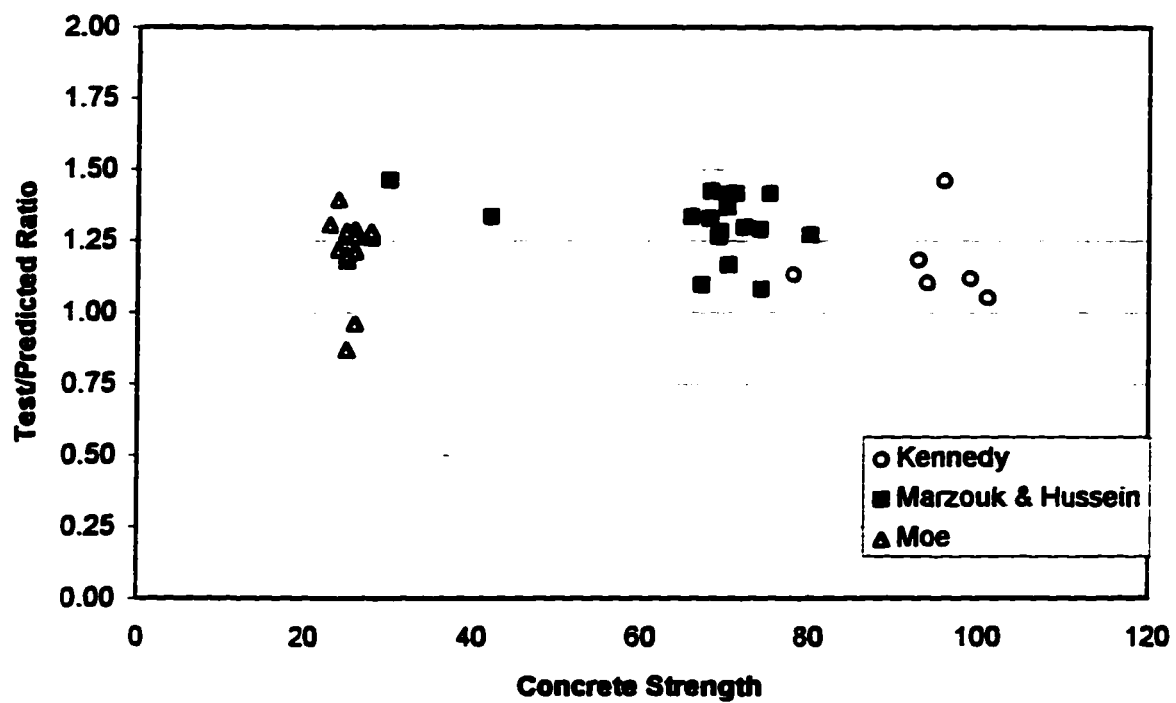


Figure 6.18 Test to Predicted Ratios - Bond Model

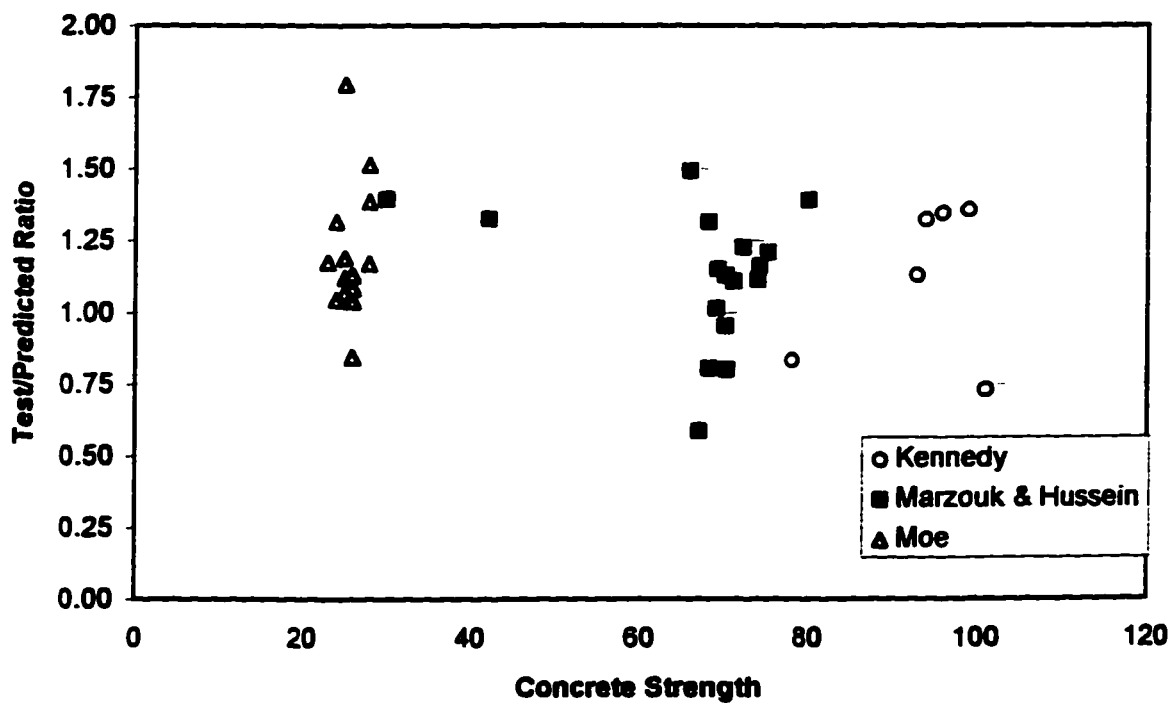


Figure 6.19 Test to Predicted Ratios - CAN3-A23.3-M94

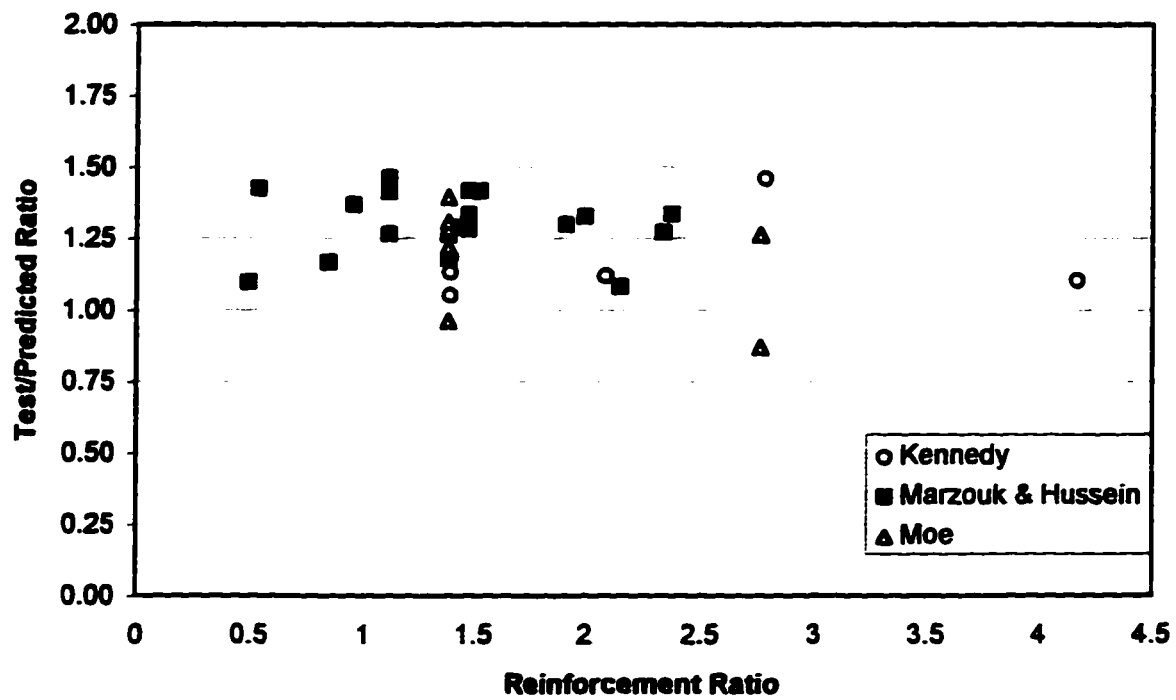


Figure 6.20 Test to Predicted Ratios - Bond Model

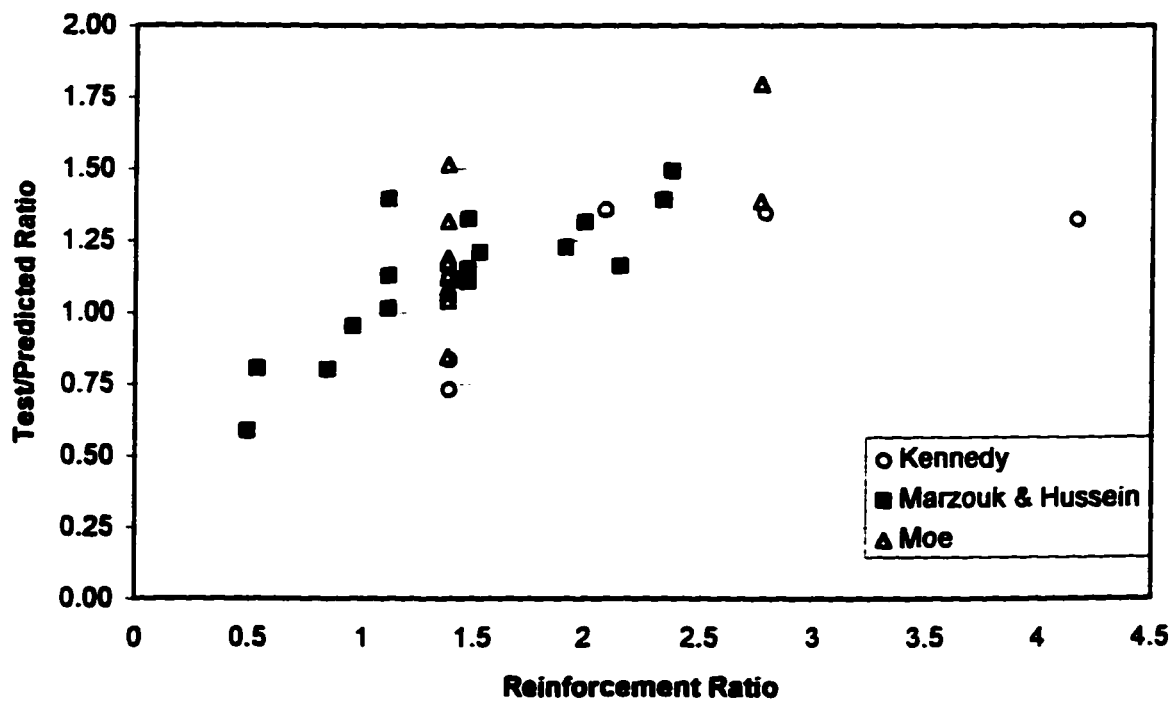


Figure 6.21 Test to Predicted Ratios - CAN3-A23.3-M94

7. CONCLUSIONS AND RECOMMENDATIONS FOR FUTURE WORK

7.1 Conclusions

1. The bond model model provides a simple and general lower bound solution for punching strength. Estimates of internal forces developed in test specimens were consistent with load transfer mechanisms described by the model. Bond model estimates of punching strength were in good agreement with test results.
2. While bond may limit the ability to develop beam action shear, other mechanisms of shear transfer are available. Additionally there are other failure mechanisms which limit capacity such as crushing/splitting of the compressive arch, anchorage of radial strip steel, and torsional capacity of the radial strips.
3. Except in the case of a corner perforation, boundary conditions do not enforce the torsional moment to be zero at the column end of the radial strip. Non-zero torsional moments may exist at this location.
4. Perforations at the column corners eliminate the ability to develop both shear and torsion on the radial strip faces at the location of the perforation. As a result less efficient load paths must be utilized resulting in decreased capacity.
5. Perforations at the column face disrupt primary shear loading of the radial strip face by preventing the development of moment gradient perpendicular to the strip over the width of the perforation. In addition the width of the strip available for the radial

compressive arch is reduced in the vicinity of the perforation. These influences reduce the capacity of the connection.

6. Perforations placed near the column reduce the ductility of slab column connections.
7. Perforations at the column corners have a greater effect on ultimate capacity than face perforations. This is due to the more pronounced influence on the development of torsion.
8. Beneficial effects of increased reinforcement within the radial even if the radial strip is not overreinforced. This can occur in situations where capacity is limited by crushing or splitting of the compressive arch. This situation is most likely to occur when the effective width of the radial strip is reduced such as in the presence of a face perforation.
9. The Canadian code method for punching strength tends to become less conservative with increasing concrete strength, suggesting its utilization of the square root of concrete strength is overestimates the influence of this parameter. The bond model, effectively using the fourth root of concrete strength, appears to more accurately reflect the influence of concrete strength on punching capacity.

7.2 Recommendations for Future Work

1. The determination of the effective reinforcement ratio for the test specimens utilized in this research was straightforward and apparent. A generic method for estimating the effective reinforcement ratio would be useful. The development of such a method,

which should be able to handle situations including banded reinforcement and asymmetric perforation, is desirable.

2. The symmetric placement of perforations in the test specimens promoted symmetric behavior enabling the analysis of internal forces to be conducted with relative ease. Tests designed to examine the influence of irregular perforation patterns as well as perforations not immediately adjacent to the column would be beneficial to a more complete understanding of the influence of perforations.
3. In situations where perforations are placed in the vicinity of columns the use of shear reinforcement is not uncommon. A study of the beneficial effects of shear reinforcement and the influence on load carrying mechanisms defined by the bond model would be valuable.

References

- Ajdukiewicz, A. and Starosolski, W. 1990. Reinforced Concrete Slab-Column Structures. Elsevier Science Publishing Company, New York, NY.
- Alexander, S.D.B., and Simmonds, S.H. 1986. Shear Moment Transfer in Slab-Column Connections. Structural Engineering Report No. 141, Department of Civil Engineering, University of Alberta, Edmonton, Alberta.
- Alexander, S.D.B., and Simmonds, S.H. 1991. Bond Model for Strength of Slab-Column Joints. Structural Engineering Report No. 174, Department of Civil Engineering, University of Alberta, Edmonton, Alberta.
- British Standards Institution, 1985. The structural use of concrete: Part 1, Code of practice for design and construction (BS8110: Part 1) British Standards Institution, London.
- CAN3-A23.3-M84:1984. Design of concrete structures. Canadian Standards Association, Rexdale, Ontario, Canada.
- CAN3-A23.3-M94:1994. Design of concrete structures. Canadian Standards Association, Rexdale, Ontario, Canada.
- MacGregor, J.G. 1992. Reinforced Concrete. Prentice Hall, Englewood Cliffs, New Jersey.
- Moe, J. 1961. Shearing Strength of Reinforced Concrete Slabs and Footings under Concentrated Loads. Development Dept. Bulletin No. D47, Portland, Cement Association, Skokie, Illinois.
- Pillai, S.O., and Kirk, D.W. 1988. Reinforced Concrete Design. McGraw-Hill Ryerson Ltd. Toronto, Ontario, Canada.

Marzouk, H., and Hussein, A. 1991. Behavior of High Strength Slabs. American Concrete Institute Structural Journal, Volume 88, No. 6, pp 701-713.

Regan, P.E., and Braestrup, M.W. 1985. Punching Shear in Reinforced Concrete. A state of the art report. Bulletin D'Information No. 168, Comite Euro-International du Beton, Lausanne, Switzerland.

Zaidi, S.T.H., and Roll, F. 1968. Shear Resistance of Perforated Reinforced Concrete Slabs. The Towne School of Civil and Mechanical Engineering, University of Pennsylvania, Philadelphia, PA.

APPENDIX A

SPECIMEN #1-SS

Load (kN)	Defl. (mm)	Bar Forces(kN)												
		C1-12S	C2-12S	P1-9S	P1-28S	P1-47S	P1-66S	P2-9S	P2-28S	P2-47S	P2-66S	P3-9S	P3-28S	P3-47S
0.0	0.00	-0.02	N/A	0.00	-0.02	0.00	-0.01	-0.01	0.00	-0.04	-0.04	0.00	-0.01	0.00
45.4	0.49	0.62	N/A	0.86	0.46	0.22	0.04	0.44	0.31	0.15	0.00	0.58	0.45	0.29
76.0	0.82	2.34	N/A	3.31	1.03	0.41	0.02	1.34	0.59	0.28	-0.02	1.98	1.03	0.51
68.5	0.80	2.48	N/A	3.36	1.06	0.36	0.02	1.42	0.59	0.29	-0.02	2.21	1.12	0.48
91.7	1.03	3.86	N/A	5.26	1.57	0.41	0.00	2.41	0.85	0.39	-0.01	3.87	1.75	0.62
111.8	1.50	7.29	N/A	10.25	2.86	0.65	-0.02	6.37	2.02	0.55	0.02	7.50	3.15	0.96
153.1	2.55	16.73	N/A	22.56	7.49	1.69	0.05	13.73	6.94	1.36	0.13	18.40	9.09	1.88
154.2	2.55	16.71	N/A	22.53	7.49	1.69	0.05	13.72	6.94	1.36	0.12	18.38	9.09	1.88
133.4	2.44	15.58	N/A	21.02	7.12	1.58	0.06	12.89	6.64	1.26	0.12	17.33	8.66	1.75
120.7	2.36	14.82	N/A	20.04	6.88	1.53	0.07	12.32	6.43	1.20	0.12	16.64	8.38	1.68
109.7	2.28	14.13	N/A	19.14	6.66	1.47	0.08	11.80	6.24	1.15	0.11	15.98	8.11	1.61
93.8	2.16	12.94	N/A	17.59	6.28	1.36	0.08	10.90	5.92	1.06	0.11	14.86	7.66	1.49
77.5	2.02	11.84	N/A	16.16	5.91	1.27	0.10	10.05	5.59	0.98	0.11	13.80	7.23	1.38
65.5	1.92	11.01	N/A	15.09	5.63	1.20	0.10	9.41	5.35	0.92	0.11	13.00	6.91	1.30
56.6	1.84	10.36	N/A	14.25	5.40	1.15	0.11	8.91	5.15	0.86	0.11	12.36	6.64	1.24
49.2	1.78	9.84	N/A	13.59	5.22	1.10	0.12	8.52	4.98	0.82	0.11	11.87	6.43	1.18
43.2	1.71	9.44	N/A	13.06	5.07	1.07	0.12	8.21	4.86	0.80	0.12	11.46	6.26	1.15
38.3	1.65	9.10	N/A	12.62	4.96	1.03	0.12	7.95	4.74	0.77	0.11	11.13	6.12	1.11
26.5	1.52	8.27	N/A	11.54	4.64	0.96	0.13	7.35	4.47	0.71	0.10	10.30	5.75	1.01
16.7	1.42	7.56	N/A	10.59	4.37	0.90	0.13	6.78	4.22	0.66	0.11	9.56	5.43	0.94
47.4	1.70	9.08	N/A	12.68	4.91	1.06	0.13	7.88	4.64	0.79	0.11	10.96	6.03	1.13
62.1	1.81	10.16	N/A	14.09	5.25	1.14	0.12	8.70	4.93	0.86	0.11	11.99	6.45	1.24
77.8	1.85	11.22	N/A	15.48	5.60	1.24	0.11	9.55	5.24	0.94	0.11	13.02	6.85	1.33
92.3	1.97	12.22	N/A	16.80	5.94	1.32	0.10	10.37	5.55	1.01	0.11	14.01	7.26	1.43
105.0	2.08	13.14	N/A	18.01	6.25	1.39	0.10	11.08	5.82	1.08	0.11	14.91	7.62	1.52
118.6	2.20	14.13	N/A	19.33	6.59	1.48	0.09	11.88	6.12	1.15	0.12	15.90	8.03	1.62
131.1	2.31	15.01	N/A	20.52	6.91	1.56	0.08	12.59	6.41	1.23	0.12	16.79	8.41	1.71
141.8	2.41	15.83	N/A	21.63	7.24	1.64	0.06	13.27	6.70	1.29	0.12	17.65	8.78	1.79
148.8	2.49	16.32	N/A	22.26	7.46	1.69	0.07	13.67	6.91	1.33	0.12	18.16	9.02	1.84
19.2	1.40	7.68	N/A	10.78	4.58	0.94	0.15	6.91	4.39	0.69	0.11	9.70	5.63	0.99
0.0	1.12	7.73	N/A	10.78	4.56	0.93	0.13	6.89	4.38	0.67	0.07	9.72	5.60	0.84
34.6	1.60	9.97	N/A	13.58	5.39	1.17	0.17	8.46	5.09	0.86	0.10	11.81	6.66	1.06
58.9	1.82	11.81	N/A	15.92	5.99	1.33	0.15	9.87	5.65	0.97	0.09	13.56	7.39	1.18
78.8	1.99	13.22	N/A	17.85	6.51	1.45	0.13	11.04	6.12	1.09	0.09	15.03	8.00	1.28
99.0	2.18	14.69	N/A	19.81	7.05	1.60	0.13	12.21	6.60	1.21	0.10	16.50	8.64	1.38
98.6	2.18	14.64	N/A	19.76	7.05	1.59	0.13	12.16	6.59	1.21	0.10	16.46	8.63	1.38
121.9	2.39	16.35	N/A	22.08	7.73	1.77	0.12	13.53	7.18	1.36	0.11	18.22	9.41	1.52
120.8	2.39	16.25	N/A	21.95	7.74	1.77	0.13	13.44	7.18	1.36	0.11	18.11	9.40	1.51
120.3	2.38	16.23	N/A	21.91	7.74	1.77	0.12	13.43	7.18	1.36	0.11	18.11	9.40	1.52
137.6	2.57	17.55	N/A	23.70	8.35	1.92	0.11	14.48	7.72	1.48	0.12	19.47	10.07	1.64
156.3	2.79	19.39	N/A	26.11	9.37	2.19	0.11	15.97	8.56	1.68	0.13	21.54	11.12	1.78
155.4	2.79	19.37	N/A	26.10	9.45	2.21	0.13	15.96	8.61	1.70	0.15	21.53	11.17	1.80
175.2	3.15	22.21	N/A	29.57	11.51	2.81	0.16	18.27	10.38	2.12	0.21	24.97	13.13	2.04
191.2	3.74	25.98	N/A	33.62	15.68	4.38	0.62	21.18	13.74	3.36	0.38	29.09	16.64	2.51
211.4	4.38	30.15	N/A	37.86	20.09	5.99	0.93	24.22	16.66	5.56	0.66	33.24	20.22	3.02
228.7	5.11	34.52	N/A	42.15	25.20	8.13	1.32	27.28	19.32	9.02	1.20	36.91	23.91	3.74
227.1	5.13	34.42	N/A	42.01	25.27	8.22	1.33	27.16	19.28	9.13	1.22	36.70	23.88	3.79
247.4	5.96	39.02	N/A	47.15	30.20	10.95	1.84	30.33	22.16	12.40	2.08	40.45	27.70	5.05
271.5	6.98	44.68	N/A	54.58	36.34	14.65	3.62	34.10	25.22	16.31	3.36	44.36	31.49	6.55
292.7	7.96	50.23	N/A	61.10	42.14	18.59	4.80	37.47	27.96	19.96	5.05	47.88	34.35	8.81
304.9	9.16	55.58	N/A	66.73	46.16	22.46	5.95	39.70	31.16	21.63	6.88	49.18	36.32	14.07
336.0	10.06	64.09	N/A	74.28	50.81	25.28	6.62	43.67	34.90	24.00	7.89	53.66	39.78	16.97
353.3	10.90	80.00	N/A	80.00	55.08	27.87	7.39	46.74	38.20	26.16	9.01	56.84	42.80	20.01
352.0	10.91	80.00	N/A	80.00	55.09	27.89	7.43	46.65	38.17	26.14	9.08	56.67	42.77	20.11

SPECIMEN #2-4F

Load (kN)	Defl. (mm)	Bar Forces(kN)												
		C1-12S	C2-12S	P1-9S	P1-28S	P1-47S	P1-66S	P2-9S	P2-28S	P2-47S	P2-66S	P3-9S	P3-28S	P3-47S
0.8	0.00	-0.03	N/A	-0.02	-0.02	0.00	-0.02	-0.03	-0.02	-0.06	-0.04	-0.01	-0.04	0.03
21.5	0.34	0.76	N/A	0.39	0.16	0.08	0.01	0.35	0.27	0.11	0.02	0.24	0.18	0.17
37.4	0.45	1.59	N/A	0.83	0.30	0.12	0.00	0.69	0.48	0.21	0.02	0.45	0.35	0.25
59.2	0.67	3.26	N/A	2.03	0.55	0.17	0.00	1.33	0.88	0.38	0.03	0.86	0.63	0.39
59.9	0.72	3.98	N/A	2.48	0.64	0.20	0.01	1.55	1.03	0.46	0.06	1.00	0.71	0.80
59.7	0.72	3.98	N/A	2.50	0.65	0.21	0.01	1.55	1.04	0.46	0.06	1.01	0.72	0.80
37.5	0.58	3.19	N/A	2.02	0.48	0.17	0.02	1.19	0.80	0.36	0.05	0.78	0.54	0.72
20.1	0.42	2.49	N/A	1.61	0.36	0.14	0.03	0.88	0.59	0.27	0.04	0.58	0.41	0.65
40.8	0.60	3.23	N/A	2.03	0.51	0.17	0.03	1.22	0.82	0.36	0.05	0.79	0.56	0.73
63.2	0.61	4.15	N/A	2.61	0.65	0.18	-0.01	1.61	1.08	0.47	0.04	1.03	0.73	0.81
72.7	0.72	4.79	N/A	3.10	0.75	0.20	-0.02	1.88	1.23	0.54	0.05	1.18	0.84	0.86
87.5	0.83	6.22	N/A	4.28	0.92	0.23	-0.05	2.93	1.52	0.65	0.05	1.54	1.06	0.96
99.1	1.03	8.64	N/A	6.99	1.16	0.28	-0.05	4.86	2.01	0.85	0.06	2.99	1.34	1.11
111.6	1.23	10.64	N/A	8.95	1.30	0.31	-0.07	6.75	2.31	1.00	0.06	4.46	1.59	1.20
126.2	1.51	13.99	N/A	12.54	1.56	0.41	-0.01	9.17	2.83	1.18	0.07	8.45	1.99	1.34
136.6	1.73	17.02	N/A	15.67	1.89	0.49	0.04	11.21	3.33	1.36	0.07	11.97	2.40	1.44
151.0	2.10	21.63	N/A	19.57	3.23	0.57	0.12	14.94	4.89	1.85	0.09	15.55	3.67	1.63
164.1	2.46	26.02	N/A	22.57	5.19	0.81	0.24	17.80	6.34	2.54	0.15	18.26	6.56	1.87
179.1	2.83	30.96	N/A	25.76	7.63	1.16	0.49	21.13	8.12	3.51	0.22	21.41	9.03	2.17
191.8	3.21	35.59	N/A	28.40	10.26	1.64	0.80	24.02	10.08	4.49	0.30	24.03	11.99	2.52
206.1	3.70	41.74	N/A	31.68	14.63	2.71	1.35	27.42	13.20	6.94	0.41	27.04	15.77	3.23
226.2	4.36	48.77	N/A	35.31	19.68	4.10	1.92	32.34	17.71	9.95	0.72	30.77	20.38	4.40
250.7	5.29	57.42	N/A	40.58	25.00	6.01	3.19	37.26	25.05	14.50	1.79	34.82	25.01	5.65
265.6	5.87	63.14	N/A	44.41	28.20	7.58	4.04	40.81	30.16	17.58	2.78	37.38	28.06	7.08
280.6	6.45	68.97	N/A	48.11	31.90	9.01	4.78	44.20	34.18	20.58	4.37	40.03	30.67	9.05
320.6	8.22	80.00	N/A	58.74	44.17	13.57	6.80	53.79	42.60	28.76	9.44	46.99	36.75	16.66
338.9	8.98	80.00	N/A	62.97	48.53	15.72	7.76	57.67	45.99	31.66	11.31	49.71	39.20	19.25
348.3	9.40	80.00	N/A	65.53	51.17	17.19	8.31	60.06	47.91	33.23	12.58	51.46	40.71	20.65
363.8	10.13	80.00	N/A	70.17	55.18	19.14	9.06	64.19	51.21	35.32	14.37	54.31	43.17	23.20
371.2	10.52	80.00	N/A	73.15	57.32	20.18	9.42	66.48	53.14	36.50	15.50	55.96	44.58	24.86
388.0	11.50	80.00	N/A	80.00	62.92	22.70	10.25	72.56	57.85	39.07	18.39	60.50	48.10	27.99
394.0	12.46	80.00	N/A	80.00	67.64	25.58	11.23	77.92	61.95	41.97	20.85	63.35	50.23	29.15
409.5	13.07	80.00	N/A	80.00	70.60	27.06	11.82	80.00	65.09	43.82	22.10	65.67	52.30	30.44
419.4	13.75	80.00	N/A	80.00	73.40	28.50	12.77	80.00	69.58	45.79	23.75	68.03	54.30	31.88
427.6	14.43	80.00	N/A	80.00	75.89	29.98	13.87	80.00	73.51	47.73	25.66	70.36	56.26	34.21
437.7	15.40	80.00	N/A	80.00	79.36	32.03	15.21	80.00	78.19	50.47	28.76	73.78	59.05	38.92
442.5	16.24	80.00	N/A	80.00	80.00	33.48	16.15	80.00	80.00	52.47	30.96	76.77	61.44	40.79

SPECIMEN #3-4C

Load (kN)	Defl. (mm)	Bar Forces(kN)												
		C1-12S	C2-12S	P1-9S	P1-28S	P1-47S	P1-66S	P2-9S	P2-28S	P2-47S	P2-66S	P3-9S	P3-28S	P3-47S
0.2	0.00	-0.05	N/A	-0.03	-0.03	-0.05	-0.03	-0.04	-0.05	-0.05	-0.05	-0.03	-0.05	0.02
17.4	0.37	0.57	N/A	0.28	0.22	0.04	0.00	0.22	0.17	0.07	0.01	0.16	0.13	0.14
39.6	0.63	1.89	N/A	0.81	0.63	0.11	-0.01	0.62	0.46	0.22	0.01	0.43	0.35	0.29
57.3	0.82	3.86	N/A	1.39	1.21	0.19	-0.02	1.04	0.80	0.36	0.03	0.73	0.60	0.43
58.8	0.83	4.40	N/A	1.63	1.49	0.23	0.00	1.17	0.90	0.45	0.04	0.82	0.72	2.00
0.5	0.12	1.62	N/A	0.47	0.59	0.02	-0.02	0.29	0.24	0.12	-0.02	0.20	0.19	1.72
0.7	0.13	1.62	N/A	0.47	0.60	0.04	0.00	0.30	0.25	0.13	0.00	0.21	0.20	1.73
17.8	0.44	2.39	N/A	0.82	0.87	0.12	0.02	0.58	0.47	0.25	0.04	0.42	0.39	1.86
36.3	0.64	3.32	N/A	1.21	1.16	0.17	0.02	0.86	0.68	0.36	0.04	0.60	0.56	1.95
57.3	0.79	4.53	N/A	1.67	1.55	0.23	0.00	1.20	0.92	0.46	0.04	0.85	0.75	2.06
76.1	0.96	6.78	N/A	2.27	2.47	0.30	-0.03	1.64	1.31	0.65	0.05	1.16	1.04	2.20
91.2	1.06	9.29	N/A	3.06	3.67	0.39	-0.05	2.14	1.79	0.86	0.06	1.53	1.40	2.58
105.7	1.24	12.22	N/A	4.51	4.93	0.62	-0.09	2.66	2.61	1.11	0.05	2.12	1.96	2.86
118.9	1.52	16.29	N/A	7.09	6.93	1.07	-0.04	4.92	4.08	1.40	0.05	4.37	3.34	3.06
136.1	2.01	22.78	N/A	12.75	8.99	1.31	-0.07	12.44	7.22	1.94	0.03	8.71	4.67	3.32
149.4	2.36	27.42	N/A	16.79	10.78	1.53	-0.10	17.72	10.45	2.42	0.01	12.59	5.84	3.49
165.6	2.88	33.23	N/A	22.49	13.80	1.65	-0.10	22.79	13.63	3.31	-0.01	18.18	8.33	3.73
179.3	3.29	37.75	N/A	26.34	16.66	1.91	-0.02	26.29	16.52	3.96	0.02	21.40	11.35	3.99
194.8	3.85	43.11	N/A	30.85	20.35	2.48	0.17	30.50	20.25	4.89	0.12	25.36	15.93	4.38
211.5	4.48	49.13	N/A	35.24	24.73	3.58	0.37	34.65	23.89	6.16	0.61	28.99	21.11	5.14
226.8	5.03	54.27	N/A	39.16	28.64	4.56	0.55	38.62	27.07	8.09	1.41	32.40	24.30	5.35
240.8	5.61	59.29	N/A	42.86	32.99	5.84	0.70	42.74	29.79	11.20	2.54	35.57	27.52	4.68
256.8	6.38	64.21	N/A	46.93	37.93	7.53	1.13	47.08	33.99	14.98	3.75	38.46	30.35	5.06
270.4	6.96	68.27	N/A	51.04	42.03	9.04	1.85	51.12	36.94	18.13	5.09	41.47	33.03	7.05
290.3	8.07	74.69	N/A	58.67	48.12	11.75	2.95	57.09	40.87	22.75	7.45	46.50	36.95	16.11
305.0	9.06	78.25	N/A	65.05	52.77	14.12	3.44	61.92	43.72	26.58	9.07	50.05	39.95	19.16
321.5	10.25	80.00	N/A	71.16	58.40	17.41	4.02	67.11	48.93	30.80	10.66	53.78	43.28	24.40
337.2	11.24	80.00	N/A	75.91	62.20	20.08	4.73	71.47	51.40	33.87	11.92	56.24	45.98	27.20
346.8	11.86	80.00	N/A	79.31	64.78	21.84	5.29	74.42	53.16	35.83	12.80	58.24	48.20	29.00
354.9	12.68	80.00	N/A	80.00	67.19	24.22	6.23	77.37	54.96	38.52	13.96	59.84	50.68	34.70
358.5	13.19	80.00	N/A	80.00	68.18	25.67	6.77	78.56	55.77	39.82	14.85	60.38	51.71	34.41
365.7	13.62	80.00	N/A	80.00	69.28	26.36	7.03	80.00	57.14	40.95	15.36	62.11	53.62	35.55

SPECIMEN #4-SS

Load (kN)	Defl. (mm)	Bar Forces(kN)															
		C1-125	C2-125	P1-95	P1-285	P1-475	P1-665	P2-95	P2-285	P2-475	P2-665	P3-95	P3-285	P3-475	P5-95	P5-285	P5-475
0.7	0.00	-0.05	N/A	0.18	0.02	0.00	0.01	0.00	-0.02	0.10	-0.02	-0.02	-0.01	0.02	0.00	0.01	0.01
18.0	0.28	0.36	N/A	0.47	0.23	0.09	0.06	0.32	0.22	0.28	0.03	0.23	0.21	0.16	0.18	0.16	0.15
39.3	0.46	0.87	N/A	0.82	0.44	0.16	0.07	0.68	0.42	0.42	0.04	0.51	0.46	0.23	0.41	0.29	0.29
58.0	0.62	1.52	N/A	1.30	0.70	0.25	0.09	1.07	0.68	0.51	0.08	0.86	0.68	0.36	0.64	0.47	0.37
57.7	0.63	1.66	N/A	1.41	0.74	0.28	0.10	1.14	0.74	0.54	0.05	0.94	0.70	0.42	0.69	0.53	0.41
76.5	0.84	3.15	N/A	2.24	1.07	0.41	0.15	1.73	1.12	0.73	0.11	1.42	1.04	0.59	1.06	0.79	0.58
75.9	0.87	3.20	N/A	2.17	1.07	0.41	0.14	1.73	1.11	0.73	0.11	1.43	1.05	0.59	1.06	0.78	0.59
-0.4	0.19	1.18	N/A	0.86	0.34	0.13	0.07	0.53	0.31	0.29	0.01	0.43	0.33	0.20	0.39	0.27	0.21
16.8	0.51	1.65	N/A	1.16	0.56	0.24	0.13	0.86	0.56	0.48	0.07	0.70	0.55	0.35	0.58	0.48	0.36
37.6	0.64	2.15	N/A	1.50	0.74	0.31	0.14	1.16	0.75	0.58	0.09	0.94	0.72	0.45	0.75	0.58	0.45
59.5	0.77	2.73	N/A	1.88	0.93	0.37	0.15	1.49	0.96	0.66	0.10	1.21	0.92	0.53	0.93	0.70	0.53
77.5	0.88	3.22	N/A	2.19	1.08	0.42	0.15	1.74	1.12	0.73	0.11	1.43	1.06	0.60	1.07	0.81	0.59
97.9	1.02	4.35	N/A	2.93	1.31	0.47	0.15	2.21	1.39	0.87	0.11	1.82	1.33	0.73	1.33	0.97	0.72
116.9	1.25	8.17	N/A	6.02	1.64	0.57	0.15	3.99	1.82	1.07	0.10	4.98	1.83	0.92	2.91	1.44	0.97
116.8	1.25	8.31	N/A	6.12	1.66	0.57	0.15	4.07	1.83	1.07	0.10	5.10	1.86	0.93	3.00	1.45	0.97
134.5	1.67	14.76	N/A	11.53	2.21	0.71	0.15	10.92	2.52	1.28	0.12	10.23	2.55	1.19	7.56	2.03	1.32
135.9	1.66	14.87	N/A	11.60	2.23	0.72	0.15	11.03	2.54	1.30	0.12	10.30	2.57	1.19	7.71	2.05	1.35
154.8	2.20	22.94	N/A	17.89	3.65	1.10	0.33	19.14	4.86	1.61	0.14	15.22	4.12	1.58	14.57	3.13	1.85
176.0	2.87	32.07	N/A	25.35	7.54	2.34	0.78	25.88	7.84	2.02	0.23	25.34	8.12	2.07	21.09	6.27	2.65
196.8	3.57	40.02	N/A	29.31	14.38	4.98	1.18	30.88	11.40	2.31	0.45	31.85	15.02	2.83	25.93	9.64	5.82
216.6	4.42	49.38	N/A	33.64	21.17	7.66	1.79	37.20	18.21	2.96	0.60	36.95	21.79	4.04	30.96	14.43	8.58
236.7	5.18	57.25	N/A	37.68	26.36	9.87	2.72	42.53	22.96	4.41	0.88	41.34	26.49	5.10	34.98	18.24	11.04
257.7	6.03	65.33	N/A	41.64	31.71	12.10	3.39	47.86	27.37	8.08	1.15	46.19	30.08	7.03	38.15	21.21	13.58
278.0	7.03	74.15	N/A	46.02	37.83	15.50	4.20	52.82	32.15	12.81	2.04	50.85	33.31	11.16	40.80	23.68	17.04
297.7	8.06	80.00	N/A	50.66	44.16	18.89	5.32	57.90	36.20	16.69	4.81	55.23	35.79	19.30	43.08	25.88	18.99
318.8	9.14	80.00	N/A	55.53	49.81	22.28	6.35	62.36	40.53	20.34	8.51	60.00	38.41	24.62	45.25	28.35	20.89
338.6	10.12	80.00	N/A	60.81	55.18	25.61	7.44	66.87	45.17	24.31	11.83	65.39	41.50	29.44	47.46	31.24	22.59
357.0	11.08	80.00	N/A	65.79	60.41	29.10	8.38	71.43	49.94	28.49	14.25	70.33	44.80	33.45	49.55	33.44	24.50
377.5	12.20	80.00	N/A	70.84	65.77	32.91	9.67	76.87	55.12	33.40	17.11	76.48	48.83	37.50	52.04	36.49	27.35
404.9	13.91	80.00	N/A	80.00	72.87	38.50	11.82	80.00	62.17	39.62	21.68	80.00	55.07	43.21	56.27	41.16	31.15
419.7	15.42	80.00	N/A	80.00	77.51	43.12	13.63	80.00	67.50	45.25	26.18	80.00	60.22	47.87	59.83	44.28	34.20
436.0	16.60	80.00	N/A	80.00	80.00	46.07	15.02	80.00	71.46	48.71	28.78	80.00	65.25	51.76	63.76	47.44	36.72
453.1	18.47	80.00	N/A	80.00	80.00	50.03	17.25	80.00	76.25	53.43	32.80	80.00	71.64	57.82	69.70	52.17	40.10
476.0	20.59	80.00	N/A	80.00	80.00	54.48	19.56	80.00	79.61	58.45	36.99	80.00	77.49	62.96	76.71	57.72	43.67
488.8	22.78	80.00	N/A	80.00	80.00	58.40	22.00	80.00	80.00	62.52	40.43	80.00	80.00	67.55	80.00	63.21	46.83
491.7	23.62	80.00	N/A	80.00	80.00	59.32	22.84	80.00	80.00	63.42	41.44	80.00	80.00	68.98	80.00	64.85	47.77

SPECIMEN #5-4C

Load (kN)	Defl. (mm)	Bar Force(kN)												
		C1-12S	C2-12S	P1-9S	P1-28S	P1-47S	P1-66S	P2-9S	P2-28S	P2-47S	P2-66S	P3-9S	P3-28S	P3-47S
0.8	0.00	-0.03	-0.07	0.05	-0.06	-0.05	-0.04	-0.04	-0.04	-0.02	-0.06	-0.01	-0.04	-0.02
18.9	0.33	0.54	0.40	0.32	0.16	0.03	-0.01	0.28	0.24	0.14	-0.02	0.18	0.13	0.09
38.6	0.56	1.52	1.17	0.69	0.46	0.09	-0.04	0.67	0.55	0.26	-0.03	0.40	0.30	0.18
58.6	0.75	3.20	3.07	1.16	0.97	0.18	-0.04	1.18	0.99	0.46	0.01	0.72	0.55	0.31
57.2	0.71	3.55	3.62	1.05	1.07	0.19	-0.05	1.25	1.06	0.51	0.02	0.83	0.59	0.32
28.8	0.50	2.57	2.70	0.65	0.76	0.11	-0.04	0.80	0.71	0.37	0.00	0.56	0.40	0.23
19.5	0.44	2.23	2.38	0.52	0.66	0.08	-0.03	0.64	0.60	0.32	-0.01	0.47	0.33	0.19
1.1	0.16	1.30	1.46	0.16	0.35	-0.01	-0.07	0.23	0.26	0.12	-0.07	0.22	0.11	0.05
19.3	0.51	1.98	2.10	0.45	0.58	0.07	-0.04	0.57	0.54	0.27	-0.01	0.41	0.28	0.16
39.7	0.64	2.84	2.94	0.78	0.84	0.15	-0.04	0.94	0.83	0.42	0.01	0.64	0.47	0.27
60.2	0.81	3.82	3.95	1.11	1.13	0.20	-0.07	1.32	1.13	0.52	0.03	0.87	0.61	0.34
80.4	0.98	5.87	6.29	1.67	1.88	0.29	-0.08	1.88	1.64	0.74	0.06	1.23	0.88	0.49
79.1	1.00	6.11	6.58	1.77	2.03	0.30	-0.06	1.95	1.74	0.79	0.07	1.30	0.93	0.52
99.2	1.21	8.42	9.19	2.58	3.07	0.35	-0.10	2.58	2.35	1.05	0.11	1.77	1.26	0.70
118.0	1.43	11.06	12.54	3.71	4.34	0.41	-0.15	4.29	3.01	1.33	0.15	2.38	1.69	0.90
137.4	1.75	14.97	17.25	6.25	6.28	0.56	-0.12	6.99	4.20	1.79	0.18	3.65	2.43	1.15
158.5	2.23	20.86	23.30	12.71	9.15	0.89	0.15	12.45	5.70	2.24	0.34	9.01	3.94	1.44
177.2	2.71	26.03	28.59	18.19	11.56	1.33	0.29	18.87	7.00	2.62	0.44	15.46	5.57	1.75
197.1	3.29	31.70	34.09	23.49	15.12	1.83	0.79	26.07	9.76	3.31	0.71	21.44	7.96	2.06
196.4	3.28	31.71	34.11	23.55	15.19	1.83	0.81	26.15	9.86	3.32	0.72	21.49	8.03	2.07
216.4	3.89	37.24	39.43	28.29	19.61	2.60	1.56	34.05	14.30	4.08	1.08	26.09	11.62	2.55
239.2	4.65	42.52	44.50	32.91	24.71	3.64	2.37	39.97	19.78	5.14	1.64	30.37	16.21	3.23
257.4	5.21	46.85	48.32	36.68	28.76	4.71	3.03	44.51	24.19	6.06	2.20	33.71	19.55	4.09
256.4	5.21	46.88	48.32	36.72	28.85	4.76	3.05	44.50	24.30	6.10	2.23	33.72	19.65	4.14
281.3	6.06	52.83	54.10	41.88	33.75	6.38	3.62	50.06	29.14	7.92	3.24	38.18	23.45	6.28
299.7	6.73	57.38	58.89	45.66	38.31	8.17	4.21	54.62	32.81	9.88	5.81	41.40	26.33	7.96
320.5	7.52	62.00	63.83	49.83	42.46	10.13	4.87	59.70	37.04	11.84	7.88	45.05	29.20	10.03
319.7	7.52	62.02	63.82	49.84	42.49	10.17	4.89	59.73	37.11	11.88	7.93	45.04	29.23	10.15
335.0	8.10	65.70	67.73	52.74	45.26	11.65	5.30	63.76	40.13	13.11	8.95	47.68	31.28	13.74
334.1	8.11	65.72	67.76	52.72	45.29	11.78	5.32	63.73	40.15	13.12	9.03	47.64	31.29	14.02
348.3	8.77	68.80	70.25	55.07	48.42	13.85	5.73	67.99	43.04	14.43	10.22	50.03	33.32	19.23
360.3	9.54	70.56	71.05	56.83	51.33	15.85	6.33	72.09	46.10	16.19	11.77	53.52	35.70	22.41
370.4	10.02	72.72	72.88	58.28	53.55	17.35	6.70	75.08	48.07	17.59	13.23	55.66	37.23	24.17
381.4	10.60	75.27	75.44	59.51	55.91	19.21	7.15	78.12	50.23	19.44	15.33	57.87	38.80	26.09
390.9	11.09	76.97	77.42	60.63	57.62	20.78	7.50	80.00	52.19	20.78	16.84	60.05	40.32	27.60
399.9	11.58	79.01	79.47	62.93	59.25	22.29	7.88	80.00	54.15	22.21	18.10	62.07	41.59	28.89
409.2	12.01	80.00	80.00	65.72	61.01	23.66	8.26	80.00	56.07	23.61	19.20	64.02	43.02	30.09
418.4	12.46	80.00	80.00	68.90	62.85	25.23	8.68	80.00	58.11	25.31	20.22	65.95	44.45	31.03
417.2	12.47	80.00	80.00	68.97	62.84	25.32	8.70	80.00	58.12	25.48	20.25	65.90	44.44	31.00
429.0	13.12	80.00	80.00	72.99	65.10	27.46	9.21	80.00	60.85	27.92	21.63	68.48	46.45	32.46
427.9	13.13	80.00	80.00	73.05	65.06	27.56	9.24	80.00	60.87	28.06	21.68	68.44	46.45	32.47
437.9	13.80	80.00	80.00	77.44	67.37	29.88	9.81	80.00	63.60	30.89	23.08	70.94	48.37	33.90
447.6	14.49	80.00	80.00	80.00	69.74	32.09	10.41	80.00	66.12	33.36	24.78	73.55	50.25	35.31
446.5	14.51	80.00	80.00	80.00	69.70	32.17	10.45	80.00	66.12	33.47	24.82	73.49	50.26	35.32
453.5	15.14	80.00	80.00	80.00	71.44	33.97	11.06	80.00	68.44	35.40	26.11	75.79	51.93	36.61

SPECIMEN #6-4F

Load (kN)	Defl. (mm)	Bar Forces(kN)												
		C1-125	C2-125	P1-95	P1-285	P1-475	P1-665	P2-95	P2-285	P2-475	P2-665	P3-95	P3-285	P3-475
0.1	0.00	0.07	N/A	-0.04	0.02	-0.04	-0.03	0.04	0.03	0.03	-0.05	0.04	0.02	-0.01
16.9	0.26	0.74	N/A	0.34	0.13	0.03	-0.01	0.31	0.23	0.11	-0.01	0.13	0.14	0.08
41.6	0.48	2.28	N/A	1.05	0.35	0.08	0.00	0.86	0.56	0.28	-0.01	0.41	0.39	0.16
59.3	0.71	3.72	N/A	1.90	0.54	0.10	-0.01	1.41	0.85	0.41	0.01	0.68	0.65	0.24
61.2	0.69	4.22	N/A	2.34	0.59	0.16	0.00	1.60	1.07	0.45	0.01	0.82	0.68	0.34
37.2	0.41	3.22	N/A	1.89	0.43	0.13	0.02	1.22	0.80	0.36	0.02	0.62	0.54	0.28
23.1	0.25	2.58	N/A	1.56	0.34	0.10	0.02	0.97	0.64	0.31	0.03	0.49	0.43	0.22
38.5	0.41	3.20	N/A	1.86	0.44	0.13	0.02	1.21	0.81	0.36	0.02	0.63	0.53	0.27
62.3	0.52	4.30	N/A	2.42	0.60	0.17	0.01	1.64	1.09	0.45	0.03	0.84	0.71	0.34
79.6	0.72	5.73	N/A	3.36	0.76	0.20	0.01	2.19	1.40	0.56	0.05	1.12	0.89	0.44
79.4	0.72	5.76	N/A	3.38	0.76	0.20	0.00	2.20	1.42	0.56	0.04	1.13	0.90	0.45
98.9	1.00	8.39	N/A	5.37	1.05	0.26	0.00	4.51	1.92	0.70	0.04	1.85	1.24	0.59
117.3	1.36	12.76	N/A	9.04	1.38	0.34	0.02	9.20	2.34	0.83	0.02	4.06	1.64	0.75
140.6	1.90	20.09	N/A	13.88	2.36	0.51	0.12	16.22	3.38	1.12	0.04	8.48	2.50	0.96
140.2	1.89	20.17	N/A	13.94	2.40	0.51	0.13	16.30	3.40	1.13	0.03	8.57	2.52	0.95
158.8	2.31	26.51	N/A	17.71	3.90	0.69	0.38	21.67	4.57	1.45	0.08	12.80	3.39	1.11
158.1	2.33	26.62	N/A	17.79	3.96	0.70	0.38	21.74	4.61	1.45	0.08	12.97	3.41	1.11
179.3	2.90	33.78	N/A	22.04	6.25	0.87	0.59	27.13	6.83	2.08	0.18	17.74	5.39	1.42
198.3	3.47	41.63	N/A	25.56	9.16	1.89	0.78	32.04	10.82	2.93	0.33	21.49	9.38	1.84
217.8	4.10	49.74	N/A	29.30	12.29	2.87	0.94	36.40	15.24	4.13	0.43	25.44	13.16	2.27
217.1	4.09	49.85	N/A	29.30	12.41	2.92	0.95	36.37	15.40	4.19	0.43	25.46	13.27	2.29
237.6	4.84	59.18	N/A	33.07	16.78	4.76	1.58	40.68	21.61	5.80	1.40	28.91	16.95	2.94
258.2	5.60	68.52	N/A	36.73	21.32	6.73	3.05	44.93	28.04	7.62	2.59	32.12	20.93	3.48
279.5	6.37	77.49	N/A	40.61	25.50	8.71	3.93	49.72	33.40	9.76	4.26	35.62	24.39	4.10
297.9	7.20	86.15	N/A	44.75	29.52	10.37	4.56	54.13	37.83	12.55	5.87	38.54	27.30	6.47
331.5	8.73	100.70	N/A	51.62	36.52	14.06	5.42	61.17	44.36	18.83	10.24	43.92	30.93	10.24
350.2	9.46	107.89	N/A	55.50	40.50	15.76	5.81	65.36	47.63	21.68	11.76	46.92	33.31	13.28
366.7	10.26	114.30	N/A	59.62	44.55	17.44	6.32	70.34	51.42	24.37	13.51	50.41	35.73	15.28
381.8	10.95	118.51	N/A	63.92	48.01	18.94	6.79	75.30	54.76	26.41	14.91	53.65	37.80	16.67
380.5	10.96	118.40	N/A	63.98	48.06	18.96	6.80	75.38	54.77	26.44	14.93	53.56	37.77	16.71
400.4	11.91	122.07	N/A	69.87	51.93	20.69	7.40	80.00	58.99	29.17	16.61	57.93	40.30	18.38
413.8	12.62	122.10	N/A	74.70	55.27	22.18	7.89	80.00	62.50	31.50	17.93	61.27	42.43	19.73
432.1	13.84	122.10	N/A	80.00	60.67	24.66	8.73	80.00	68.25	36.15	20.38	66.80	45.85	22.13
430.6	13.85	122.10	N/A	80.00	60.78	24.69	8.75	80.00	68.30	36.24	20.49	66.82	45.85	22.17